

2014

Modeling human muscle metabolism: using constraint-based modeling to investigate nutrition supplements, insulin resistance, and type 2 diabetes

<https://hdl.handle.net/2144/15223>

"Downloaded from OpenBU. Boston University's institutional repository."

BOSTON UNIVERSITY
GRADUATE SCHOOL OF ARTS AND SCIENCES
AND
COLLEGE OF ENGINEERING

Dissertation

**MODELING HUMAN MUSCLE METABOLISM:
USING CONSTRAINT-BASED MODELING TO INVESTIGATE
NUTRITION SUPPLEMENTS, INSULIN RESISTANCE, AND
TYPE 2 DIABETES**

by

CHRISTOPHER DOMENIC NOGIEC

B.S., Boston College, 1999
M.S., Northeastern University, 2003

Submitted in partial fulfillment of the

requirements for the degree of

Doctor of Philosophy

2014

© Copyright by
CHRISTOPHER D. NOGIEC
2014

Approved by

First Reader

Simon Kasif, PhD, Professor of Biomedical Engineering, Bioinformatics and Computer Science, Boston University; and Staff Scientist, Children's Hospital Informatics Program, Harvard-MIT Division of Sciences and Technology

Second Reader

Mary-Elizabeth Patti, MD, Investigator and Adult Endocrinologist, Joslin Diabetes Center; and Assistant Professor of Medicine, Harvard Medical School

Acknowledgements

I would like to thank my advisors, Simon Kasif, PhD, and Mary-Elizabeth Patti, MD. Without their support and guidance, I would not have been able to start, let alone finish, my dissertation. I would never be able to express how much their mentoring and tutelage have helped me throughout this entire process and have helped me become a better scientist.

I would also like to thank Alison Burkart, PhD. Her feedback and support were invaluable throughout the process. And, her superb laboratory work has been vital in validating the simulation and predictions from the computational model. In addition, I thank Carles Lerin, PhD, for his help in creating the model used in the insulin resistance research, and Ana Luis Coelho, PhD, who also provided laboratory results to support biological validation

I thank members of the Palsson laboratory and other members of the metabolic network community for the free software packages and optimization tools. I thank Jonathan Dreyfuss and Tomer Shlomi for multiple discussions and suggestions.

I thank the Bioinformatics program at Boston University for enabling me to pursue a PhD: the training fellowship during my first year and sharing in the publication costs of my papers.

I thank members of the Kasif and Patti laboratories for many comments and suggestions on my presentations during my PhD.

**MODELING HUMAN MUSCLE METABOLISM:
USING CONSTRAINT-BASED MODELING TO INVESTIGATE
NUTRITION SUPPLEMENTS, INSULIN RESISTANCE, AND TYPE
2 DIABETES**

CHRISTOPHER DOMENIC NOGIEC

Boston University, Graduate School of Arts and Sciences

and College of Engineering, 2014

Major Professor: Simon Kasif, PhD, Professor of Biomedical Engineering, Bioinformatics and Computer Science, Boston University; and Staff Scientist, Children's Hospital Informatics Program, Harvard-MIT Division of Sciences and Technology

Abstract

Human muscle metabolism, the biochemical reactions which to lead storage and usage of energy, is complex, but important in understanding human health and disease. Optimal muscle metabolism can help maintain a healthy organism by adequately storing and utilizing energy for subsequent use in contraction and recovery and adaption from contraction and exercise. Dysregulated muscle metabolism can lead to insulin resistance and obesity among other health problems.

Flux balance analysis (FBA) and constraint-based modeling have successfully elucidated important aspects of metabolism in single-celled organisms. However, limited work has been done with multicellular organisms. The foci of this dissertation are (1) to show how novel applications of this technique can aid in the investigation of human nutrition and (2) to elucidate metabolic phenotypes associated with the insulin resistance (IR) characteristics of Type 2 Diabetes (T2D).

First, for human nutrition a novel steady-state constraint-based model of skeletal muscle tissue was constructed to investigate the effect of amino acid supplementation on protein synthesis. Several *in silico* supplementation strategies implemented showed that amino acid supplementation could increase muscle contractile protein synthesis, which is consistent with published data on protein synthesis. These results suggest that increasing bioavailability of methionine, arginine, and the branched-chain amino acids can increase the flux of contractile protein synthesis.

Second, the cause(s) of the altered muscle metabolism in IR remain(s) unknown. Attempting to elucidate this complexity, systematic perturbations of the metabolic network identified reactions which mimic IR phenotypes. Reduced flux through a single reaction is not sufficient to recapitulate the IR phenotypes, but knockdowns in pyruvate dehydrogenase in combination with either reduced lipid uptake or lipid/amino acid oxidative metabolism do so. These combinations also decrease complete lipid oxidation and glycogen storage.

Table of Contents

Acknowledgements	iv
Abstract	v
Table of Contents	vii
List of Tables	x
List of Figures	xi
List of Abbreviations	xii
Introduction	1
Description of Flux Balance Analysis and Model Development	3
Brief FBA Review.....	3
Model Development.....	4
Model Implementation	8
A Metabolic Network Framework for Human Nutritional Supplements	9
Introduction	9
Methods	11
<i>Modeling Assumptions</i>	11
<i>Experimental Method</i>	12
<i>Data Analysis</i>	15
Results	18
<i>Single Amino Acid Supplementation</i>	18
<i>Multiple Amino Acid Supplementation</i>	19
Discussion.....	20
<i>Comparison to Literature – BCAA</i>	26

<i>Comparison to Literature – Arginine</i>	27
<i>Comparison to Literature – Glutamine</i>	27
Metabolic Modeling of Muscle Metabolism Identifies Key Reactions Linked to Insulin	
Resistance Phenotypes	29
Introduction	29
Methods	31
<i>Choosing the Objective Function</i>	31
<i>Modeling the Dynamics of Normal Metabolism</i>	32
<i>Nutrient Conditions</i>	34
<i>In Silico Knockdowns</i>	35
<i>Modeling Insulin Resistance Phenotypes</i>	36
<i>Pathway Analysis</i>	40
<i>Modeling Assumptions</i>	40
<i>RT-PCR of S961 IR Mouse Model</i>	41
<i>Primary Cell Preparation and Transfection</i>	41
<i>Western Blot Analysis</i>	42
<i>Respiration Studies</i> ⁵	42
<i>Citrate Synthase Activity Assay</i>	43
<i>Adenosine Nucleotide Measurements</i>	43
Results	44
<i>Model Development and Validation</i>	44
<i>Impact of Nutrient Availability</i>	47
<i>Simulating Metabolic Phenotypes of Insulin Resistance</i>	53
<i>Pathway Analysis of Knockdown Phenotypes</i>	59
<i>Multiple Simultaneous Knockdowns are Required to Fully Recapitulate Metabolic Phenotypes Associated with Insulin Resistance</i>	61

<i>Biological Validation of In Silico Results</i>	66
Discussion.....	71
Conclusion.....	81
Appendix A – Pathway Assignments.....	87
Bibliography	95
Curriculum Vitae	104

List of Tables

Table 1. Table of the contractile protein complexes in different types of muscle tissue	7
Table 2. Fasting and Post-prandial control for glucose, fatty acid and amino acid levels.....	12
Table 3. Amino Acids Needed Compared to the Amino Acids Available to produce one contractile protein complex in Type 2a.	15
Table 4. Type 2a contractile protein flux synthesis in fasting and post-prandial states for every combination of 1 -7 amino acids.	20
Table 5. Basal concentrations used as maximal uptake fluxes in the Flux Balance Model.	34
Table 6. Major qualitative changes induced by increased glucose and fatty acid substrate availability.....	48
Table 7. KDs in 1xFA-1xGluc causing significant reductions in the three screened phenotype...	54
Table 8. Top KDs causing reduced metabolic flexibility in basal nutrient condition	56
Table 9. KDs in 2xFA-2xGluc causing significant reductions in the three screened phenotypes .	57
Table 10. Top KDs causing reduced metabolic flexibility in the 2xFA-2xGluc increased nutrient condition.....	58
Table 11. Pathways enriched in causing IR phenotypes in 1xFA-1xGluc basal nutrient conditio.	59
Table 12. Pathways enriched in causing IR phenotypes in the 2xFA-2xGluc increased nutrient condition.....	60
Table 13. Summary of scores for the top DOUBLE KDs causing reduced metabolic flexibility....	63
Table 14. RT-PCR results from skeletal muscle tissue from the Control (PBS) and S961 IR induced mice for candidate genes from <i>in silico</i> analysis.	67

List of Figures

Figure 1. Experimental Procedure for Amino Acid Supplementation.....	14
Figure 2. Flux differences compared to control show how increased amino acids could be used.	25
Figure 3. Simulating fasting to fed transition by reducing CPT1 activity and increasing a modifiable glucose uptake component.....	34
Figure 4. Work flow for the <i>in silico</i> knockdown experiments.	36
Figure 5. Modeling muscle metabolism under normal nutrient conditions	46
Figure 6. Fluxes through all reactions in the model from fasting to fed transition for four different nutrient states.....	51
Figure 7. Predicted fluxes through pathways and substrate uptake/production	52
Figure 8. Combined knockdowns can induce metabolic phenotypes associated with insulin resistance.....	62
Figure 9. Double knockdowns (PDH/ETFDH or PDH/FAT) alter carbohydrate and fatty acid metabolism.....	66
Figure 10. Double knockdowns in myoblasts recapitulate the IR phenotypes predicted by <i>in silico</i> experiments.....	70
Figure 11. Predicted fluxes through pathways and substrate uptake, production, and release ...	74
Figure 12. Schematic of targeted knockdowns that model phenotypes of insulin resistance.....	76

List of Abbreviations

AA	Amino Acid
ACSL	Long-chain Acyl-CoA Synthase
ADP	Adenosine Di-Phosphate
ALA	Alanine
AMP	Adenosine Mono-Phosphate
ARG	Arginine
ASN	Asparagine
ASP	Aspartate
AST	Aspartate Transaminase
ATP	Adenosine Tri-Phosphate
bas	Basal
BCAA	Branched-chain Amino Acids
BCAT-2	Branched-chain amino acid transaminase
CPT1	Carnitine Palmitoyl-transferase 1
Cr-P	Creatine Phosphate
CYS	Cysteine
E. C.	Enzyme Commission
ECAR	Extracellular Acidification Rate
Eq.	Equation
ETC	Electron Transport Chain
ETFD(H)	Electron-Transferring Flavoprotein Dehydrogenase
FA	Fatty Acid
FAD/H	Flavin Adenine Dinucleotide
FAT	Fatty Acid Transport
FBA	Flux Balance Analysis
FDR	False Discovery Rate
GLAST	Glutamate-Aspartate Mitochondrial Exchange

GLN	Glutamine
GLPK	GNU Linear Programming Kit
GLU	Glutamate
Gluc	Glucose
GLUT	Glucose Transport
GLY	Glycine
glyc3P	Glycerol-3-phosphate
GU	Glucose Uptake
HIS	Histidine
ILE	Isoleucine
IR	Insulin Resistance
IS	Insulin Sensitive
KD(s)	Knockdown(s)
KEGG	Kyoto Encyclopedia of Genes and Genomes
LEU	Leucine
LYS	Lysine
MET	Methionine
Met. Flex	Metabolic Flexibility
mM	milli Molar
mMol	milli mole
mod	modifiable
mTOR	mammalian target of rapamycin
NAD/H	Nicotinamide Adenine
NCBI	National Center for Biotechnology Information
NMR	Nuclear Magnetic Resonance
OCR	Oxygen Consumption Rate
OXPHOS	Oxidative Phosphorylation
PBS	Phosphate Buffer Saline
PDH	Pyruvate Dehydrogenase

PEP	Phosphoenolpyruvate
PHE	Phenyl-Alanine
PK	Pyruvate Kinase
PPAR γ	Peroxisome proliferator-activated receptor gamma
PRO	Proline
ROS	Reactive oxygen species
RQ	Respiratory Quotient
S	Matrix of reactions and metabolites used in the model
SBML	Systems Biology Markup Language
siRNA	Small interfering RNA
SER	Serine
T2D	Type 2 Diabetes
TAG	Tri-Acyl Glycerides
TCA	Tri-Carboxylic Acid
THR	Threonine
TRP	Tryptophan
TYR	Tyrosine
v	Variable for flux solution
VAL	Valine
WT	Wild Type

Introduction

Human muscle metabolism, the biochemical reactions which lead to storage and usage of energy, is complex, but important in understanding human health and disease. Optimal muscle metabolism can help maintain a healthy organism by adequately storing and utilizing energy for subsequent use in contraction and recovery and adaption from contraction and exercise. Dysregulated muscle metabolism can lead to insulin resistance and obesity among other health problems. However, given the complexities and redundancy of human metabolism, it is often difficult, time-consuming, inefficient, and expensive to fully investigate hypotheses. However, with recent advances in metabolic modeling, one is now more able to study multiple hypotheses and obtain insight into the entire known metabolic network. Flux Balance Analysis (FBA), a constraint-based modeling framework, has been an effective tool at simulating, predicting, and elucidating metabolism (Oberhardt et al., 2009; Cakir et al., 2007; Duarte et al., 2007; Jerby et al., 2010; Thiele et al., 2013; Folger et al., 2011). The work described in this dissertation showcases a novel metabolic model of muscle metabolism and novel applications for and results of FBA: (1) studies into human nutrition and (2) investigation into insulin resistance (IR)/Type 2 Diabetes (T2D). Specifically, it is used to determine causal relationships between dysregulated metabolism leading to diseased phenotypes for the latter, and increasing bioavailability of nutrients leading to increased protein synthesis. Before

describing these findings, a short review describes the FBA framework. This is followed by a report of the development of an original metabolic model of human skeletal muscle created for use in the work described here. The next two chapters elaborate on novel methodologies and findings which demonstrate how FBA (1) is an effective tool for studying human nutrition in the form of amino acid supplementation related to post-exercise protein synthesis and (2) provides novel approaches in determining causes of metabolic phenotypes specifically related to IR and T2D. The final section contains concluding remarks and broader perspectives of the work which will have been presented.

Description of Flux Balance Analysis and Model Development

Brief FBA Review

Flux balance analysis (FBA) (Varma and Palsson, 1994) is a constraint-based modeling framework which captures the relationships between input and output fluxes associated with biochemical reactions in metabolic networks under different conditions and systemic objectives. FBA has been successfully used to model both bacterial (Oberhardt et al., 2009) and human metabolism (Cakir et al., 2007; Duarte et al., 2007; Jerby et al., 2010; Thiele et al., 2013; Folger et al., 2011; Nogiec and Kasif, 2013).

FBA models are developed by collating reactions from public databases (e.g. KEGG (Kanehisa et al., 2012), BioCyc (Romero et al., 2005)), and by manual curation (Nogiec and Kasif, 2013). These reactions are converted into mathematical expressions as a matrix of linear equations (S) where the columns represent the set of reactions and the rows represent the set of metabolites. The system is subsequently additionally augmented by linear constraints to increase biological feasibility (v). For example, one can add thermodynamic information by constraining the directionality of each reaction (e.g. if irreversible), limit storage of metabolites by setting upper limits, and limit substrate availability. These constraints are provided as linear inequalities. This framework provides one with

the capability to use modern computational methods to find specific solutions to the system of linear equalities and inequalities that optimize a relevant objective function. Objective functions can be manually assigned to represent biological objectives of cells. The model predicts the optimal flux distributions (v), at steady state, under specific optimization parameters and perturbations: $S * v = 0$.

Optimizing a system of equations with inequalities can lead to multiple solutions which satisfy the constraints. Many techniques have been used to optimize prediction accuracy (Segre et al., 2002; Oberhardt et al., 2009). However, in this dissertation, a simplified approach has been used, assuming cells will re-optimize after perturbations.

Model Development

While there has been an increased attempt to create human tissue specific models (Cakir et al., 2007; Shlomi et al., 2008; Jerby et al., 2010; Agren et al., 2012), some a subset of the human metabolic model (Duarte et al., 2007), these models are not curated, and the authors have not specifically reported on the skeletal muscle tissue models (Shlomi et al., 2008; Agren et al., 2012). While the model presented in this dissertation is smaller than previously published skeletal muscle models, it was built by manually identifying key reactions specific in muscle tissue, similar to the method used by Cakir (2007). This curation process is different than methods used by Shlomi et al. (2008) and Agren et al. (2012) which used various algorithms incorporating gene expression to predict a tissue specific model from the general

human model from Palsson's lab (Duarte et al., 2007). One main difference is this muscle model includes detailed fluxes for specific muscle proteins (the contractile complexes for Type 1, 2a, 2x, and 2b muscle tissue) while the larger models do not have these specific reactions.

The goal for this model was to capture metabolism from the major macronutrients (carbohydrates, lipids, and protein/amino acids) in muscle tissue. In addition, beyond major catabolic reactions, fatty acid and amino acid biosynthesis and protein synthesis for the major contractile muscle proteins have been included. The flux model developed here combines the previously published flux model of the mitochondria (Ramakrishna et al., 2001) with critical additions to uniquely capture muscle-specific metabolism: amino acid metabolism, protein synthesis, fatty acid oxidation and synthesis, and pentose phosphate metabolism. For example, Aconitase was added (EC 4.2.1.3) which catalyzed the reversible reaction between isocitrate and citrate. In addition, the entire electron transport complex (ETC) was modeled, including electron transfer flavoprotein-ubiquinone oxidoreductase which oxidizes flavin adenine dinucleotide (EC 1.5.5.1). Further modifications were made to fatty acid oxidation. The fatty acid used by Ramakrishna (2001), palmitate, is a 16 carbon fatty acid. Although the same enzymes are used in each cycle of the fatty acid oxidation, each cycle here is detailed. In other words, there are reactions which oxidize an 18 carbon fatty acid,

a 16 carbon fatty acid, etc. This makes it possible to add other fatty acids as substrates and to incorporate amino acid oxidation into the same cycle.

The model was also expanded to include amino acid and protein metabolism. During certain conditions, the muscle will oxidize certain amino acids for energy supply (Jungas et al. 1992), and thus amino acids, which are known to be metabolized in human muscles, were also included. The branched-chain amino acids (BCAA), isoleucine, leucine, and valine, are used as an energy supply during certain conditions, and the byproducts enter fatty acid oxidation cycle and Tri-Carboxylic Acid (TCA) cycle. In addition to the BCAAs, serine can be converted to pyruvate (EC 4.3.1.17), which can be used in the glycolytic pathway. The oxidative products of lysine also enter the fatty acid oxidation pathway. Proline oxidation produces flavin adenine dinucleotide (FADH), which can be incorporated into the electron transport chain (ETC). The enzymes, which catalyze these reactions, were found in the *Homo sapiens* KEGG pathway map. Expression in muscles of the enzymes was confirmed using UniProt information on tissue specificity for each of these enzymes involved in amino acid metabolism.

In addition to the amino acid metabolism, protein metabolism is included: specifically, the synthesis of the major contractile proteins actin, myosin, tropomyosin, and troponin. Their amino acid make-up was determined from NCBI database. Different muscle tissue type expresses different myosin, tropomyosin, and troponin. The myosin complex is made of a heavy chain, which differs between type 1/2x, 2a, and 2b muscle types; a light chain kinase; and a light chain

phosphatase. Tropomyosin is expressed as two sub-types, type 1 and type 2, and form dimers within the respective tissue type. Troponin is composed of three subtypes specific to each muscle tissue type 1 or 2: troponin C, troponin I, and troponin T. The entire contractile protein complex is composed in the ratio of 7 actin to 7 myosin to 1 tropomyosin dimer to 1 troponin complex (Gordon et al., 2000) (**Table 1**).

Table 1. Table of the contractile protein complexes in different types of muscle tissue

Muscle Type	Protein	GI (from NCBI)
Type 1	Actin	4501881
	Myosin Heavy Chain type 1/2x	115527082
	Myosin Light Chain Kinase	14993776
	Myosin Light Chain Phosphatase	28372499
	Tropomyosin type 1	114155140
	Troponin C type 1	4507615
	Troponin I type 1	56682969
	Troponin T type 1	187173288
Type 2a	Actin	4501881
	Myosin Heavy Chain type 2a	153792663
	Myosin Light Chain Kinase	14993776
	Myosin Light Chain Phosphatase	28372499
	Tropomyosin type 2	114155144
	Troponin C type 2	4507617
	Troponin I type 2	4507621
	Troponin T type 2	5803203
Type 2x	Actin	4501881
	Myosin Heavy Chain type 1/2x	115527082
	Myosin Light Chain Kinase	14993776
	Myosin Light Chain Phosphatase	28372499
	Tropomyosin type 2	114155144
	Troponin C type 2	4507617

	Troponin I type 2	4507621
	Troponin T type 2	5803203
Type 2b	Actin	4501881
	Myosin Heavy Chain type 1/2x	110611903
	Myosin Light Chain Kinase	14993776
	Myosin Light Chain Phosphatase	28372499
	Tropomyosin type 2	114155144
	Troponin C type 2	4507617
	Troponin I type 2	4507621
	Troponin T type 2	5803203

Nogiec Muscle model v1.0 includes 374 reactions and 341 metabolites (Nogiec and Kasif, 2013). The model is available in standard XML systems biology markup language (Nogiec and Kasif, 2013).

Model Implementation

Once all the reactions were identified and collected, the text was converted into a matrix for use in Mat Lab software package (Version 7.8.0.347 64 bit). The optimization software is the open-source GLPK MatLab interface (Version 4.39): ©2001-2007, Nicolo' Giorgetti, which uses linear programming to optimize a specified objective function; all default settings were used.

A Metabolic Network Framework for Human Nutritional Supplements¹

Introduction

The Nutrition Business Journal (2010) estimates the supplement industry at \$23.7 billion. However, the claims and efficacy of these supplements are not routinely regulated by the Federal Drug Administration. The question of whether to supplement and what to supplement to increase muscle mass has given rise to many studies over the years (Blomstrand et al., 2006; Paddon-Jones et al., 2004; Gleeson, 2008). Much focus has been on protein and amino acid supplementation. However, human studies can be difficult due to small sample sizes and length of time per study. In addition, only a limited number of variables can be investigated at a time (i.e., one amino acid or a few combinations at a time). Although some results show clear evidence for the efficacy of certain amino acids at increasing muscle mass (Blomstrand et al., 2006), others still show inconclusive results (Paddon-Jones et al., 2004; Gleeson, 2008).

¹ This chapter is based on material from the PLOS One publication, "To Supplement or Not to Supplement: A Metabolic Network Framework for Human Nutritional Supplements" by Christopher D. Nogiec and Simon Kasif (2013). Both authors have agreed to have the material included in this dissertation.

One goal of supplementation research in exercise physiology, fitness, and health is to determine which metabolites have the biggest effect on increasing muscle protein synthesis during the recovery phase. One method has been to increase the bioavailability of amino acids, as these are the building blocks of muscle proteins. Some amino acids and combinations have been investigated in great detail. Branched-chain amino acids (BCAAs) have been shown to increase protein synthesis, specifically in muscle tissue, in response to resistance exercise (Blomstrand et al., 2006). Of the three BCAAs, leucine seems to have the most prominent effect, and one hypothesis put forth is that leucine may signal an increase in enzymes involved in protein synthesis through mammalian target of rapamycin (mTOR) (beyond the scope of this introduction) (Blomstrand et al., 2006). In addition to the BCAAs, other amino acids have been investigated with mixed results. For example, supplementing with arginine, a conditionally essential amino acid, shows that it alone does not seem to increase protein synthesis nor does it increase protein synthesis in the presence of the eight essential amino acids. However, some studies indicate that arginine can increase protein synthesis in conjunction with other amino acids or with meals (Paddon-Jones et al., 2004). However, it is unclear which combination of amino acids is most beneficial. Furthermore, many studies show no effect of some amino acids, but these amino acids are still highly promoted among nutrition and supplement companies. Glutamine is promoted by supplement manufacturers for numerous positive effects, one of which helps muscle protein synthesis. However, a recent

review suggests that glutamine supplementation does not provide any of these benefits (Gleeson, 2008).

It is challenging to determine the individual effects of supplements and their combinations in human studies. Also, without trying every combination, it is unclear which are the most beneficial and whether there is a specific combination that is most effective. The advent of metabolic modeling of human tissues opens the door to using this platform for studying multiple hypotheses in this space including nutrition and supplementation. Multiple regimes of supplementation can be investigated efficiently and predictively. In this dissertation I introduce perturbation in the form of additional supplementation and measure the effect of individual and combinations of supplements on the protein synthesis flux in the model.

Methods

Modeling Assumptions

In addition to assumptions made with FBA (Oberhardt et al., 2009) I add three postulates. First, I assume muscle tissue is in a recovery state and primed for contractile protein synthesis. For example, the assumption is that all the hormones and enzymes available to support protein synthesis are available. In other words, this approach investigates an acute response to supplementation. Next, because of the difficulty in obtaining amino acid uptake fluxes for all amino acids into muscle tissue, I assume the uptake flux is proportional to amino acid concentration levels,

as levels are maintained by the liver and red blood cells (Cynober, 2002; MacLaren et al., 2000). Last, I assume the system reaches a steady state over enough time to exhaust the concentrations available in the plasma levels, as the goal is to seek qualitative results with this exploratory study.

Experimental Method

The goal of the experiment is to determine if supplementation of amino acids above a normal, fasting state can improve the protein synthesis flux. The normal fasting amino acid profile is based on Cynober (2002) (**Table 2**). The post-prandial (2 hours post ingestion of a 200g sirloin steak) is based on the average of Aoki et al. (1976), Tessari et al. (1996), and Pozefsky et al. (1969) (**Table 1**).

Table 2. Fasting and Post-prandial control for glucose, fatty acid and amino acid levels

Metabolite	Fasting (mmol/L) ¹	Post-prandial (mmol/L) ²
Glucose	5	7
Palmitate	0.125	0.125
Tetradecanoate	0.230	0.230
Arginine	0.080 ± 20	0.115 ± 14
Histidine	0.082 ± 10	0.118 ± 7
Isoleucine	0.062 ± 14	0.128 ± 14
Leucine	0.123 ± 25	0.271 ± 14
Lysine	0.188 ± 32	0.294 ± 24
Methionine	0.025 ± 4	0.030 ± 2
Phenylalanine	0.057 ± 9	0.068 ± 4
Threonine	0.140 ± 33	0.182 ± 13
Tryptophan	0.044 ± 7	0.036 ± 3.6
Valine	0.233 ± 43	0.349 ± 36
Alanine	0.333 ± 74	0.309 ± 46
Asparagine	0.041 ± 10	0.045 ± 2

Metabolite	Fasting (mmol/L) ¹	Post-prandial (mmol/L) ²
Aspartate	0.003 ± 1	0.067 ± 10
Cysteine	0.052 ± 11	0.093 ± 10
Glutamate	0.024 ± 15	0.152 ± 22
Glutamine	0.586 ± 84	0.541 ± 25
Glycine	0.230 ± 52	0.281 ± 33
Proline	0.168 ± 60	0.299 ± 23
Serine	0.114 ± 19	0.175 ± 11
Tyrosine	0.059 ± 12	0.092 ± 9

1. *Cynober 2002*

2. *Average of levels from Aoki et al., 1976; Tessari et al., 1996; and Pozefsky et al., 1969*

Supplementation was modeled by changing the available flux for each metabolite to an “unlimited” flux (99999 mmol/L/time). For single amino acid supplementation, each amino acid was supplemented one at a time. For multiple supplementations, all combinations of double, triple, quadruple... up to 7 amino acids were supplemented. (Computational time and resources dramatically increased after that, and the interest here is finding a minimum number of amino acids, rather than increasing all the amino acids.) If the protein synthesis flux increased compared to the normal condition, then it’s assumed that the increase in availability of the amino acid increased protein synthesis flux.

Using the model, I first determined the protein synthesis flux for the contractile proteins in each of the four muscle tissues (Type 1, Type 2a, Type 2x, and Type 2b) under both fasting and post-prandial states. I then optimized protein synthesis (contractile protein complex) in both control and supplement conditions, and I

compared the resulting fluxes after optimization. Simulating supplementation was achieved by removing the constraint on the supplemented amino acid(s). I then optimized protein synthesis through the contractile protein complex described. The method is outlined in **Figure 1**.

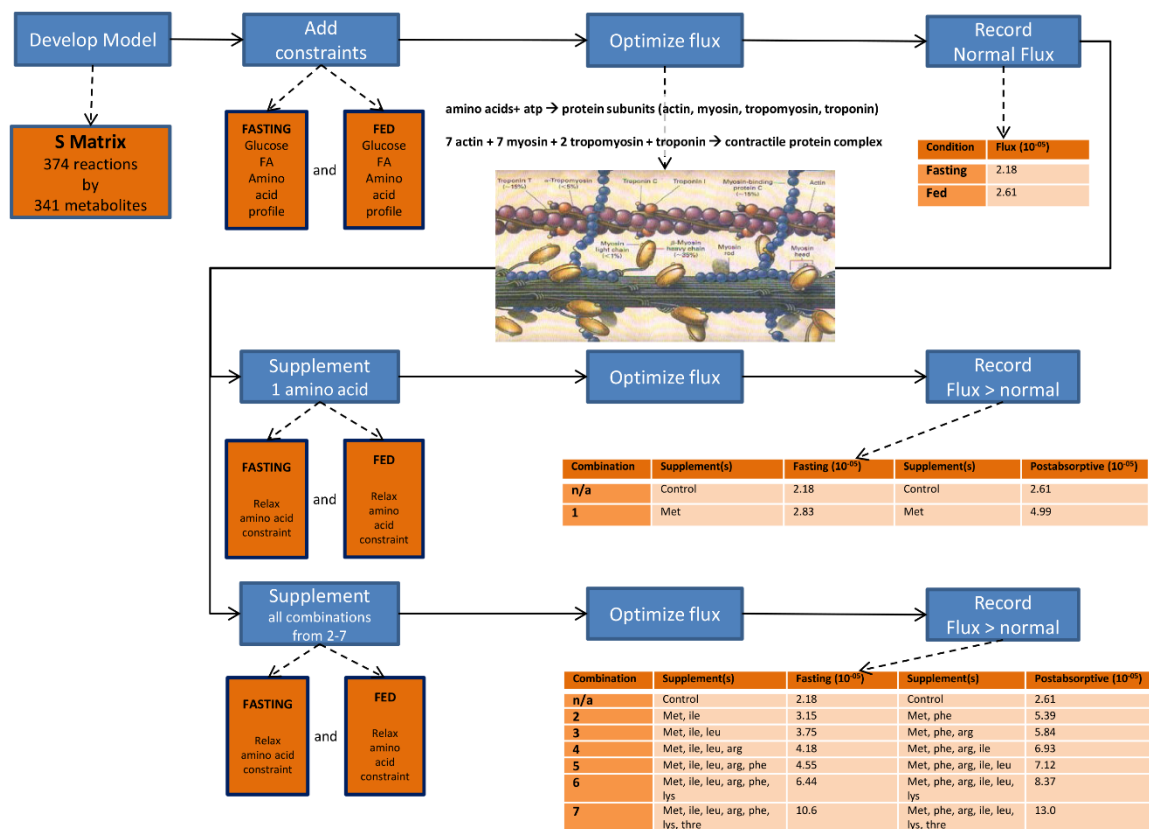


Figure 1. Experimental Procedure for Amino Acid Supplementation. This figure describes the work flow used for the experiment. A flux balance model of 374 reactions and 341 metabolites describing human muscle tissue was developed. Flux constraints based on fasting (Cynober 2002) and fed (Cynober et al. 2002, Aoki et al. 1976, Pozefsky et al. 1969) levels of glucose, fatty acids, and amino acids in blood were added. With the given constraint, the contractile protein flux was determined. Supplementation was simulated by relaxing the constraint on amino acids singly and in all combinations from 2-7 amino acids. If the resultant flux was greater than the control flux, then the flux and conditions were recorded. (The contractile protein schematic is from Spirito et al., 1997.)

Data Analysis

To make sense of the data and which amino acids are actually an artifact of being important or just available in lower quantities, the number of amino acids that are needed were compared to the number that were available (**Table 3**). The number of each amino acid that is needed is based on a count of the amino acids in each of the protein and subunits of the proteins which make up the protein complex unit (**Table 1**). The amount that is available was determined by converting the amount available in mmol divided by the control protein flux: 2.18×10^{-5} mmol/time (**Table 4**). Next, the difference of what is needed from what is available was determined and the amino acids were ranked by difference (*Expected Supplementation Effect*). The *Actual Supplementation Effect* is which amino acids were effective at increasing protein flux from single to 7 amino acid combinations (**Table 3**).

Table 3. Amino Acids Needed Compared to the Amino Acids Available to produce one contractile protein complex in Type 2a. Table 3A is the fasting state ranked by difference. Table 3B is the fasting state ranked by essentiality (ce and e considered essential) and then by difference. Table 3C is the post-prandial state ranked by difference. Table 3D is the post-prandial state ranked by essentiality (ce and e considered essential) and then by difference. (Act Sup Eff—Actual Supplementation Effect; AA Ess—Amino Acid Essentiality; ce—conditionally essential; e – essential; ne – non-essential)

Table 3A. Fasting state ranked by difference

AA	Needed	Available	Difference	Rank	Act Sup Eff	AA Ess
GLU	4996	1102	-3894	1	n/a	ne
ASP	2162	138	-2024	2	n/a	ne
MET	1148	1148	0	3	1	e
ASN	1592	1883	291	4	n/a	ne

AA	Needed	Available	Difference	Rank	Act Sup Eff	AA Ess
ILE	2191	2847	656	5	2	e
PHE	1363	2617	1254	6	5	e
ARG	2133	3674	1541	7	4	ce
LEU	3909	5648	1739	8	3	e
TRP	227	2020	1793	9	n/a	e
TYR	798	2709	1911	10	n/a	ne
CYS	472	2388	1916	11	n/a	ne
HIS	735	3765	3030	12	n/a	ce
SER	2118	5235	3117	13	n/a	ne
THR	2174	6429	4255	14	7	e
LYS	4132	8633	4501	15	6	e
PRO	1308	7715	6407	16	n/a	ne
GLY	2165	10562	8397	17	n/a	ne
VAL	1938	10699	8761	18	n/a	e
ALA	3668	15291	11623	19	n/a	ne
GLN	2390	26909	24519	20	n/a	ne

Table 3B. Fasting state ranked by essentiality (ce and e are both considered essential) and then by difference

AA	Needed	Available	Difference	Rank	Act Sup Eff	AA Ess
MET	1148	1148	0	1	1	e
ILE	2191	2847	656	2	2	e
PHE	1363	2617	1254	3	5	e
ARG	2133	3674	1541	4	4	ce
LEU	3909	5648	1739	5	3	e
TRP	227	2020	1793	6	n/a	e
HIS	735	3765	3030	7	n/a	ce
THR	2174	6429	4255	8	7	e
LYS	4132	8633	4501	9	6	e
VAL	1938	10699	8761	10	n/a	e
GLU	4996	1102	-3894	11	n/a	ne
ASP	2162	138	-2024	12	n/a	ne
ASN	1592	1883	291	13	n/a	ne
TYR	798	2709	1911	14	n/a	ne
CYS	472	2388	1916	15	n/a	ne
SER	2118	5235	3117	16	n/a	ne
PRO	1308	7715	6407	17	n/a	ne

AA	Needed	Available	Difference	Rank	Act Sup Eff	AA Ess
GLY	2165	10562	8397	18	n/a	ne
ALA	3668	15291	11623	19	n/a	ne
GLN	2390	26909	24519	20	n/a	ne

Table 3C. Post-prandial state ranked by difference

AA	Needed	Available	Difference	Rank	Act Sup Eff	AA Ess
GLU	4996	918	-4078	1	n/a	ne
ASP	2162	115	-2047	2	n/a	ne
MET	1148	957	-191	3	1	e
ASN	1592	1569	-23	4	n/a	ne
ILE	2191	2373	182	5	4	e
LEU	3909	4707	798	6	5	e
PHE	1363	2181	818	7	2	e
ARG	2133	3061	928	8	3	ce
TRP	227	1684	1457	9	n/a	e
TYR	798	2258	1460	10	n/a	ne
CYS	472	1990	1518	11	n/a	ne
SER	2118	4362	2244	12	n/a	ne
HIS	735	3138	2403	13	n/a	ce
LYS	4132	7194	3062	14	6	e
THR	2174	5357	3183	15	7	e
PRO	1308	6429	5121	16	n/a	ne
GLY	2165	8801	6636	17	n/a	ne
VAL	1938	8916	6978	18	n/a	e
ALA	3668	12743	9075	19	n/a	ne
GLN	2390	22425	20035	20	n/a	ne

Table 3D. Post-prandial state ranked by essentiality (ce and e considered essential) and then by difference

AA	Needed	Available	Difference	Rank	Act Sup Eff	AA Ess
MET	1148	957	-191	1	1	e
ILE	2191	2373	182	2	4	e
LEU	3909	4707	798	3	5	e
PHE	1363	2181	818	4	2	e
ARG	2133	3061	928	5	3	ce
TRP	227	1684	1457	6	n/a	e

AA	Needed	Available	Difference	Rank	Act Sup Eff	AA Ess
HIS	735	3138	2403	7	n/a	ce
LYS	4132	7194	3062	8	6	e
THR	2174	5357	3183	9	7	e
VAL	1938	8916	6978	10	n/a	e
GLU	4996	918	-4078	11	n/a	ne
ASP	2162	115	-2047	12	n/a	ne
ASN	1592	1569	-23	13	n/a	ne
TYR	798	2258	1460	14	n/a	ne
CYS	472	1990	1518	15	n/a	ne
SER	2118	4362	2244	16	n/a	ne
PRO	1308	6429	5121	17	n/a	ne
GLY	2165	8801	6636	18	n/a	ne
ALA	3668	12743	9075	19	n/a	ne
GLN	2390	22425	20035	20	n/a	ne

Results

Single Amino Acid Supplementation

The purpose of this study is to determine if constraint based modeling is an effective tool for investigating nutrition supplementation. To achieve this, I ask a specific question: can increasing single or multiple amino acid uptake flux lead to increased muscle synthesis of the contractile protein complexes (see methods) assuming the muscle tissue is primed for protein synthesis (post-exercise stimulus) without including genetic and regulatory controls (an acute response). The first step was to investigate single acid supplementation, and after optimizing the model for contractile protein synthesis under fasting and post-prandial conditions, I relaxed each amino acid constraint one at a time. For single amino acid supplementation in both fasting and post-prandial states, methionine was the only

amino acid effective at increasing the protein flux above the control condition (**Table 4**).

Multiple Amino Acid Supplementation

Quite often supplementation regimes occur in combinations with many supplements/amino acids. The next step was to determine if the model predicted that specific combinations of supplements result in increased protein synthesis. I then relaxed the constraints for every combination of 2-7 amino acids to determine what combinations would increase contractile protein synthesis above the control fasting and post-prandial states. Once I supplemented with methionine the combination in the fasting and post-prandial states vary slightly. For instance, the combination of three amino acids in the fasting state differs than the optimal combination in the post-prandial state (**Table 4**). In fasting, methionine, isoleucine, and leucine were most optimal at increasing protein synthesis, yet in the post-prandial state, the optimal combination of amino acids is methionine, arginine, and phenylalanine, due to differing amino acid concentrations in the two different nutrient states.

However, when investigating the optimal condition for five supplements, the results in both the fasting and post-prandial states were the same: methionine, arginine, isoleucine, leucine, and phenylalanine (**Table 4**). In six and seven combinations, the addition of lysine and threonine increased protein synthesis, respectively (**Table 4**).

Table 4. Type 2a contractile protein flux synthesis in fasting and post-prandial states for every combination of 1 -7 amino acids. Post-abs: post-prandial

Combination	Supplement: Fasting	Fasting: (10^{-05} mmol/L/time*)	Supplement: Post-abs	Post-prandial (10^{-05} mmol/L/time*)
n/a	Control	2.18	Control	2.61
1	Methionine	2.83	Methionine	4.99
2	Methionine, Isoleucine	3.15	Methionine, Phenylalanine	5.39
3	Methionine, Isoleucine, Leucine	3.75	Methionine, Phenylalanine, Arginine	5.84
4	Methionine, Isoleucine, Leucine, Arginine	4.18	Methionine, Phenylalanine, Arginine, Isoleucine	6.93
5	Methionine, Isoleucine, Leucine, Arginine, Phenylalanine	4.55	Methionine, Phenylalanine, Arginine, Isoleucine, Leucine	7.12
6	Methionine, Isoleucine, Leucine, Arginine, Phenylalanine, Lysine	6.44	Methionine, Phenylalanine, Arginine, Isoleucine, Leucine, Lysine	8.37
7	Methionine, Isoleucine, Leucine, Arginine, Phenylalanine, Lysine, Threonine	10.6	Methionine, Phenylalanine, Arginine, Isoleucine, Leucine, Lysine, Threonine	13.0

**time is not defined.*

Discussion

I focused on Type 2A muscle tissue because it responds to exercise by increasing the contractile proteins, while other tissue types respond to exercise through other means (like increasing mitochondrial content). The significance of these results is

apparent when comparing the amount of amino acids needed to build one contractile protein complex to what is available (**Table 3**). One would expect that methionine and isoleucine, respectively, should be the top two amino acids needed to increase protein flux because these essential amino acids have the largest differences between what is available and what is needed (**Table 3B**). As expected, this is also what the model shows. However, it is interesting the model then predicts that leucine and valine are the next important essential amino acids necessary at increasing the protein flux even though, based on availability differences, one would expect phenylalanine and tryptophan would be the next effective supplements (**Table 3B**). Arginine, a conditionally essential amino acid is also greater than expected in supplementation affect based on essentiality and availability differences (**Table 3B**). Results are similar when investigating the data in post-prandial state. According to the rank between what is available and what is needed, methionine, isoleucine, and leucine should be the most effective, but in fact the model shows that phenylalanine and arginine are more effective.

The advantage of using this metabolic modeling is being able to track the fluxes for each of the metabolites. Thus, one can predict why the results differ than what is expected if availability is the only factor. Not only is there an increase in contractile protein synthesis when relaxing the constraint on methionine, the model predicts that there is a change in how energy is produced in support for protein synthesis (**Figure 2B**). As seen in **Figure 2B**, there is a decrease in glycolysis

from glucose and a decrease in fatty acid oxidation from palmitate. Some of the energy for the synthesis process comes from increased lysine oxidation among changes in other amino acid catabolism, such as asparagine, serine, and glycine. Glutamine is predicted to be made in excess and transported out of the muscle tissue. This process increases the TCA cycle and the NADH shuttle to the mitochondria (facilitated by the malate and alpha-ketoglutarate exchange seen in **Figure 2B**).

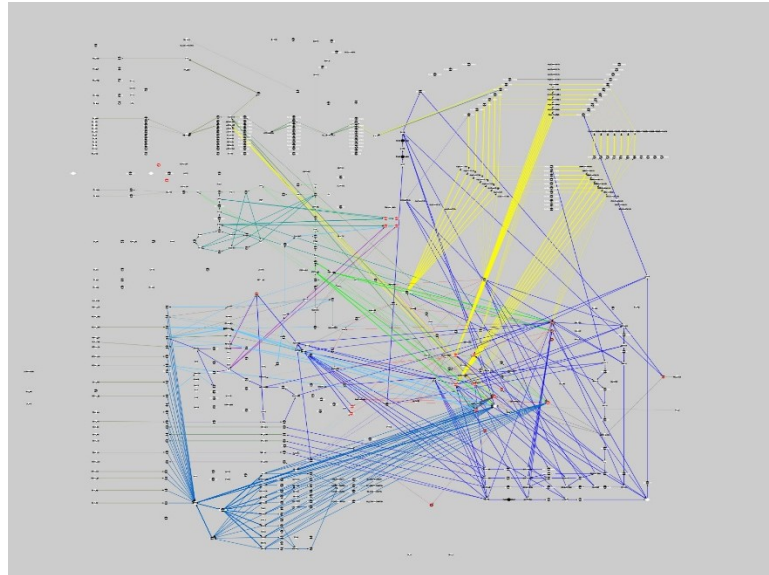
Although relaxing the constraints on the other single amino acid supplementation conditions did not increase contractile protein synthesis, it did alter the metabolic profile of the network compared to the control condition. Here I will describe a few of the different profiles based on different supplementation conditions. For example, the model predicts the usage of the BCAAs as a preferred energy source, even in single amino acid supplementation (**Figures 2D** and **2E**). Thus, it is predicted that all the available BCAAs (isoleucine, leucine, and valine) will be absorbed and used, whether as a building block for proteins or an energy source for ATP production. Increasing the available BCAAs increases the flux through the branched-chain amino acid transaminase enzyme (BCAT-2). Increased flux through BCAT-2 increases the byproduct of glutamate. The increased BCAT-2 flux requires an increase in the fluxes through the malate-aspartate shuttles and ultimately leads to an increase in serine production. This process reduces the need of serine, and as such, less serine is taken into the cell compared to no BCAA

supplementation. In summary, the model shows that if the availability of BCAAs is increased, then the muscle tissue doesn't require as much serine to build contractile proteins (**Figures 2D** and **2E**). This is also a similar process for supplementation of alanine, aspartate, glutamate, and proline. Under these conditions less serine is required to achieve the same result in protein synthesis flux. Also, when extra glutamine is supplied to the model, less asparagine is needed.

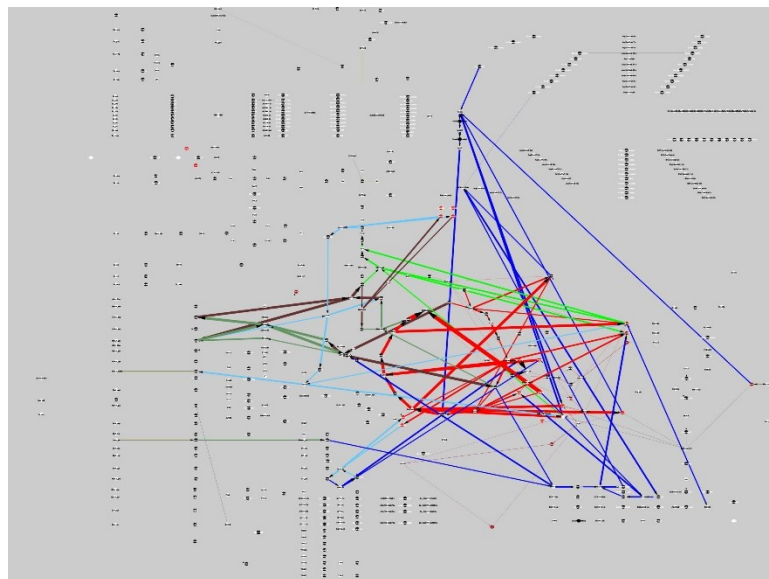
A. Pathway Assignment

Pathways	Color
Objective	
Glycolysis	Green
Fatty Acid	Yellow
Amino Acid Catabolism	Blue
Fatty Alcohol	Orange
Pentose Phosphate Pathway	Teal
TCA	Red
Electron Transport Chain	Red
Amino Acid Biosynthesis	Light Blue
Muscle	Dark Blue
Polymerization	Blue
Protein Synthesis	Blue
Translation	Blue
Glycogen Synthesis	Green
TAG	Yellow
Amino Acid Mit Transport	Purple
Mitochondrial Transport	Green
Cellular Uptake	Olive
Cellular Export	Olive
Exchange	Olive
Nutrient	Olive
Shuttle Cytosolic	Brown
Shuttle Mitochondrial	Brown
Creatine	Purple
Vitamin Metabolism	Purple
Glutathione biosynthesis	Purple
Glutathione Redox	Purple
Signaling/Hormone	Brown

B. Methionine Supplementation



C. Isoleucine Supplementation



D. Leucine Supplementation



E. 3 AA Supplementation

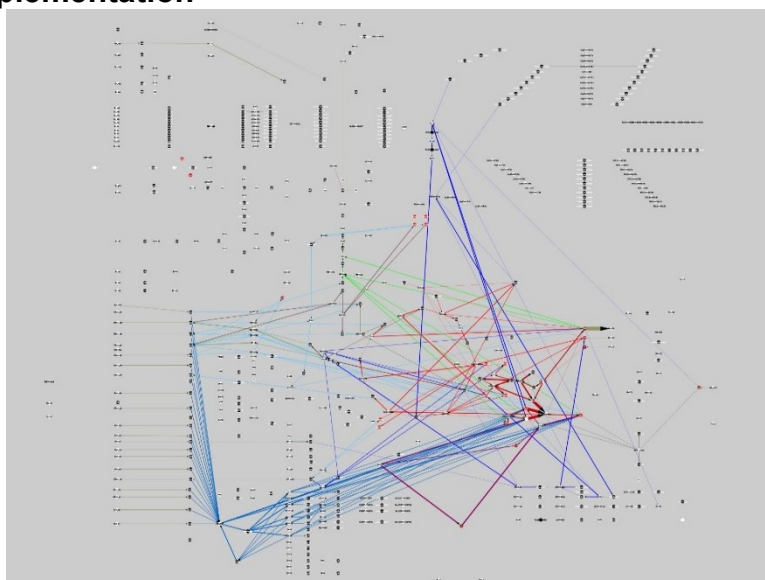


Figure 2. Flux differences compared to control show how increased amino acids could be used. This figure shows the changes in fluxes from the control

solution described in methods. (A) Manually assigned color key for pathways in the model. (B) Shows the differences in fluxes between methionine supplementing and control. (C) Shows the differences in fluxes between isoleucine supplementing and control. (D) Shows the differences in fluxes between leucine supplementing and control. (E) Shows the differences in fluxes between the three amino acid supplementation (methionine, isoleucine, and leucine (**Table 4**) and control results

Comparison to Literature – BCAA

The model's predictions are more similar to what is found in literature than what is expected based on availability differences. BCAAs have been found to greatly increase protein synthesis. Even though BCAA catabolism increases after exercise (Spirito et al., 1997), a popular current hypothesis is that they have a signaling effect and increase enzymes necessary for protein synthesis through activation of mTOR (Blomstrand et al., 2006; Spirito et al., 1997). The model used here is void of any genetic controls, yet it still shows that increasing the bioavailability of these amino acids is enough to predict an increase in protein synthesis flux (**Table 4**). The model predicts that the BCAAs are preferentially oxidized over glucose and fatty acids and used as an energy source rather than as a building block for the contractile proteins (**Figure 2B**). It is possible that in addition to a signaling effect, BCAAs are effective at increasing protein synthesis by adding a more efficient acute energy source when energy is needed quickly for protein synthesis.

Comparison to Literature – Arginine

Another pertinent revelation from the model is an amino acid combination where arginine is required to increase protein synthesis (**Table 4**, row 4 Fasting, row 3 post-prandial). In the literature, arginine supplementation had equivocal results. It was hypothesized that arginine is only effective under certain amino acid profiles (Paddon-Jones et al., 2004), but the exact profile is unknown. As summarized in **Table 4**, row 4 in the fasting condition, the model shows that arginine is effective when supplemented with methionine, isoleucine, and leucine in the fasting state and effective in the post-prandial state when combined with methionine and phenylalanine (**Table 4**). Most of the studies with arginine have been compared to either all the essential amino acids or none. The model predicts two different scenarios where arginine is effective at increasing protein synthesis and could explain the mixed results seen in the literature. This could indicate that during fasting conditions, in between meals, or other times throughout the day different supplementation strategies could be important compared to supplementation with meals.

Comparison to Literature – Glutamine

Lastly, contrary to nutrition/supplement companies but consistent with the literature (Gleeson, 2008), glutamine supplementation is not predicted by the model to have an effect on protein synthesis. It is the most abundant amino acid found in fasting blood at concentrations above what is needed for protein synthesis

of the contractile complexes (**Table 3**). Glutamine is a byproduct of many reactions and easily synthesized in the body. The model also shows glutamine is not found in the top seven amino acids which show an increase in protein synthesis (**Table 4**). In fact, the model predicts an abundance of glutamine is made and eliminated from muscle tissue in some conditions (data not shown).

Metabolic Modeling of Muscle Metabolism Identifies Key Reactions Linked to Insulin Resistance Phenotypes²

Introduction

Type 2 diabetes (T2D) has reached epidemic proportions worldwide, in parallel with the dramatic increase in obesity (Centers for Disease Control and Prevention, 2011). Insulin resistance plays a particularly important role in T2D pathophysiology, as it is present years before the onset of hyperglycemia and can predict the subsequent development of diabetes decades later (Martin et al., 1992; Tabak et al., 2009). Although insulin resistance occurs in multiple tissues, skeletal muscle is a key tissue, being responsible for over 80% of insulin-stimulated glucose uptake (DeFronzo et al., 1985).

While the molecular basis of insulin resistance remains unknown, insulin resistance in skeletal muscle is intimately linked to alterations in metabolism. These include (1) reductions in glucose uptake, non-oxidative glucose metabolism, and glycogen synthesis (Eriksson et al., 1989; Vaag et al., 1992); (2) reduced lipid oxidation (Kelley and Simoneau, 1994; Boyle et al., 2012) and accumulation of

² This chapter is based on material from a forthcoming publication, "Muscle Metabolic Modeling of Insulin Resistance" by Christopher D. Nogiec, Alison Burkart, Carles Lerin, Simon Kasif, and Mary-Elizabeth Patti. Alison Burkart performed the *in vitro* studies and corresponding data analysis. All authors have agreed to have the material included in this dissertation.

multiple lipid species (Jacob et al., 1999; Malenfant et al., 2001); (3) reduced TCA cycle activity (Befroy et al., 2007; Simoneau and Kelley, 1997); and (4) increased reactive oxygen species (ROS) (Anderson et al., 2009). Moreover, *in vivo* NMR spectroscopy in insulin resistant humans has demonstrated abnormal energetics, including reductions in ATP and creatine phosphate (Cr-P) synthesis at rest (Petersen et al., 2004) and in response to insulin (Petersen et al., 2005) and exercise training (Kacarovsky-Bielesz et al., 2009). Transcriptome analysis has similarly demonstrated dysregulation of mitochondrial regulatory genes in insulin resistance and established T2D (Patti et al., 2003; Mootha et al., 2003; Boyle et al., 2011). While these data highlight the close relationship between disordered metabolism and insulin resistance, it remains unknown which alterations in metabolic reactions might cause the changes in metabolic phenotypes associated with or contributing to insulin resistance.

Given the complexity and redundancy of metabolism, it is difficult to address this question experimentally. To approach this challenge, I used a constraint-based modeling framework and FBA muscle model. Specifically, I incorporate reciprocal modulation of lipid oxidation and glucose uptake in order to model the fasted-to-fed transition, under conditions of both normal and increased substrate availability. Using this model, I then systematically perturb the metabolic network by performing *in silico* knockdowns of each of the 388 reactions within the model and identify those perturbations which produce metabolic phenotypes associated with

IR: (1) reduced ATP+Cr-P synthesis, (2) reduced cumulative TCA cycle flux, and (3) reduced metabolic flexibility. The analysis suggests that single-enzyme knockdowns do not reproduce these phenotypes. However, knockdowns in the pyruvate dehydrogenase flux in combination with either reduced fatty acid uptake or fatty acid/amino acid oxidative metabolism (electron-transferring-flavoprotein dehydrogenase) reduces ATP+Cr-P synthesis, reduces cumulative TCA cycle flux, and induces metabolic inflexibility. These combined knockdowns also reduce glycogen storage and lipid oxidation and increase incomplete lipid oxidation, other phenotypes associated with IR. Thus, this computational model serves as a novel tool to identify candidate enzymes linked to the pathogenesis of dysregulated metabolism in IR.

Methods

Choosing the Objective Function

I made the assumption that the main objectives of resting muscle tissue (either during the fasting state or fed state) is to maximize a complex objective function combining storage of energy in the forms of high-energy phosphates (ATP+ Cr-P), glycogen, and TAG for energy needs during subsequent contraction. Given the importance of ATP+Cr-P as an acute energy source in muscle, I weighted the sum of ATP+Cr-P production to be twice that of the other energy storage molecules.

For ATP production, I maximize a reaction within the model describing ATP storage (**Eq. 1**), encompassing both aerobic and non-aerobic ATP production.

Eq.1:

$$ATP\ storage = \sum(aerobic\ ATP\ production) + \sum(nonaerobic\ ATP\ Production)$$

For Cr-P, glycogen, and TAG, I maximize flux through reactions describing storage for each substrate. Since muscle tissue can only store a finite amount of ATP+Cr-P, I set an upper limit of 33.3 and 116.7 mmol/time for ATP+Cr-P production, respectively, based on prior data demonstrating an approximate 3.5-fold ratio of Cr-P to ATP content (Sleigh et al., 2011; Gray et al., 2008). This allows extra substrate to be stored optimally in glycogen, triacylglycerols, or muscle protein.

Modeling the Dynamics of Normal Metabolism

Flux balance analysis (FBA) typically models metabolism in a steady state, but to properly model the conditions associated with a disease state, it was necessary to simulate the metabolic transitions between fasting and fed conditions. To this aim, I reciprocally modulate lipid oxidation and glucose uptake. Given that lipid substrate utilization is maximal in the fasting state and reduced in the fed state, I first modulated lipid oxidation by limiting CPT1—the enzyme controlling fatty acid transfer into mitochondria for subsequent oxidation—from a maximum activity of 100% (fasted) to a minimum of 0% (fed) through a progressive stepwise reduction

in activity (**Figure 3**). I simultaneously modeled glucose uptake in two distinct components: basal and modifiable. First, I estimated basal glucose uptake (GU_{bas}) to be 5% of the glucose concentration in plasma, constant across the fasted to fed transition (Kraegen et al., 1993; Kelley et al., 1993; Kelley et al., 1992; Mandarino et al., 1993). In addition to the constant GU_{bas} , I modeled a modifiable glucose uptake (GU_{mod}), specified by adjusting the maximal glucose uptake from 0% to 100% of the concentration found in plasma (**Figure 3**). I defined three steady states across this continuum: **fasted** (90% CPT1, 10% GU_{mod}), **mixed** (50% CPT1, 50% GU_{mod}), and **fed** (10% CPT1, 90% GU_{mod}) (**Figure 3**). These steady states were used to examine the impact of the metabolic condition on *in silico* KDs (see **In Silico Knockdowns** below). In all conditions, I allow free uptake of fatty acids and amino acids up to the values found in plasma in healthy fasting individuals (Jin et al., 2011; Cynober, 2002).

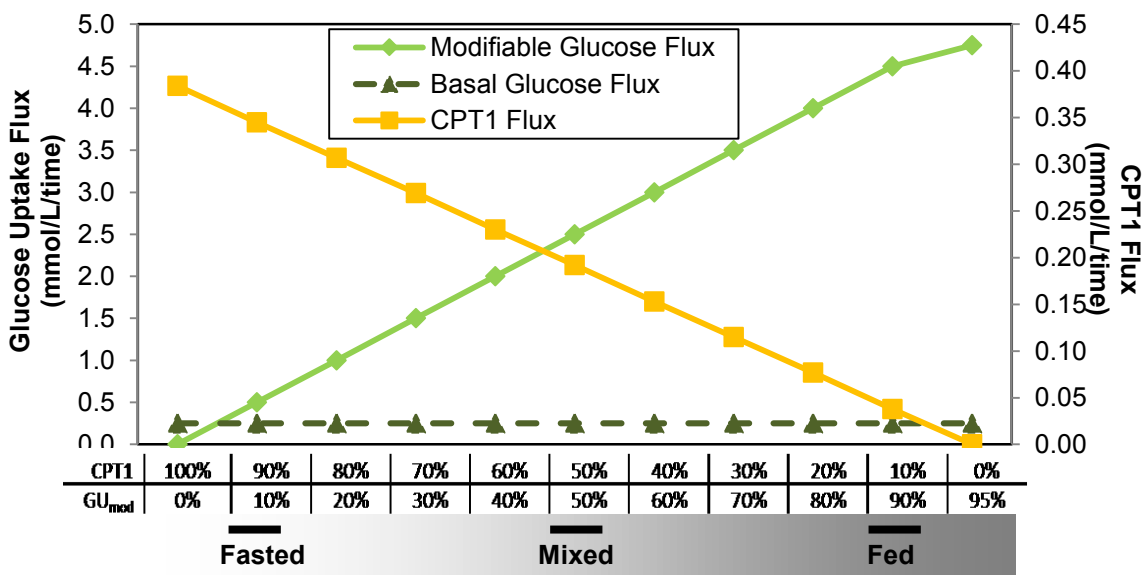


Figure 3. Simulating fasting to fed transition by reducing CPT1 activity and increasing a modifiable glucose uptake component. To simulate the fasting-to-fed transition, and associated shifts from fatty acid to glucose metabolism, I experimentally modulated flux through carnitine palmitoyl-transferase 1 (CPT1) and a modifiable component of glucose uptake (GU_{mod}). Flux is sampled at discrete percentages of maximal flux through CPT1 and GU_{mod} . I define fasted (90% CPT1: 10% GU_{mod}), mixed (50% CPT1: 50% GU_{mod}), and fed states (10% CPT1: 90% GU_{mod}).

Nutrient Conditions

Since prevailing nutrient conditions are a key determinant of cellular metabolism, I assigned basal (1x) concentrations of extracellular glucose, fatty acids, and amino acids as extrapolated from measurements obtained from healthy subjects (Jin et al., 2011; Cynober, 2002) (**Table 5**). To examine the impact of increased substrate availability, as seen in patients with insulin resistance and T2D, I also created three additional nutrient conditions, yielding increased fatty acids and glucose independently (2xFA-1xGluc or 1xFA-2xGluc) and in combination (2XFA-2XGluc).

Table 5. Basal concentrations used as maximal uptake fluxes in the Flux Balance Model.

Metabolite	Concentration (mmol/L) ¹
Glucose [‡]	5.00
Palmitate [‡]	0.3875
Arginine	0.080 ± 20
Histidine	0.082 ± 10
Isoleucine	0.062 ± 14
Leucine	0.123 ± 25
Lysine	0.188 ± 32
Methionine	0.025 ± 04

Phenylalanine	0.057 \pm 09
Threonine	0.140 \pm 33
Tryptophan	0.044 \pm 07
Valine	0.233 \pm 43
Alanine	0.333 \pm 74
Asparagine	0.041 \pm 10
Aspartate	0.003 \pm 01
Cysteine	0.052 \pm 11
Glutamate	0.024 \pm 15
Glutamine	0.586 \pm 84
Glycine	0.230 \pm 52
Proline	0.168 \pm 60
Serine	0.114 \pm 19
Tyrosine	0.590 \pm 12

1. Cynober et al. (2002), Jin et al. (2011) and MacLaren (2000),
 ¥Glucose and Fatty Acid are based on internal data collected in the Patti Lab

***In Silico* Knockdowns**

I simulated knockdowns (KDs) of each reaction **R** by constraining the flux for **R** to 50% its normal, optimal value. This was done for each of the three defined states (fasted, mixed, and fed) resulting in possibly three different KD flux values—one for each of the states, respectively. After constraining the reaction to this new, reduced value, I re-optimized the model to obtain another set of fluxes (**Figure 4**) and compared metabolic phenotypes to the basal (no knockdown) condition.

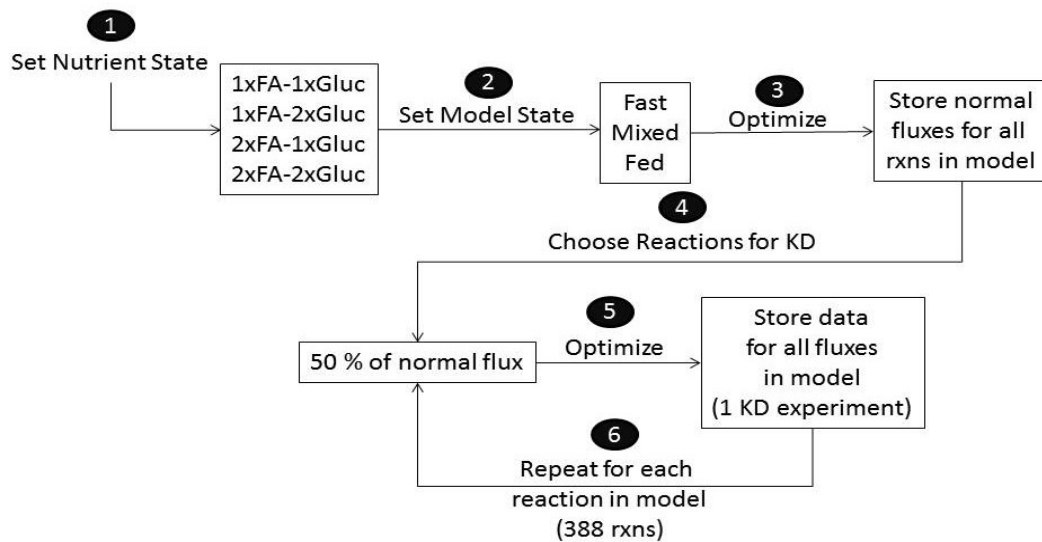


Figure 4. Work flow for the *in silico* knockdown experiments.

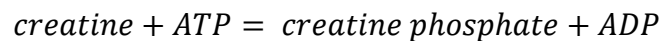
In the first step, I select the nutrient state. Next, I then select the model state: fasted (90% CPT1:10% GU_{mod}), mixed (50% CPT1:50% GU_{mod}), or fed (10% CPT1:90% GU_{mod}). In the third step, the model produces a normal set of optimized fluxes for each reaction. In the fourth step, I define the KD flux for a single reaction (50% of normal flux) and set that as an additional constraint to the model. Fifth, I again optimize to obtain a new set of fluxes reflecting the KD. Then, I repeat steps 4 and 5 for each of the 388 reactions in the model (Nogiec Muscle Model v1.1).

Modeling Insulin Resistance Phenotypes

The goal is to identify metabolic reaction(s) or network(s) whose dysregulation may perturb muscle metabolism sufficiently to yield metabolic phenotypes observed in IR. Given that this model does not incorporate insulin signaling networks, three key metabolic phenotypes characteristic of human insulin resistance are used as a proxy for insulin resistance: (1) reduced ATP+Cr-P production (Petersen et al., 2004; Petersen et al., 2005), (2) reduced flux through TCA cycle (Befroy et al., 2007; Simoneau and Kelley, 1997), and (3) reduced metabolic flexibility (Kelley

and Mandarino, 2000). In order to determine the effect of *in silico* KDs on these phenotypes, I define them mathematically for the model. For ATP production, I monitor a reaction within the model describing ATP storage (**Eq. 1**), encompassing both aerobic and non-aerobic ATP production. For Cr-P, I examine the creatine kinase reaction (**Eq. 2**). To quantify TCA cycle activity, I sum the fluxes through all reactions within the TCA cycle (**Eq. 3**).

Eq. 2:



Eq. 3:

$$\begin{aligned} \sum(\textit{TCA Flux}) = & \textit{citrate synthase} + \textit{aconitase} + \textit{isocitrate dehydrogenase 2} \\ & + \alpha \textit{ ketoglutarate dehydrogenase} \\ & + \textit{succinyl CoenzymeA synthetase} \\ & + \textit{succinate dehydrogenase (Complex II)} + \textit{fumarase} \\ & + \textit{malate dehydrogenase 2} \end{aligned}$$

Metabolic flexibility, defined as the ability to modulate between fatty acid and glucose oxidation in response to feeding or insulin stimulation (Kelley and Mandarino, 2000), is quantified in clinical research by examining changes in the

respiratory quotient (RQ), which reflects the ratio of carbon dioxide produced relative to the oxygen consumed (**Eq. 4**).

Eq. 4:

$$RQ = \frac{CO2\ production}{O2\ consumption}$$

To determine whether experimental disruption in flux for a metabolic reaction causes changes in these characteristic metabolic phenotypes, I compared phenotypic scores from each KD to the corresponding phenotypic score from the normal (control) score. Since ATP and Cr-P production are closely linked in muscle, I summed these high-energy phosphate molecules to simplify the analysis (ATP+Cr-P). Thus, I assessed the ratio of KD to control for the ATP+Cr-P-production and cumulative-TCA-flux phenotypes (**Eq. 5** and **6**):

Eq. 5:

$$ATP+Cr-P\ ratio = \frac{\Sigma (KD\ ATP+Cr-P\ production)}{\Sigma (Control\ ATP+Cr-p\ production)}$$

Eq. 6:

$$TCA\ ratio = \frac{\Sigma\ KD\ TCA\ flux}{\Sigma\ Control\ TCA\ Flux}$$

In normal metabolism, RQ (**Eq. 4**) increases as the individual shifts from fatty acid oxidation in the fasting state to glucose oxidation in the fed state (Kelley and Mandarino, 2000). In contrast to healthy, insulin sensitive individuals, insulin resistant and obese individuals have (1) higher fasting RQs **AND** (2) lower fed RQs. Since both of the above phenotypes need to be true to indicate metabolic inflexibility, I thus define it as a logical, binary equation (**Eq. 7**):

Eq. 7:

$$\text{metabolic inflexibility} = (KD RQ_{fast} > \text{Control } RQ_{fast}) \text{ AND } (KD RQ_{fed} < \text{Control } RQ_{fed})$$

If **Eq. 7** is true, I then assess the magnitude of difference between fasted and fed RQ values: a greater difference indicates more decreased flexibility/increased inflexibility (**Eq. 8**).

Eq. 8:

$$\begin{aligned} \text{Metabolic inflexibility score} &= \text{IF} (\text{metabolic inflexibility} = \text{TRUE}), \\ &\quad \text{then } (|KD RQ_{fast} - \text{Control } RQ_{fast}| + (KD RQ_{fed} - \text{Control} \\ &\quad RQ_{fed})) \\ &\quad \text{else } 0 \end{aligned}$$

Ratios less than one for either ATP+Cr-P production (**Eq. 5**) or cumulative TCA flux (**Eq. 6**) and any non-zero score for metabolic flexibility (**Eq. 8**.) are considered to reflect IR phenotypes. Significance of each score was determined by comparing the score to the distribution of the scores for each phenotype.

Pathway Analysis

I assigned each of the 388 model reactions to a KEGG pathway(s) based on its EC number, or if none were available, I assigned one manually (**Appendix A**). I also created pathways including reactions utilizing common energy substrates (e.g. creatine, nicotinamide adenine dinucleotide (NAD(H)), and flavin adenine dinucleotide (FAD(H))) and defined a cytosolic-mitochondrial NADH shuttle pathway. Finally, an “All Reactions Pathway,” containing all 388 reactions in the model, was used as the background distribution. I then used the Fisher’s exact test to determine if any of the pathways was significantly enriched in modulating the three metabolic phenotypes in any of the 3 defined states (fasted, mixed, fed) or four nutrient conditions—i.e., whether the number of perturbations in a specific pathway that alter the phenotype is greater than expected by chance. To account for multiple-hypothesis testing, I used the Benjamini-Hochberg method to calculate false discovery rate (FDR).

Modeling Assumptions

In addition to assumptions made with the FBA model (Oberhardt et al., 2009), I add three additional assumptions. First, this modeling approach assumes that necessary hormones and enzymes are in place to seamlessly modulate fuel metabolism between fatty acid and glucose metabolism. Secondly, because the flux into muscle of all lipid and amino acid species is unknown, I assume the uptake flux is proportional to plasma concentrations (Cynober, 2002; MacLaren et al.,

2000). Finally, I assume the system reaches a steady state over enough time to maintain constant flux, and that concentrations of substrates in plasma will be stably maintained over time.

RT-PCR of S961 IR Mouse Model³

Mice were treated with S961 at 10 nMol/week to induce insulin resistance (Yi et al., 2013). Total RNA was extracted from gastrocnemius muscle by using RiboZol reagent (AMRESCO, Solon, OH, USA). For quantitative mRNA analysis, 1 µg of total RNA was reverse-transcribed with High Capacity cDNA Reverse Transcription Kit (Life Technologies, Carlsbad, CA, USA). The cDNA reaction was subjected to quantitative real-time PCR analysis using iTaq Universal SYBR Green Supermix (Bio-Rad, Hercules, CA, USA) and ABI 7900HT Real-Time PCR System (Life Technologies), following the manufacturer's instructions. *Tbp* was used as an internal housekeeping gene. Relative gene expression was calculated by the $2^{-\Delta\Delta CT}$ method.

Primary Cell Preparation and Transfection⁴

All leg muscles were isolated from 4-week-old PDK2/4 KO mice (Jeoung and Harris, 2007) and wild type control mice by digesting with 2.4 U/mL dispase and

³ Ana-Luisa Coelho, PhD, performed these methods.

⁴ Alison Burkart, PhD, performed these methods.

1% collagenase. Cells were grown in F10 medium supplemented with 20% fetal bovine serum and penicillin/streptomycin. Myoblasts were selected for by differential plating upon successive passages until cultures were over 97% pure. We used specific siRNA oligonucleotides against ETFDH or a scrambled control that were transfected by HiPerFect, based on manufacturer's instructions.

Western Blot Analysis⁵

At 72 hours post KD, total protein was obtained by lysis with 1% sodium dodecyl sulfate in phosphate-buffered saline (PBS). Protein concentrations were determined with a bicinchoninic acid assay (BCA; Pierce – ThermoScientific Fisher, Rockford, IL, USA). Equal amounts of protein were run on a 10% SDS-PAGE gel and transferred to nitrocellulose. Membranes were blocked in 5% milk for one hour and then incubated with primary antibodies as indicated. Specific secondary antibodies and enhanced chemiluminescence reagents were used to visualize bands.

Respiration Studies⁵

Cellular respiration was assessed using a Seahorse XF24 Flux Analyzer. Cells were treated overnight with 250 μ M palmitate in BSA. The following day, cells were washed twice in PBS, then put in KRB buffer with 5.5 mM glucose and 250 μ M palmitate in BSA for 1 hr. Basal oxygen consumption rate (OCR) and extracellular

⁵ Alison Burkart, PhD, carried out these methods.

acidification rate (ECAR) were measured 4 times over a period of 20 mins. Then, 5.5 mM glucose was injected into each well and the OCR and ECAR were measured 4 times over 20 mins. After the assay, media was aspirated and DNA was isolated for normalization.

Citrate Synthase Activity Assay⁶

Citrate synthase (CS) activity was determined using an enzymatic method based on a commercially available assay kit (CS0720 Sigma, St. Louis, MO, USA). Cells were lysed in RIPA buffer and added to a 96 well plate. Assay buffer (100 mM Tris pH 7.5) with 300 nM Acetyl-CoA and 100 nM DTNB (5,5'-dithiobis-(2-nitrobenzoic acid) was added to all wells. Plate was read at 412 nm for 1.5 mins, with a read every 10 seconds to determine endogenous CS activity. The curve slope was used to calculate the enzymatic activity, a BCA assay was used to normalize the data per milligram of protein.

Adenosine Nucleotide Measurements⁷

Levels of adenine nucleotides were measured by a coupled enzymatic assay (Detimary et al., 1995). Cells were grown in an opaque 96-well plate with clear bottom. Cells were washed twice in PBS, then put in KRB buffer with 5.5 mM

⁶ Alison Burkart, PhD, carried out these methods.

⁷ Alison Burkart, PhD, carried out these methods.

glucose for 1 hr. Next, 100 μ l of the CellTiter-Glo luminescent assay reagent (Promega, Fitchburg, WI, USA) was added and incubated for 15 min. Luminescence was read using a multiplate reader. Untreated wells were used to determine relative protein content by BCA assay to normalize the data.

Results

Model Development and Validation

As described more fully in Methods, I have developed a model of muscle metabolism incorporating 388 distinct reactions. I use the technique of flux balance analysis (FBA), which optimizes flux through a set of reactions (in this case, the metabolic network of muscle tissue) to achieve a specific objective function. Given that muscle metabolism at rest is focused on energy storage in preparation for subsequent physical activity, I assigned the objective function as storage of ATP, creatine phosphate (Cr-P), glycogen, and triacylglycerols (TAG). I limited maximal ATP and Cr-P to 33.3 and 116.7 mmol/L/time, respectively, to achieve a dynamic range during the fasting to fed transition and to allow for storage of excess energy in the fed state. This ratio of 3.5 Cr-P to 1 ATP was chosen on the basis of prior metabolite assays in muscle (Sleigh et al., 2011; Sleigh et al., 2012; Gray et al., 2008). I did not constrain glycogen nor TAG, given their wide variation in distinct nutrient conditions and training states (Sacchetti et al., 2004). While FBA typically models steady-state metabolism, I simulated dynamic shifts across the fasting-fed

transition by modulating mitochondrial fatty acid uptake and cellular glucose uptake. Specifically, I constrained activity of CPT1 (the rate-limiting step of mitochondrial fatty acid uptake), assigning maximal activity in fasting state with progressive stepwise reductions toward the fed spectrum (**Figure 3**). For glucose uptake, I similarly assigned both a constant basal component and a modifiable component which increased progressively from fasted to fed states (**Figure 3**). In each state, the model allows free uptake of fatty acids and amino acids up to the concentrations found in fasting human plasma (Cynober, 2002; MacLaren et al., 2000), as needed to meet the energetic objective functions.

I next examined flux through key reactions at each step in the fasted-fed spectrum to confirm that this model mirrored expected metabolic profiles in normal human subjects. ATP+Cr-P production reach maximal levels in the fed state, with excess energy stored as glycogen and triacylglycerols (**Figure 5A**). Similarly, TCA cycle cumulative flux increases in the fed state (**Figure 5B**). As expected, glycolytic flux increases in the fed state, concurrent with increased glucose availability, while substrate exchange (including amino acid uptake) and amino acid oxidation remain constant. Consistent with the net increase in glucose oxidation and reduction in fatty acid oxidation in the fasted to fed transition, respiratory quotient (RQ) increased in the fed state (**Figure 5C**). Changes in flux through all the reactions are represented in the model across the fasted-to-fed transition are visualized in **Figure 6**. This analysis demonstrates the metabolic model faithfully recapitulates

the basic transitions in human metabolism in fasted and fed states allowing one to compare these states to hypothetical disease conditions.

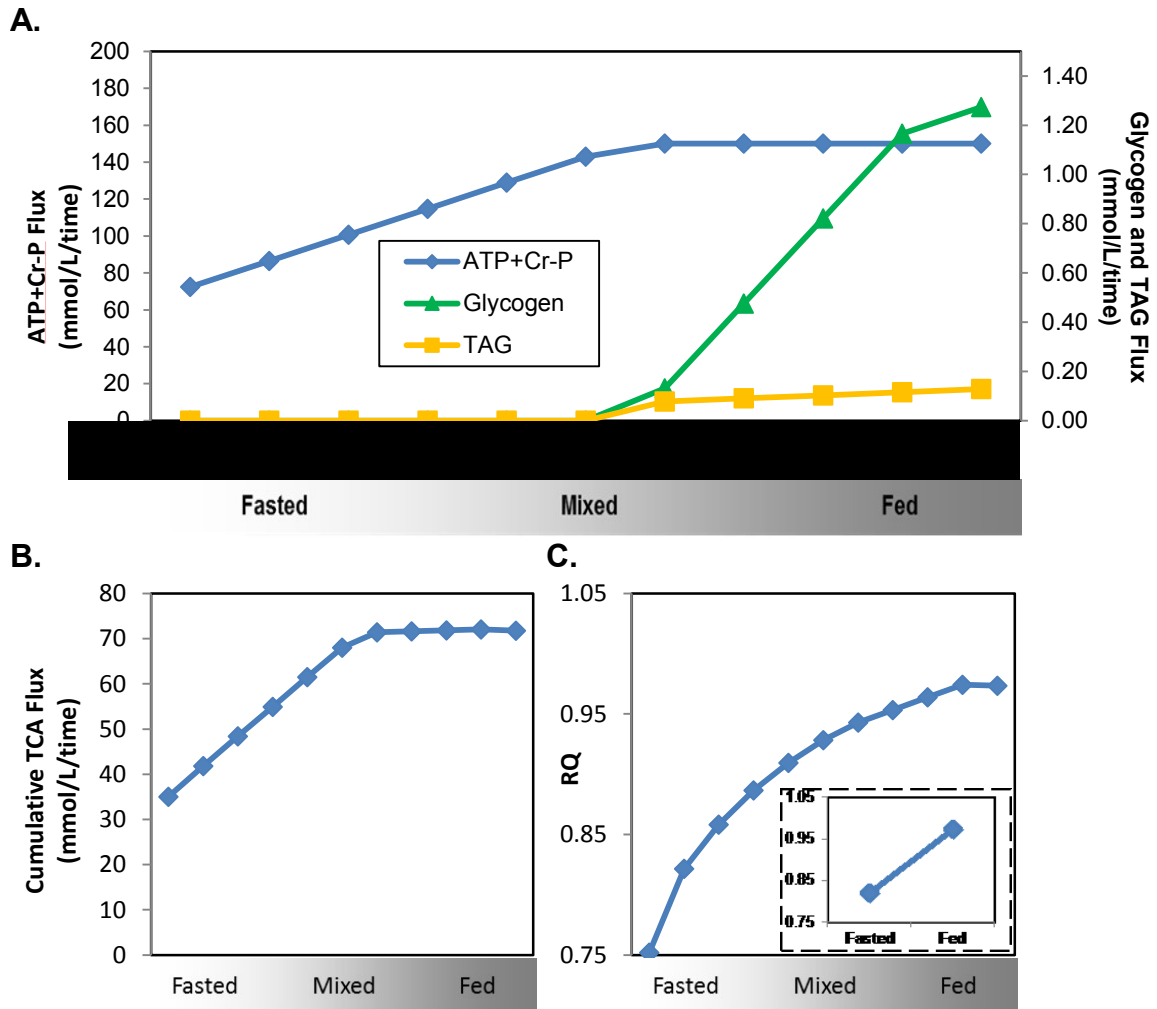


Figure 5. Modeling muscle metabolism under normal nutrient conditions. (A) Fluxes for ATP+Cr-P, glycogen storage, and TAG storage. (B) Cumulative TCA flux increases across the fasted to fed spectrum. (c) Respiratory quotient (RQ) increases across the fasted to fed spectrum, as predicted from in vivo analysis. .

Impact of Nutrient Availability

Since the obesity/diabetes metabolic environment is characterized by increases in plasma levels of nutrient substrates, which may themselves contribute to altered flux, I tested the impact of increasing extracellular glucose and fatty acid availability by 2-fold over the fasting level (2X Gluc and 2X FA, respectively), both independently and in combination. With increased glucose availability (2x Gluc), there is a leftward shift in glucose-dependent fluxes, occurring earlier in the fasted-to-fed transition (**Table 1** and **Figure 6**, *panel B vs. panel A*), including increased flux through glycolysis, glycogen storage, and TAG storage. There was no major effect of 2X Gluc on substrate uptake, fatty acid/amino acid metabolism, TCA or OXPHOS, or creatine metabolism fluxes.

Increased fatty acid availability (2X FA) (**Table 6** and **Figure 6C**) increased flux through TCA, OXPHOS, glycogen storage, and TAG storage. In each case, fluxes through these reactions occurred earlier in the fasted-to-fed transition, potentially consistent with increased energy availability in this state. Increased availability of FA without an increase in energy demand (as dictated by model constraints on maximal ATP+Cr-P production) also promotes increased storage of FA as triacylglycerol (**Figure 7E**). Glycerol for triacylglycerol synthesis is predicted to derive from conversion of glycolytic intermediates into glycerol-3-phosphate (glyc3P), as indicated by increased flux through glycerol-3-phosphate dehydrogenase (**Figure 7H**).

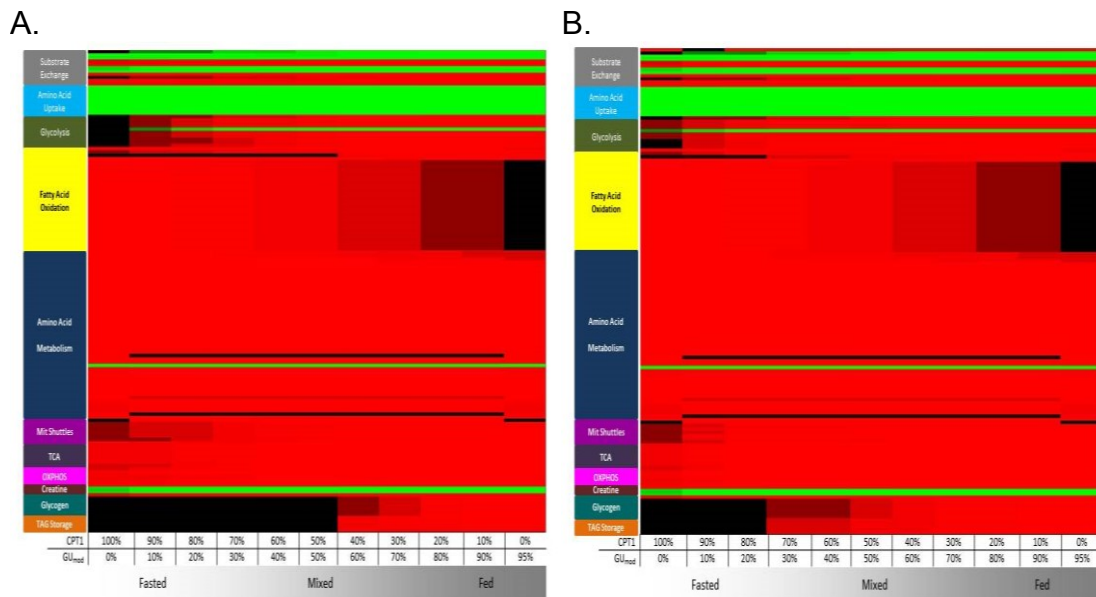
Table 6. Major qualitative changes induced by increased glucose and fatty acid substrate availability (1xFA = 0.3838 mmol/L; 1xGluc = 5.0 mmol/L).

Condition	Major Qualitative Changes Compared to 1xFA1xGluc
2xGluc	Increased: <ul style="list-style-type: none"> • Glycolytic fluxes • Glycogen storage • TAG storage
2xFA	Increased: <ul style="list-style-type: none"> • TCA • OXPHOS • Glycogen storage • TAG storage
2xFA-2xGluc	Increased: <ul style="list-style-type: none"> • Glycolytic fluxes • TCA • OXPHOS • Glycogen storage • TAG storage

Finally, increased availability of both glucose and fatty acids (2X Gluc, 2X FA, **Table 6** and **Figure 6D**) largely produces effects reflecting a combination of effects from each nutrient independently.

To further examine the impact of nutrient state on key parameters dysregulated in insulin resistance, I examined net ATP+Cr-P production, cumulative TCA cycle flux, and the RQ. The increases in ATP+Cr-P production (**Figure 5A**) and TCA

flux (**Figure 5B**) during the transition from fasted to fed states are similar in each of the four different nutrient conditions (**Figure 7A/B**), paralleling oxygen consumption and OXPHOS flux (**Figure 7F/G**). By contrast, nutrient availability has marked effects on RQ. With increased glucose availability, there is a leftward shift in the respiratory quotient curve (**Figure 7C**), indicating increased glucose oxidation even in the fasting spectrum. With increased FA availability, the RQ decreases, reflecting increased lipid oxidation.



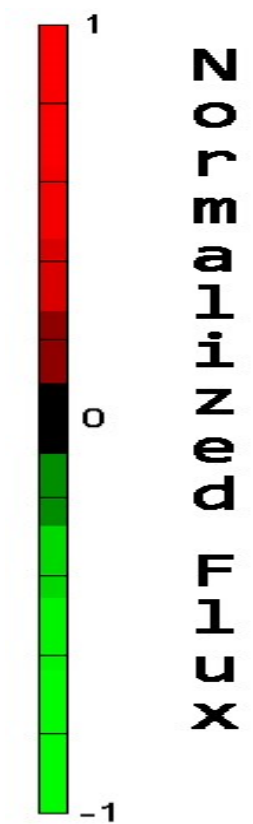
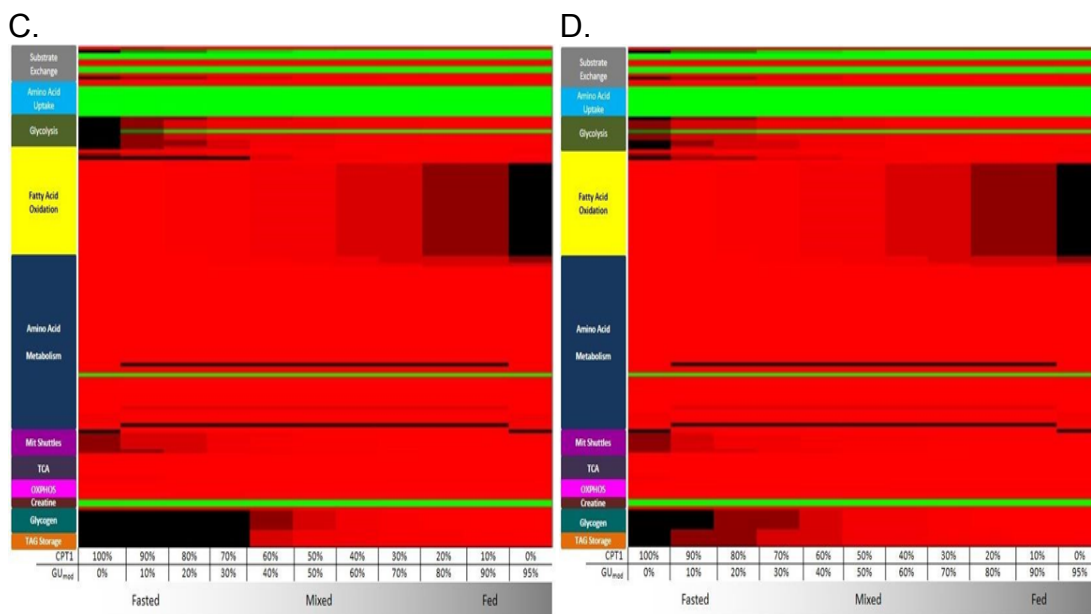
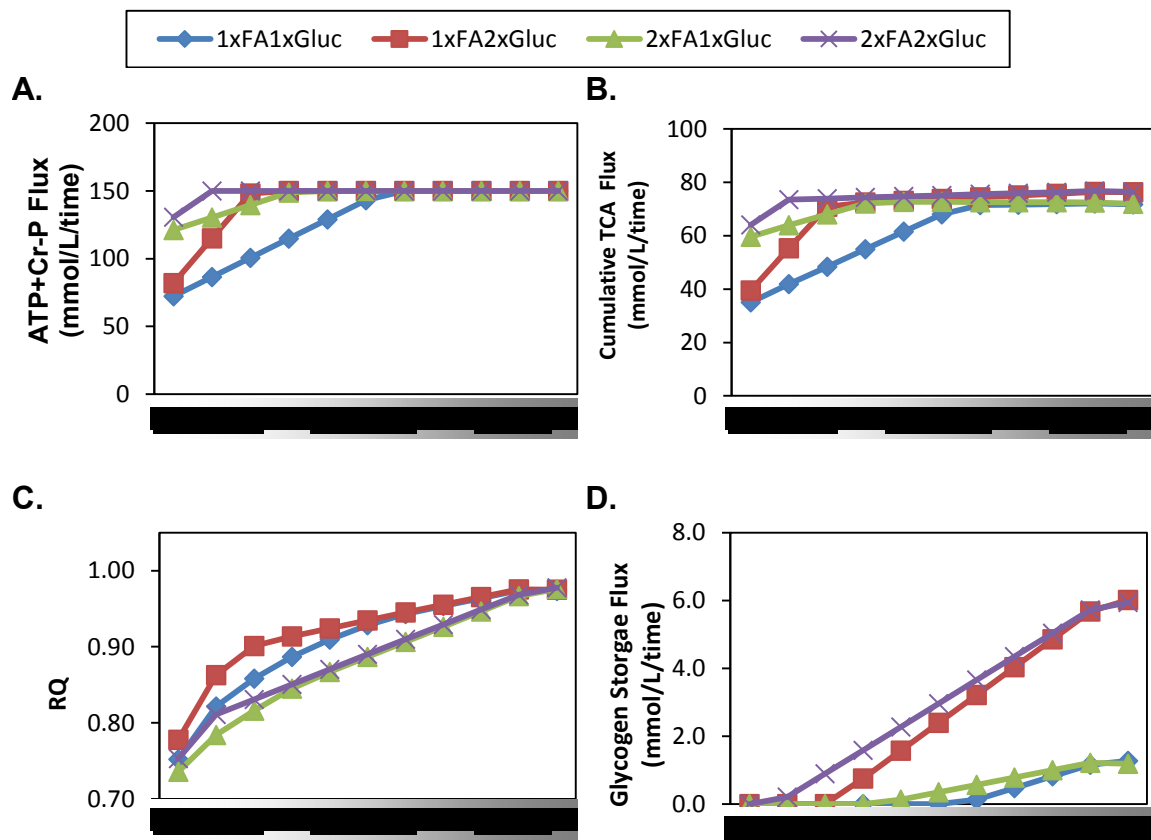


Figure 6. Fluxes through all reactions in the model from fasting to fed transition for four different nutrient states.

Each row represents a reaction in the model, which are grouped and color-coded by pathway based on KEGG classification or manual curation. Each column represents discrete sampling from the defined fasting to fed states, with colors indicating the flux through the reaction at each discretely sampled point. All zero fluxes across the entire spectrum were removed, and the remaining fluxes are normalized to the maximum flux specific to each row. Red indicates that flux is proceeding in a positive direction (as indicated for each reaction in Supplemental File MuscleModelv1.1.pdf); green indicates flux in the opposite direction. Nutrients taken into the system have a negative flux (green), while nutrients and metabolites produced and/or released have a positive flux (red). (A) Normalized fluxes through each reaction based on substrate availability in the fasting state (1xFA-1xGluc). (B) Normalized fluxes with 2-fold increase in glucose availability (1xFA-2xGluc). (C) Normalized fluxes with 2-fold increase in fatty acid availability (2xFA-1xGluc). (D) Normalized fluxes with 2-fold increases in both glucose and fatty acid availability (2xFA-2xGluc).



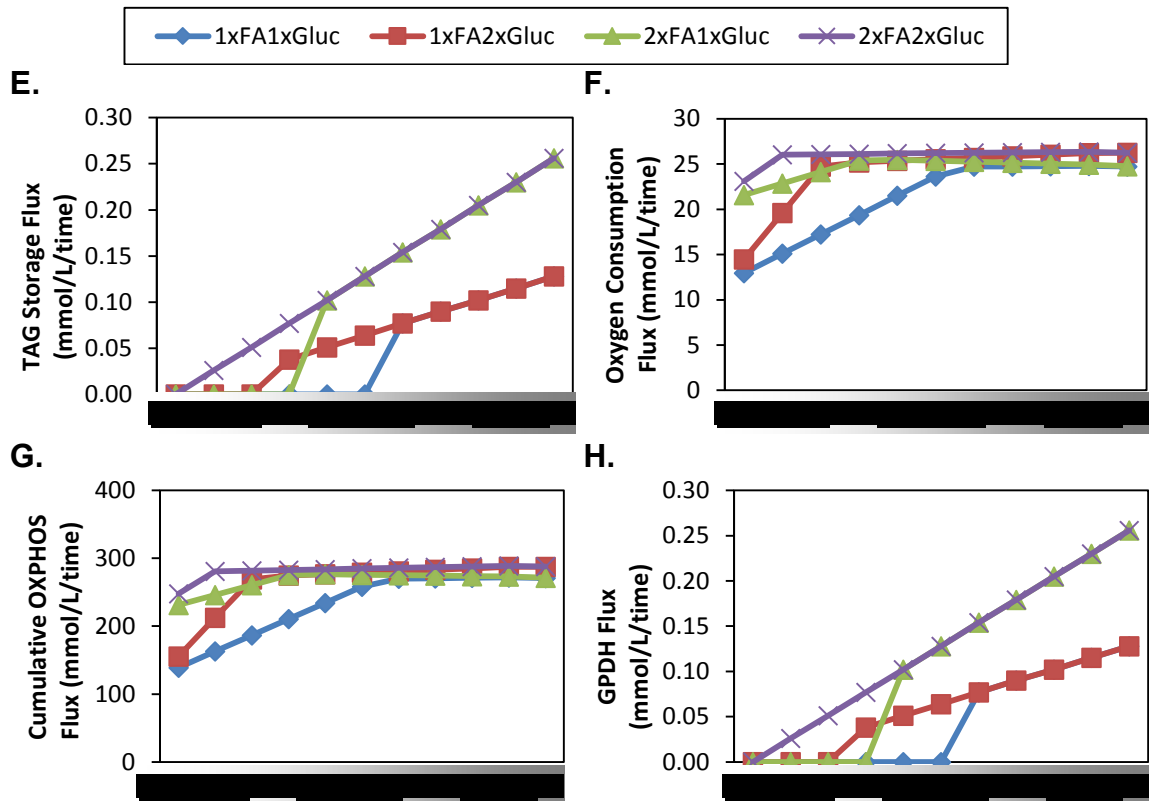


Figure 7. Predicted fluxes through pathways and substrate uptake/production. Chart shows the flux in mmol/L/time on the Y-axis. The x-axis shows the flux at the discrete points from our defined fasting to fed states, as defined by conversely constraining the flux through CPT1 and modifiable glucose uptake from 0-100% of the maximum flux. The different nutrient states, defined in the text, are indicated by different colored lines and symbols: 1xFA/1xGluc (blue/diamonds), 1xFA/2xGluc (red/boxes), 2xFA/1xGluc (green/triangle), and 2xFA/2xGluc (purple/x). (A) Predicted ATP+Cr-P production, constrained to a maximum of 150 mmol/time (ATP limit 33.3 mmol/time; Cr-P limit 116.7 mmol/time). (B) Predicted cumulative flux through the TCA cycle, including citrate synthase, aconitase, isocitrate dehydrogenase-2, α -ketoglutarate dehydrogenase, succinyl coenzyme-A synthetase, succinate dehydrogenase, fumarase, and malate dehydrogenase-2 reactions. (C) Predicted respiratory quotient (RQ). (D) Predicted glycogen storage. (E) Predicted TAG storage. (F) Predicted oxygen consumption. (G) Cumulative flux through electron transport chain (complexes I-V). (H) Glucose oxidation, as measured by flux through glycerol-3-phosphate dehydrogenase (GPDH) reaction.

Simulating Metabolic Phenotypes of Insulin Resistance

Given that the model recapitulated key aspects of muscle metabolism in different nutrient conditions across a simulated fasting to fed spectrum, I next utilized the model to determine if I could reproduce metabolic phenotypes associated with insulin resistance by systematically perturbing the flux in each of the 388 reactions in the model. I performed *in silico* knockdowns (KD), defined as a 50% reduction in the normal (control) flux for each nutrient condition and state in the model (fasted, mixed, and fed) (**Figure 3**) and examined the impact of each KD on the three predefined insulin resistance phenotypes. For ATP+Cr-P production or TCA cycle flux, a ratio (KD/control) less than one was considered to reflect insulin resistance. I examined each knockdown's impact on metabolic flexibility by determining whether the KD yielded an RQ pattern similar to insulin resistance (increased RQ_{fasted} and decreased RQ_{fed}). Values indicating reduced RQ change in the fasting-fed transition (score >0) were considered to reflect insulin resistance, and significance determined by comparing data to the distribution of RQ changes (see Methods for more details).

In the basal nutrient condition (1xFA-1xGluc), KDs in 34 reactions in the fasted state, 30 in the mixed state, and 26 in the fed state significantly reduced ATP+Cr-P production ($p \leq 0.05$, **Table 7A**). Top-ranking reactions included all OXPHOS complexes, NADH shuttling between cytosol and mitochondria, and TCA cycle. In

4.2.1.17	EnoCoADeh-12c	0.82	0.05
1.1.1.35	3HA-CoADeh-12c	0.82	0.05
2.3.1.16	AcylCoAAT-12c	0.82	0.05

Table 7B. KDs in 1xFA-1xGluc causing significant reductions in cumulative TCA flux.

<i>TCA Fasted</i>				<i>TCA Mixed</i>				<i>TCA Fed</i>			
EC Number	Reaction	Score	p	EC Number	Reaction	Score	p	EC Number	Reaction	Score	p
n/a	Nut_o2	0.50	0.00	n/a	Nut_o2	0.46	0.00	n/a	Nut_o2	0.51	0.00
1.10.2.2	UCytC-III	0.50	0.00	1.10.2.2	UCytC-III	0.46	0.00	1.10.2.2	UCytC-III	0.51	0.00
1.9.3.1	CytCO-IV	0.50	0.00	1.9.3.1	CytCO-IV	0.46	0.00	1.9.3.1	CytCO-IV	0.51	0.00
3.6.3.14	ATPSynth-V	0.51	0.00	3.6.3.14	ATPSynth-V	0.52	0.00	3.6.3.14	ATPSynth-V	0.53	0.00
1.2.4.2	AKGDeh	0.57	0.00	1.2.4.2	AKGDeh	0.57	0.00	1.1.1.37	MalDehM	0.55	0.00
1.3.99.1	SucDeh-II	0.57	0.00	1.3.99.1	SucDeh-II	0.57	0.00	1.2.1.12	D3PDeh	0.56	0.00
4.2.1.2	Fum	0.57	0.00	4.2.1.2	Fum	0.57	0.00	2.7.2.3	PGK	0.56	0.00
1.5.5.1	ETFUO	0.60	0.00	1.1.1.37	MalDehM	0.58	0.00	n/a	MalDehC	0.59	0.00
n/a	Nut_co2	0.60	0.00	n/a	Nut_co2	0.59	0.00	n/a	Mal-AKGEX	0.59	0.00
4.2.1.3	Acon	0.66	0.00	4.2.1.3	Acon	0.63	0.00	1.2.4.2	AKGDeh	0.61	0.00
2.3.3.1	CitSynth	0.66	0.00	2.3.3.1	CitSynth	0.63	0.00	1.3.99.1	SucDeh-II	0.61	0.00
1.1.1.37	MalDehM	0.66	0.00	2.7.7.9	Nut_cr	0.64	0.00	4.2.1.2	Fum	0.61	0.00
1.6.5.3	NADHDeh-I	0.70	0.00	n/a	CKM	0.64	0.00	n/a	Nut_co2	0.61	0.00
2.7.7.9	Nut_cr	0.71	0.00	2.4.1.186/	St_cr	0.64	0.00	1.6.5.3	NADHDeh-I	0.63	0.00
n/a	CKM	0.71	0.00	2.4.1.11				2.7.7.9	Nut_cr	0.63	0.00
2.4.1.186/	St_cr	0.71	0.00	n/a	Ex_gluc	0.64	0.00	n/a	CKM	0.63	0.00
2.4.1.11				1.2.1.12	D3PDeh	0.64	0.00	2.4.1.186/	St_cr	0.63	0.00
n/a	Ex_pal	0.74	0.01	2.7.2.3	PGK	0.64	0.00	2.4.1.11			
n/a	FAT-CD36	0.74	0.01	2.7.1.2	Hex	0.64	0.00	n/a	ASTC	0.64	0.00
6.2.1.3	ACSL/PalTK	0.74	0.01	1.6.5.3	NADHDeh-I	0.65	0.00	n/a	Glu-AspEx	0.64	0.00
n/a	SLC25A20-CACT	0.74	0.01	1.5.5.1	ETFUO	0.67	0.00	2.6.1.1	ASTM	0.64	0.00
2.3.1.21	CPT2	0.74	0.01	n/a	MalDehC	0.67	0.00	1.5.5.1	ETFUO	0.65	0.00
1.3.99.3	AcylCoADeh	0.74	0.01	n/a	Mal-AKGEX	0.67	0.00	n/a	MCT	0.66	0.00
4.2.1.17	EnoCoADeh	0.74	0.01	n/a	MCT	0.69	0.00	2.3.3.1	CitSynth	0.67	0.00
1.1.1.35	3HA-CoADeh	0.74	0.01	n/a	ASTC	0.72	0.01	4.2.1.3	Acon	0.67	0.00
2.3.1.16	AcylCoAAT	0.74	0.01	n/a	Glu-AspEx	0.72	0.01	n/a	Ex_gluc	0.72	0.01
1.3.99.3	AcylCoADeh-14-c	0.77	0.02	2.6.1.1	ASTM	0.72	0.01	2.7.1.2	Hex	0.72	0.01
4.2.1.17	EnoCoADeh-14c	0.77	0.02	1.2.4.1	PyrSynth-pdh	0.80	0.02	1.2.4.1	PyrSynth-pdh	0.73	0.01
1.1.1.35	3HA-CoADeh-14c	0.77	0.02								
2.3.1.16	AcylCoAAT-14c	0.77	0.02								
4.2.1.17	EnoCoADeh-12c	0.81	0.04								
1.1.1.35	3HA-CoADeh-12c	0.80	0.04								

Table 7C. KDs in 1xFA-1xGluc causing significant reductions in metabolic flexibility as measured by RQ differences.

EC Number	Reaction	Score	p
1.2.4.1	PyrSynth-pdh	-0.09	0.01
n/a	Ex_pal	-0.03	0.43
n/a	FAT-CD36	-0.03	0.43
6.2.1.3	ACSL/PalTK	-0.03	0.43
n/a	Glu-AspEx	-0.01	0.71
2.6.1.1	ASTM	-0.01	0.71
n/a	ASTC	-0.01	0.73
n/a	NEAA_asp	0.00	0.88

By contrast, KDs of only one reaction significantly reduced metabolic flexibility: pyruvate dehydrogenase (PDH) (**Table 7C**). All other candidates were not statistically significant: fatty acid transport (e.g., Ex_pal; FAT-CD36), long-chain

acyl-CoA synthase (ACSL), glutamate-aspartate mitochondrial exchange (GLAST), and both cytosolic and mitochondrial aspartate transaminase (AST) (**Table 7C**). These reactions are key regulatory nodes for glucose metabolism, lipid uptake and metabolism, aspartate metabolism, and the transport of extra-mitochondrial hydrogen to the respiratory chain. KDs of these also reduced ATP+Cr-P production and cumulative TCA flux (**Table 8**).

Table 8. Top KDs causing reduced metabolic flexibility in basal nutrient condition (1xFA-1xGluc). For metabolic flexibility, data indicate cumulative difference in RQ (Eq. 8 in text). For each KD, data indicate ratio of KD compared to control (Eq. 6 and 7 in text).

KD Reaction	EC Number	Met. Flex	ATP+Cr-P Production			Cumulative TCA Flux		
		ΔRQ	<i>Fasted</i>	<i>Mixed</i>	<i>Fed</i>	<i>Fasted</i>	<i>Mixed</i>	<i>Fed</i>
PDH	1.2.4.1	0.09	0.94	0.78	0.80	0.93	0.77	0.73
FAT-CD36	n/a	0.03	0.75	0.92	1.00	0.74	0.91	1.00
PalTK	6.2.1.3	0.03	0.75	0.92	1.00	0.74	0.91	1.00
ASTM	2.6.1.1	0.01	0.96	0.73	0.68	0.97	0.91	0.64
ASTC	n/a	0.01	0.95	0.73	0.68	0.96	0.72	0.64
Glu-Asp Ex	n/a	0.01	0.96	0.73	0.68	0.97	0.72	0.64

With increased nutrient availability (2xFA-2xGluc), the model predicts that the objective functions (ATP, Cr-P, glycogen and TG storage) can be achieved more readily. In agreement, fewer KDs produce insulin resistance phenotypes. Significant reductions in ATP+Cr-P production were observed with 31 KDs in fasting, 18 in mixed, and 17 in the fed state (**Table 9A**), with similar patterns for TCA flux (**Table 9B**). Once again, only the KD in PDH yielded significant alterations in respiratory quotient; similar trends were observed for FAT and ACSL (**Tables 9C and 10**).

Table 9. KDs in 2xFA-2xGluc causing significant reductions in the three screened phenotypes: ATP+Cr-P production, cumulative TCA flux, and metabolic inflexibility.

Table 9A. KDs in 2xFA-2xGluc causing significant reductions in ATP+Cr-P production.

<i>ATP+Cr-P Fasted</i>				<i>ATP+Cr-P Mixed</i>				<i>ATP+Cr-P Fed</i>			
EC Number	Reaction	Score	p	EC Number	Reaction	Score	p	EC Number	Reaction	Score	p
3.6.3.14	ATPSynth-V	0.53	2.1E-07	3.6.3.14	ATPSynth-V	0.60	5.4E-10	n/a	CKM	0.61	2.8E-09
n/a	Nut_o2	0.53	2.9E-07	n/a	Nut_o2	0.60	9.9E-10	2.4.1.186/	St_cr	0.61	2.8E-09
1.10.2.2	UCytC-III	0.53	2.9E-07	1.10.2.2	UCytC-III	0.60	9.9E-10	2.4.1.11			
1.9.3.1	CytCO-IV	0.53	2.9E-07	1.9.3.1	CytCO-IV	0.60	9.9E-10	2.7.7.9	Nut_cr	0.61	3.0E-09
n/a	CKM	0.61	1.9E-05	n/a	CKM	0.61	2.8E-09	1.2.1.12	D3PDeh	0.63	1.2E-08
2.4.1.186/	St_cr	0.61	1.9E-05	2.4.1.186/	St_cr	0.61	2.8E-09	2.7.2.3	PGK	0.63	1.2E-08
2.4.1.11				2.4.1.11				n/a	Nut_o2	0.66	1.5E-07
2.7.7.9	Nut_cr	0.61	1.9E-05	2.7.7.9	Nut_cr	0.61	3.0E-09	1.10.2.2	UCytC-III	0.66	1.5E-07
n/a	Nut_p	0.63	4.2E-05	1.1.1.37	MalDehM	0.69	1.6E-06	1.9.3.1	CytCO-IV	0.66	1.5E-07
1.5.5.1	ETFUO	0.65	9.6E-05	n/a	Nut_p	0.69	1.6E-06	3.6.3.14	ATPSynth-V	0.66	1.7E-07
n/a	Nut_co2	0.67	0.00025	1.6.5.3	NADHDeh-I	0.72	1.6E-05	1.1.1.37	MalDehM	0.69	2.8E-06
1.1.1.37	MalDehM	0.67	0.00028	1.2.1.12	D3PDeh	0.74	5.1E-05	n/a	Nut_p	0.75	9.0E-05
1.6.5.3	NADHDeh-I	0.68	0.00045	2.7.2.3	PGK	0.74	5.1E-05	n/a	MalDehC	0.75	0.00014
1.3.99.1	SucDeh-II	0.69	0.00054	n/a	MalDehC	0.82	0.0039	n/a	Mal-AKGEX	0.75	0.00014
4.2.1.2	Fum	0.69	0.00054	n/a	Mal-AKGEX	0.82	0.0039	1.6.5.3	NADHDeh-I	0.76	0.00017
1.2.4.2	AKGDeh	0.69	0.00064	n/a	Nut_co2	0.84	0.011	n/a	ASTC	0.79	0.0014
2.3.3.1	CitSynth	0.71	0.0014	n/a	ASTC	0.86	0.022	n/a	Glu-AspEx	0.80	0.0016
4.2.1.3	Acon	0.71	0.0014	n/a	Glu-AspEx	0.86	0.024	2.6.1.1	ASTM	0.80	0.0016
2.3.1.21	CPT1B-CHKL	0.77	0.012	2.6.1.1	ASTM	0.856	0.024				
n/a	SLC25A20-CACT	0.77	0.012								
2.3.1.21	CPT2	0.77	0.012								
1.3.99.3	AcylCoADeh	0.77	0.012								
4.2.1.17	EnoCoADeh	0.77	0.012								
1.1.1.35	3HA-CoADeh	0.77	0.012								
2.3.1.16	AcylCoAAT	0.77	0.012								
n/a	Ex_pal	0.81	0.031								
n/a	FAT-CD36	0.81	0.031								
6.2.1.3	ACSL/PalTK	0.81	0.031								
1.3.99.3	AcylCoADeh-14c	0.81	0.036								
4.2.1.17	EnoCoADeh-14c	0.81	0.036								
1.1.1.35	3HA-CoADeh-14c	0.81	0.036								
2.3.1.16	AcylCoAAT-14c	0.81	0.036								

Table 9B. KDs in 2xFA-2xGluc causing significant reductions in cumulative TCA flux.

<i>TCA Fasted</i>				<i>TCA Mixed</i>				<i>TCA Fed</i>			
EC Number	Reaction	Score	p	EC Number	Reaction	Score	p	EC Number	Reaction	Score	p
n/a	Nut_o2	0.50	4.6E-07	3.6.3.14	ATPSynth-V	0.52	1.5E-07	n/a	Nut_o2	0.51	3.3E-05
1.10.2.2	UCytC-III	0.50	4.6E-07	n/a	Nut_o2	0.52	1.6E-07	1.10.2.2	UCytC-III	0.51	3.3E-05
1.9.3.1	CytCO-IV	0.50	4.6E-07	1.10.2.2	UCytC-III	0.52	1.6E-07	1.9.3.1	CytCO-IV	0.51	3.3E-05
3.6.3.14	ATPSynth-V	0.51	5.7E-07	1.9.3.1	CytCO-IV	0.52	1.6E-07	3.6.3.14	ATPSynth-V	0.53	6.3E-05
1.2.4.2	AKGDeh	0.55	5.8E-06	1.1.1.37	MalDehM	0.61	2.3E-05	1.1.1.37	MalDehM	0.55	0.00016
1.3.99.1	SucDeh-II	0.55	5.8E-06	1.2.4.2	AKGDeh	0.64	9.6E-05	1.2.1.12	D3PDeh	0.58	0.00032
4.2.1.2	Fum	0.55	5.8E-06	1.3.99.1	SucDeh-II	0.64	9.6E-05	2.7.2.3	PGK	0.58	0.00032
n/a	Nut_co2	0.60	5.7E-05	4.2.1.2	Fum	0.64	9.6E-05	n/a	MalDehC	0.61	0.00092
4.2.1.3	Acon	0.60	6.4E-05	2.7.7.9	Nut_cr	0.65	0.00013	n/a	Mal-AKGEX	0.61	0.00092
2.3.3.1	CitSynth	0.61	6.8E-05	n/a	CKM	0.65	0.00013	n/a	NADHDeh-I	0.63	0.0017
1.5.5.1	ETFUO	0.62	0.00010	2.4.1.186/	St_cr	0.65	0.00013	1.6.5.3	NADHDeh-I	0.63	0.0017
n/a	CKM	0.64	0.00024	2.4.1.11				n/a	ASTC	0.65	0.0028
2.4.1.186/	St_cr	0.64	0.00024	1.6.5.3	NADHDeh-I	0.67	0.00029	1.2.4.2	AKGDeh	0.65	0.0029
2.4.1.11				4.2.1.3	Acon	0.69	0.00065	1.3.99.1	SucDeh-II	0.65	0.0030
				2.3.3.1	CitSynth	0.69	0.00069	4.2.1.2	Fum	0.65	0.0030
				n/a	Nut_co2	0.69	0.00074	n/a	Glu-AspEx	0.65	0.0030
				1.2.1.12	D3PDeh	0.71	0.0014	2.6.1.1	ASTM	0.65	0.0030

2.7.7.9	Nut_cr	0.64	0.0002	2.7.2.3	PGK	0.71	0.0014	2.7.7.9	Nut_cr	0.66	0.0032
1.1.1.37	MalDehM	0.65	0.0003	n/a	MalDehC	0.74	0.0040	n/a	CKM	0.66	0.0032
1.6.5.3	NADHDeh-I	0.70	0.0028	n/a	Mal-AKGEX	0.74	0.0040	2.4.1.186/	St_cr	0.66	0.0032
2.3.1.21	CPT1B-CHKL	0.76	0.014	n/a	ASTC	0.78	0.014	2.4.1.11			
n/a	SLC25A20-CACT	0.76	0.014	n/a	Glu-AspEx	0.78	0.015	2.3.3.1	CitSynth	0.70	0.0088
2.3.1.21	CPT2	0.76	0.014	2.6.1.1	ASTM	0.78	0.015	4.2.1.3	Acon	0.70	0.0088
1.3.99.3	AcylCoADeh	0.76	0.014	1.5.5.1	ETFUO	0.80	0.022	1.5.5.1	ETFUO	0.70	0.0088
4.2.1.17	EnoCoADeh	0.76	0.014	n/a				n/a	Nut_co2	0.73	0.019
1.1.1.35	3HA-CoADeh	0.76	0.014					n/a	MCT	0.7	0.037
2.3.1.16	AcylCoAAT	0.76	0.014								
n/a	Ex_pal	0.79	0.033								
n/a	FAT-CD36	0.79	0.033								
6.2.1.3	ACSL/PalTK	0.79	0.033								
1.3.99.3	AcylCoADeh-14-c	0.80	0.037								
4.2.1.17	EnoCoADeh-14c	0.80	0.037								
1.1.1.35	3HA-CoADeh-14c	0.80	0.037								
2.3.1.16	AcylCoAAT-14c	0.80	0.037								

Table 9C. KDs in 2xFA-2xGluc causing significant reductions in metabolic flexibility as measured by RQ differences.

EC Number	Reaction	Score	p
1.2.4.1	PyrSynth-pdh	-0.22	0.0004
n/a	Ex_pal	-0.046	0.21
n/a	FAT-CD36	-0.046	0.21
6.2.1.3	ACSL/PalTK	-0.046	0.21

Table 10. Top KDs causing reduced metabolic flexibility in the 2xFA-2xGluc increased nutrient condition. For metabolic flexibility, data indicate cumulative difference in RQ (Eq. 8 in text). For each KD, data indicate ratio of KD compared to control (Eq. 6 and 7 in text).

KD Reaction	EC Number	Met. Flex	ATP+Cr-P Production			Cumulative TCA Flux		
		Δ RQ	Fasted	Mixed	Fed	Fasted	Mixed	Fed
PDH	1.2.4.1	0.22	0.96	0.78	0.80	0.96	0.90	0.82
FAT-CD36	n/a	0.05	0.81	1.00	1.00	0.74	1.00	1.00
ACSL/PalTK	6.2.1.3	0	0.81	1.00	1.00	0.74	1.00	1.00

Pathway Analysis of Knockdown Phenotypes

To determine whether experimental alterations in flux within specific metabolic pathways were more likely to yield insulin resistance phenotypes, I performed a pathway-based analysis. I used Fisher's exact test and the Benjamini-Hochberg method to assess significance and calculate false discovery rate (FDR), respectively.

In the control nutrient state, three pathways were significantly enriched for reduction in ATP+Cr-P production ($p < 0.05$, $Q < 0.25$) in the fasting and mixed conditions: BCAA, butanoate, and lysine metabolism (**Table 11**). Similarly, seven pathways were significantly enriched for reducing TCA flux: BCAA, butanoate, lysine, propanoate, tryptophan, FAD metabolism, and the TCA cycle itself. Only three pathways were enriched for reductions in metabolic flexibility: glycerophospholipid metabolism, lysine metabolism, and NADH shuttle.

Table 11. Pathways enriched in causing IR phenotypes ($p < 0.05$; $Q < 0.25$) in 1xFA-1xGluc basal nutrient condition.

ATP + Cr-P Production	Cumulative TCA Flux	Metabolic Inflexibility
<ul style="list-style-type: none"> •BCAA (fast and mixed) •Butanoate (fast and mixed) •Lysine (fast and mixed) 	<ul style="list-style-type: none"> •BCAA (fast and mixed) •Butanoate (fast and mixed) •Lysine (fast and mixed) •Propanoate (fast and mixed) •TCA Cycle (fast only) •Tryptophan (fast and mixed) •FAD metabolism (fast only) 	<ul style="list-style-type: none"> •Glycerophospholipid •Lysine •NADH shuttle

Increasing glucose and fatty acid availability (2xFA-2xGluc) yielded similar pathway results. OXPHOS, TCA cycle, glycolysis, fatty acid metabolism, and the NADH shuttle remained significantly enriched for modulating ATP+Cr-P production, while the BCAA pathway was no longer significantly enriched. Similarly, increased nutrient availability (2xFA-2xGluc) also reduced the number of pathways significantly enriched for reduced-cumulative-TCA-flux phenotype: glycerophospholipid, glycolysis, lysine, OXPHOS, and NADH shuttle. The only pathway enriched ($p < 0.05$) for reduced metabolic flexibility under conditions of increased glucose and fatty acid availability was glycerophospholipid metabolism, but the FDR value ($Q = 0.73$) was above the threshold (**Table 12**).

Table 12. Pathways enriched in causing IR phenotypes ($p < 0.05$; $Q < 0.25$, except otherwise indicated) in the 2xFA-2xGluc increased nutrient condition.

ATP + Cr-P Production	Cumulative TCA Flux	Metabolic Inflexibility
<ul style="list-style-type: none"> • Fatty Acid Metabolism (Fasted only) • Glycolysis (fasted only) • OXPHOS (fasted and mixed) • TCA Cycle (fasted and mixed) • NADH Shuttle (fasted and mixed) 	<ul style="list-style-type: none"> • Glycerolipid/glycerophospholipid (fasted and mixed) • Glycolysis (fasted and mixed) • Lysine (fasted only) • OXPHOS (fasted and mixed) • NADH Shuttle (fasted and mixed) 	<ul style="list-style-type: none"> • Glycerophospholipid ($p < 0.05$; $Q = 0.73$)

Multiple Simultaneous Knockdowns are Required to Fully Recapitulate Metabolic Phenotypes Associated with Insulin Resistance

It is notable that reduced flux in any single reaction did not produce all three metabolic phenotypes associated with insulin resistance in all conditions sampled. This is potentially an important observation, and if true in biological systems, it is likely a result of the extensive redundancy in cellular metabolism. Thus, I next asked whether simultaneous KDs in more than one reaction could more readily induce insulin resistance phenotypes. I performed a KD for each of the top three reactions causing decreased metabolic flexibility (PDH, FAT, and AST) and then systematically performed a second knockdown of all other reactions in combination. Interestingly, two knockdown pairs, either PDH and electron-transferring-flavoprotein dehydrogenase (ETFD), or PDH and FAT, did reduce ATP+Cr-P production and cumulative TCA flux and induce metabolic inflexibility (**Figure 8**, *open shapes*). While the PDH&ETFD and PDH&FAT double KDs both led to the insulin resistance phenotype in the 1xFA-1xGluc nutrient state, the PDH&ETFD double KD was the only combination which recapitulated all three insulin resistance phenotypes in all four nutrient conditions. By contrast, other combinations were not as robust at recapitulating the phenotypes in each condition (**Table 13**).

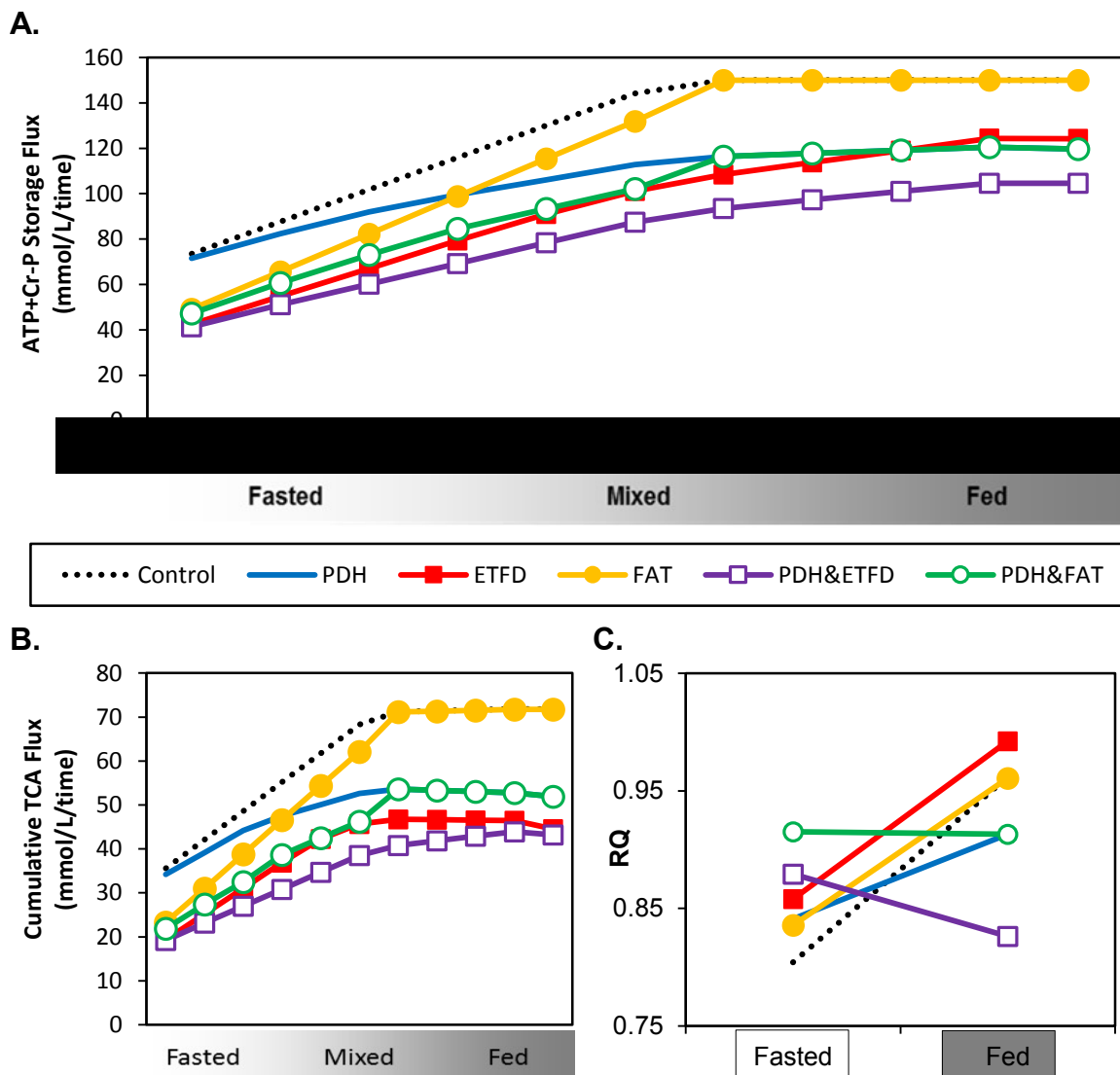


Figure 8. Combined knockdowns can induce metabolic phenotypes associated with insulin resistance. (A) ATP + Cr-P storage and (B) TCA cycle flux, and (C) respiratory quotient (RQ) under control conditions and in response to single or combined knockdowns.

Table 13. Summary of scores for the top DOUBLE KDs causing reduced metabolic flexibility. For metabolic flexibility, data indicate cumulative difference in RQ (Eq. 8 in text). For each KD, data indicate ratio of KD compared to control (Eq. 6 and 7 in text).

Table 13A. Basal nutrient condition (1xFA-1xGluc)

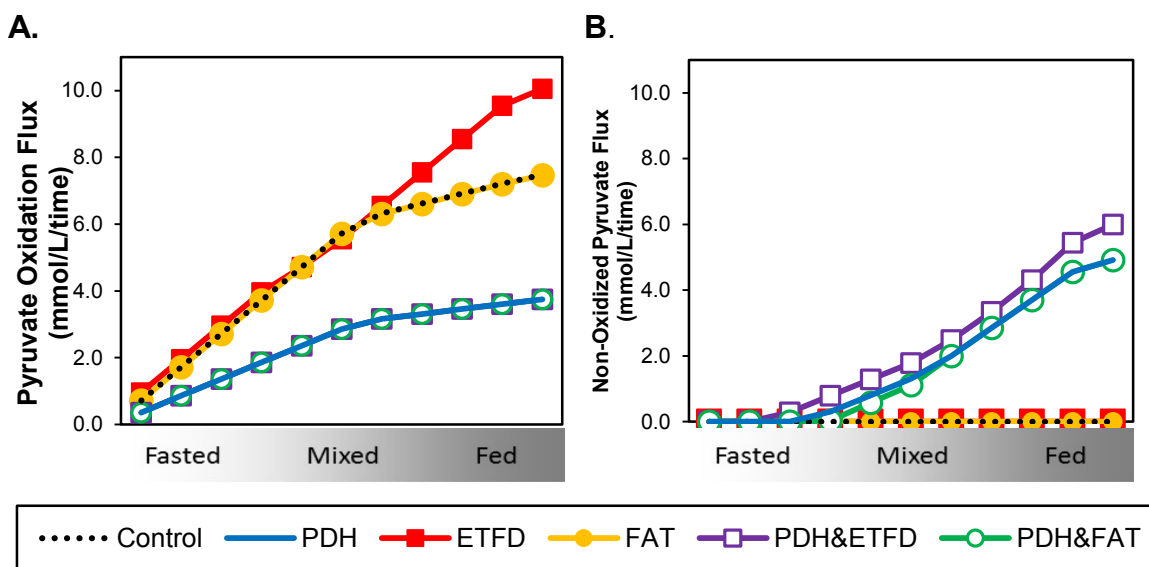
KD Reactions	EC Numbers	Met. Flex	ATP+Cr-P Production			Cumulative TCA Flux		
		ΔRQ	Fasted	Mixed	Fed	Fasted	Mixed	Fed
PDH & ETFD	1.2.4.1 & 1.5.5.1	0.21	0.58	0.61	0.70	0.55	0.56	0.61
PDH & FAT-CD36	1.2.4.1 & n/a	0.16	0.69	0.71	0.80	0.65	0.68	0.73
PDH & ASN Synth	1.2.4.1 & 2.7.2.11	0.15	0.94	0.76	0.78	0.93	0.73	0.69
FAT-CD36 & MCT	n/a & n/a	0.29	0.68	0.66	0.75	0.61	0.60	0.66
AST & FAT-CD36	2.6.1.1 & n/a	0.10	0.73	0.65	0.68	0.69	0.62	0.63
AST & ETFD	2.6.1.1 & 1.5.5.1	0.06	0.60	0.58	0.61	0.58	0.59	0.58

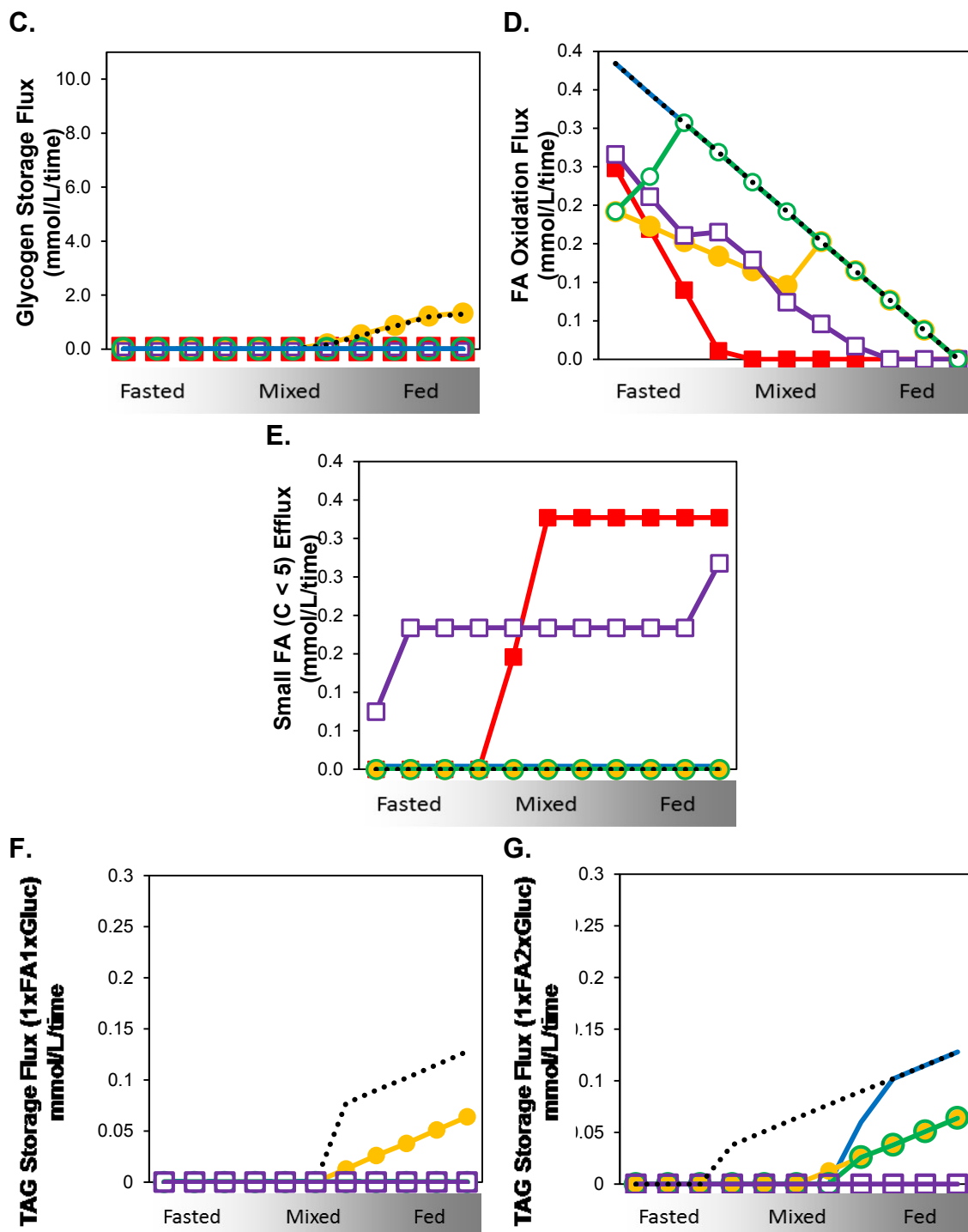
Table 13B. Increased nutrient condition (2xFA-2xGluc)

KD Reactions	EC Numbers	Met. Flex	ATP+Cr-P Production			Cumulative TCA Flux		
		ΔRQ	Fasted	Mixed	Fed	Fasted	Mixed	Fed
PDH & ETFD	1.2.4.1 & 1.5.5.1	0.32	0.58	0.78	0.98	0.53	0.63	0.73
PDH & FAT-D36	1.2.4.1 & n/a	0.37	0.72	1.00	1.00	0.66	0.90	0.82
PDH & ASN Synth	1.2.4.1 & 2.7.2.11	0.24	0.96	1.00	1.00	0.92	0.86	0.79
FAT-CD36 & MCT	n/a & n/a	0.41	0.68	0.98	1.00	0.60	0.83	0.77
AST & FAT-CD36	2.6.1.1 & n/a	0.15	0.71	0.85	0.79	0.65	0.77	0.64
AST & ETFD	2.6.1.1 & 1.5.5.1	0.02	0.57	0.64	0.70	0.55	0.62	0.58

Interestingly, the combination of reduced flux through PDH&ETFD or PDH&FAT also produced other phenotypes associated with insulin resistance. KDs in PDH decreased PDH activity, as expected, but also increased non-oxidized pyruvate

(lactate) production (**Figures 9A** and **9B**); this was most striking with the PDH&ETFD combination. Similarly, the model predicts that a KD in PDH or ETFD alone or in combination, or combined KD in PDH& FAT lead to reduced glycogen storage – also a key phenotype of insulin resistance (Eriksson et al., 1989) (**Figure 9C**). Strikingly, double KDs in PDH&ETFD or PDH&FAT reduce complete fatty acid oxidation (**Figure 9D**) and increase release of short-chain acyl-carnitines (**Figure 9E**), suggesting incomplete fatty acid oxidation, as described in both humans and rodents with insulin resistance (Koves et al., 2008). I also observed reduced TAG storage with this combination (**Figure 9F**), and found reduced TAG storage in the increased nutrient conditions (2xFA1xGluc, 1xFA2xGluc, and 2xFA2xGluc) with the PDH&ETFD double KD.





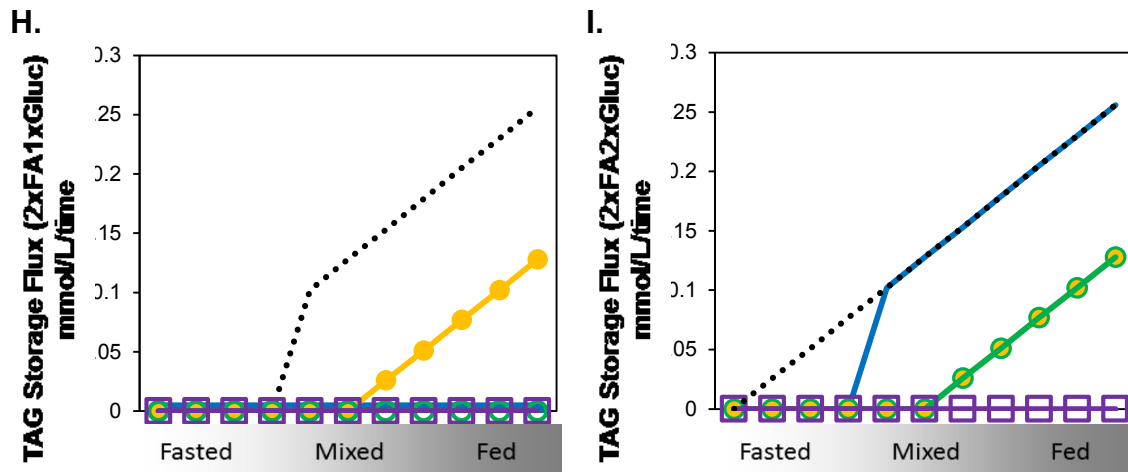


Figure 9. Double knockdowns (PDH/ETFDH or PDH/FAT) alter carbohydrate and fatty acid metabolism, including (A) PDH activity, (B) reduced non-oxidized pyruvate, (C) reduced glycogen storage, (D) reduced complete fatty acid oxidation, (E) increased release of short-chain acyl-carnitines. (F) 1xFA1xGluc TAG Storage Flux, (G) 1xFA12Gluc TAG Storage Flux, (H) 2xFA1xGluc TAG Storage Flux, and (I) 2xFA2xGluc TAG Storage Flux

Biological Validation of *In Silico* Results

RT-PCR of candidate genes from skeletal muscle cells from IR induced mice show altered gene expression

In silico predictions and FBA modeling provide insight into the possible metabolic dysregulations which cause the metabolic alterations observed in IR phenotypes. However, the next step is to use these predictions to help design *in vivo/vitro* experiments to validate these predictions/simulations. Yi et al. (2013) recently published a mouse model where IR is induced by a small peptide S961 (43 amino acids in length). S961 binds the insulin receptor in mice and antagonizes the insulin signaling pathway. After a week of S961 treatment, mice become hyperglycemic and glucose intolerant (Yi et al, 2013). To examine the impact of acute IR-induction

on expression of candidate enzymes identified by the *in silico* analysis, mice were treated with 10 nMol/week S961 or PBS, and RT-PCR was performed for the genes which encode for the candidate enzymes: PDH, ETFDH, and FAT/CD36.⁸ Of the genes tested PDHb, ETFb, and CD36 had significantly lower expression levels in skeletal muscle cells which were S961 treated compared to the PBS group ($p \leq 0.05$). The expression in S961 treated group for genes PDHA1 and FATP2, while not significant ($0.05 > p \leq 0.10$), trended lower than control (**Table 14**).

Table 14⁹. RT-PCR results from skeletal muscle tissue from the Control (PBS) and S961 IR induced mice for candidate genes from *in silico* analysis.

Gene:	ETFDH	ETFa	ETFb*	PDHa1 [‡]	PDHa2	PDHb*	PDHx	CD36*	FATP1	FATP2 [‡]
PBS (control)	1.04 +0.15	1.03 +0.13	1.05 +0.17	1.01 +0.08	1.13 +0.28	1.08 +0.23	1.03 +0.12	1.02 +0.11	1.02 +0.10	1.06 +0.20
S961 treated	0.91 +0.15	0.91 +0.14	0.59 +0.14*	0.78 +0.13[‡]	2.18 +0.80	0.64 +0.09*	0.82 +0.12	0.66 +0.10*	0.86 +0.21	0.66 +0.15[‡]

* $p \leq 0.05$; [‡] $p \leq 0.10$ (1-tailed t-test)

Lower PDH protein expression and siRNA ETFDH Knockdown Cause IR-like Phenotypes from Mouse Myotubes

To determine if alterations in flux through the enzymes identified in our *in silico* analysis would also recapitulate IR metabolic phenotypes *in vivo*, we analyzed the impact of modulating candidate genes in mouse myocytes. Given the difficulty in establishing robust knockdowns of two genes in combination using siRNA, we utilized primary myoblasts derived from mice in which PDH flux was decreased by dual genetic ablation of the PDH inhibitors pyruvate dehydrogenase kinase 2/4

⁸ Ana-Luisa Coelho, PhD, extracted gastrocnemius tissue and performed RT-PCR.

⁹ Alison Burkart, PhD, collected and analyzed the data in this table.

(PDK2/4). Pyruvate dehydrogenase kinase (PDK) is an important regulatory enzyme of PDH, deactivating PDH via phosphorylation (Bowker-Kinley et al. 1998). Without PDK's inhibitory effect, PDH phosphorylation and flux are increased, as compared to WT cells (**Figure 10A**); thus, PDK 2/4-KO and WT cells allow analysis of the metabolic impact of relative reductions in PDH activity. We then superimposed siRNA-mediated KD of ETFDH in PDK2/4 KO and WT cells to examine the impact of decreased activity of both candidate enzymes, independently and in combination. We confirmed decreased mRNA expression of PDK2/4 and ETFDH by qRT-PCR analysis (**Figure 10B**). Similarly, Western blots demonstrated reduced PDH phosphorylation in PDK2/4-KO cells and reduced ETFDH protein expression in cells transfected with ETFDH siRNA (**Figure 10C**). After confirming successful experimental knockdowns, we analyzed IR-associated metabolic phenotypes. We first measured ATP levels; consistent with model predictions, cells with lower PDH activity (WT) had significantly lower ATP content (**Figure 10D**). Although KD of ETFDH alone did not significantly reduce ATP levels, ATP levels were significantly lower with combined reduction in PDH and ETFDH activity. (**Figure 10D**). We next examined flux through the TCA cycle by analyzing the activity of the key TCA cycle enzyme citrate synthase (CS), a key TCA cycle enzyme. Myoblasts with lower PDH activity had decreased CS activity, and ETFDH siRNA reduced CS activity (**Figure 10E**).

To determine the impact of experimental manipulation of PDH and ETFDH on metabolic flexibility, we assessed cellular substrate utilization and responses to

nutrient modulation. Specifically, we measured extracellular acidification rate (ECAR), a readout of glycolytic glucose metabolism, and oxygen consumption rate (OCR), a measure of aerobic respiration, and determined the ECAR/OCR ratio as a surrogate for substrate utilization. In the fasted state, lipid substrate utilization would dominate, with more oxygen consumption and less glycolysis, yielding a lower ECAR/OCR ratio. By contrast, in the fed state, the ECAR/OCR ratio is higher, consistent with predominant glucose utilization. To assess metabolic flexibility, or the ability of cells to modulate substrate utilization, cells were incubated with palmitate (to promote lipid oxidation) and then acutely treated with glucose to provoke a switch from lipid to carbohydrate metabolism. As expected, glucose increased the ECAR/OCR ratio, consistent with a shift to glycolytic metabolism (**Figure 10F**). Consistent with model predictions, cells with lower PDH flux displayed a reduced shift to glycolytic metabolism (decreased slope of ECAR/OCR change) upon addition of glucose, as compared to cells with higher PDH flux. Moreover, knockdown of ETFDH tended to reduce this shift (**Figure 10F**). Thus, experimental reductions in PDH and ETFDH flux result in reduced metabolic flexibility.

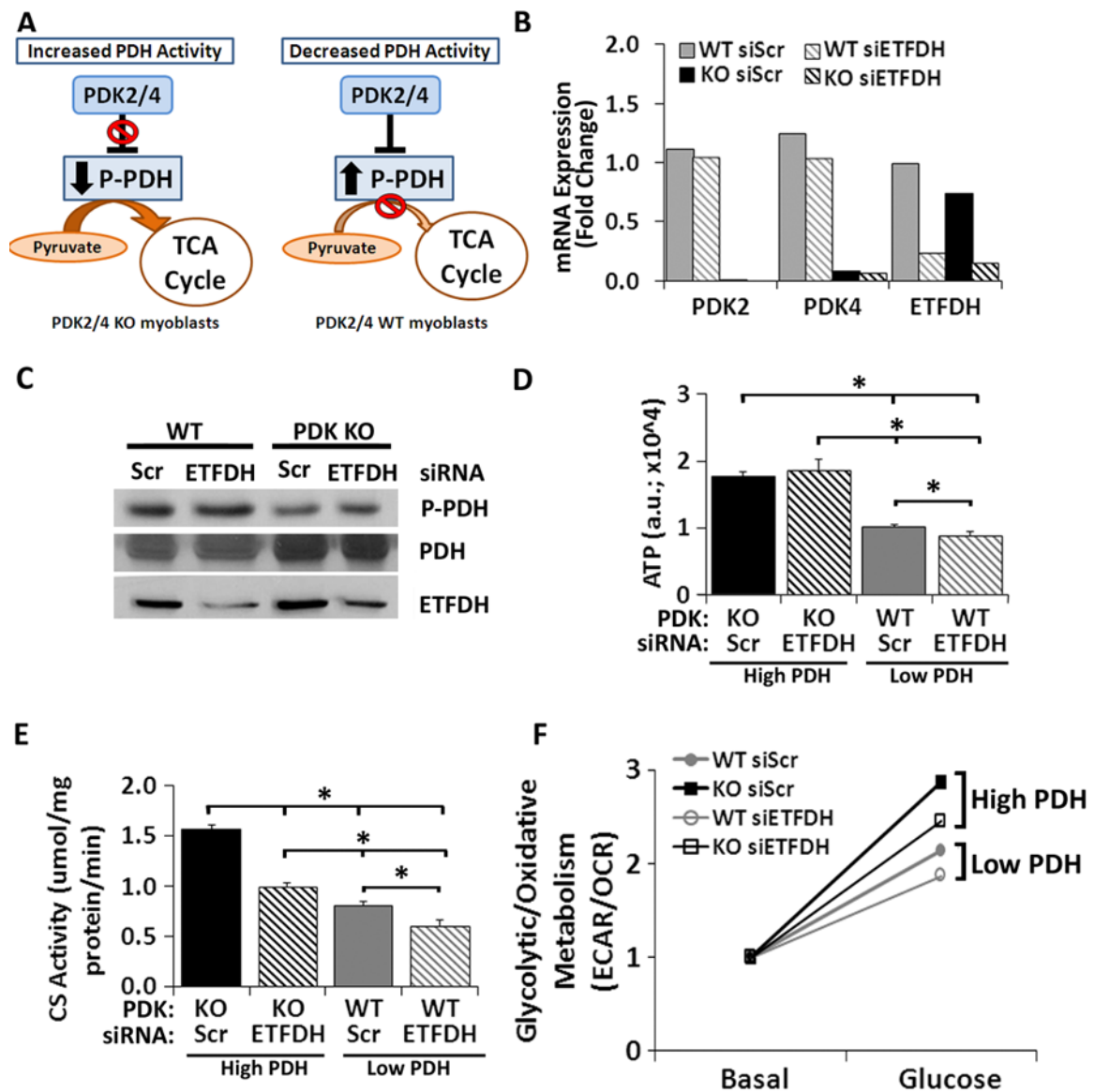


Figure 10. Double knockdowns in myoblasts recapitulate the IR phenotypes predicted by *in silico* experiments. PDK2/4 wild type and knockout myoblasts (KO) were transfected with ETFDH siRNA or a control scrambled siRNA (Scr). (A) Schematic of PDH regulation by PDK 2/4 (B) qRT-PCR analysis shows decreased PDK2 and PDK 4 mRNA expression in PDK2/4 KO cells and decreased ETFDH mRNA with ETFDH siRNA transfection. (C) Western blot analysis of the inactive phosphorylated PDH (P-PDH; top panel) and total PDH protein expression (middle panel) show decreased PDH

phosphorylation in KO cells. ETFDH protein expression (bottom panel) was decreased in both the WT and PDK 2/4-KO cells with the ETFDH siRNA compared to the scrambled (Scr). (D) ATP levels (normalized to protein) show a significant reduction in cells with lower levels of PDH activity (WT Scr) with ETFDH KD further decreasing the ATP levels in WT cells. (E) Citrate synthase (CS) activity is decreased in the WT cells and ETFDH KD decreases CS activity in both PDK2/4 KO and WT cells. (F) ECAR/OCR values under basal conditions (250 μ M palmitate) and after addition of 5.5 mM glucose, shown relative to the basal level.

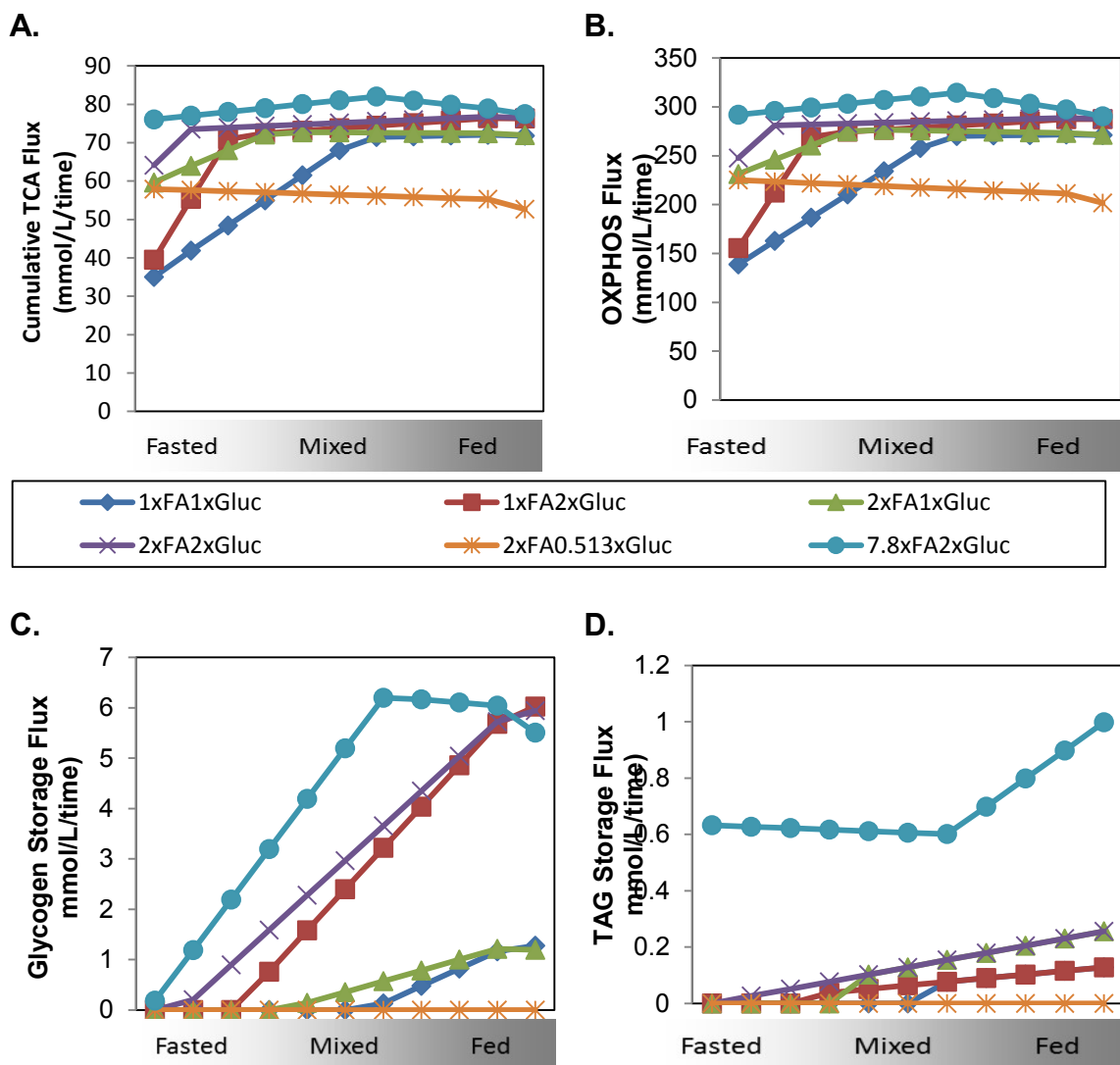
Discussion

Skeletal muscle is a key tissue for determining whole-body energy usage and a very sensitive mirror of insulin sensitivity (DeFronzo et al., 1985). Not surprisingly, muscle insulin resistance is associated with dysregulation in multiple metabolic pathways. However, it remains unknown which specific metabolic reactions might directly cause or contribute to these phenotypes and whether they also play a pathogenic role in insulin resistance. I have approached this important question by developing a novel *in silico* constraint-based FBA model of muscle metabolism. As with any modeling approach, flux balance analysis requires several key assumptions (Oberhardt et al., 2009). Most importantly, flux balance modeling assumes that flux across each metabolic reaction is modulated to achieve the defined objective functions of the entire model. In the case of muscle, I defined this objective function (goal) as both energy production (ATP+Cr-P) and storage (glycogen and triacylglycerols) for subsequent contraction. In addition, flux balance modeling also assumes that a steady state can be achieved. While this

is more readily achieved *in vivo* during fasting, I extended this assumption to the fasting-to-fed transition by examining steady-state fluxes at discrete points along this continuum. To model the fasting state, which is characterized by increased fatty acid utilization, I allow maximal flux through CPT1. Similarly, I relax the constraint I put on modifiable glucose uptake in order to mimic increased glucose uptake in the fed state. Analysis of the flux transitions observed in fasted and fed states demonstrate that the proposed model mirrors alterations in metabolic flux in response to prevailing nutrient and metabolic conditions *in vivo*.

I first used this model to examine the impact of increased availability of glucose and fatty acids, as seen in individuals with insulin resistance and T2D, on flux patterns. A two-fold increase in glucose availability resulted in increased flux through glycolysis, glycogen storage, and TAG storage, while a two-fold increase in fatty acid availability increased TCA cycle, OXPHOS, glycogen storage, and TAG storage. With increases in both glucose and fatty acids, glucose effects dominate, with increases in glycolytic fluxes even in fasting states. The predominant effect of glucose is likely to result from its higher extracellular concentration (2x Gluc = 10.00 mM Gluc) as compared with fatty acids (2xFA = 0.7675 mM FA). I found that increasing the FA availability (7.8xFA = 3.000 mM FA) to that of equal energy production of 2x Gluc did shift the metabolism to be primarily fatty acid focused until the 30% CPT1:70%GU_{mod} sampling point. As expected, it increased TCA cycle, OXPHOS, glycogen storage, and TAG storage compared to all other conditions (**Figure 11**). Thus, isolated increases in

extracellular glucose or lipid substrates can alter metabolic flux in the model, even in the absence of hormonal signals. However, it is important to note that modest elevations in either glucose or fatty acid availability (or both) in the model *increase* energy production, did not markedly change RQ patterns (higher in fasted AND lower in fed), and thus do not recapitulate the metabolic phenotypes characteristic of insulin resistance.



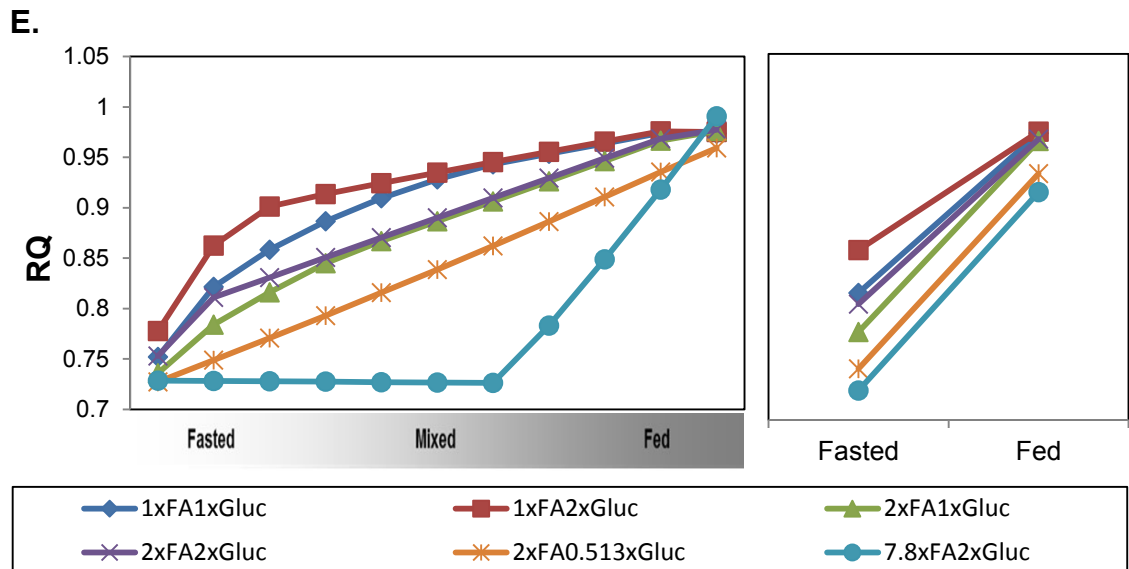


Figure 11. Predicted fluxes through pathways and substrate uptake, production, and release. Chart shows the flux in mmol/L/time on the Y-axis. The x-axis shows the flux at the discrete points from our defined fasting to fed states, as defined by conversely constraining the flux through CPT1 and modifiable glucose uptake from 0-100% of the maximum flux. The different nutrient states, defined in the text, are indicated by different colored lines and symbols: 1xFA/1xGluc (blue/diamonds), 1xFA/2xGluc (red/boxes), 2xFA/1xGluc (green/triangle), 2xFA/2xGluc (purple/x), 2xFA/0.513xGluc (orange/star), and 7.8xFA/2xGluc (aqua/circle). (A) Predicted cumulative flux through the TCA cycle, including citrate synthase, aconitase, isocitrate dehydrogenase-2, α -ketoglutarate dehydrogenase, succinyl coenzyme-A synthetase, succinate dehydrogenase, fumarase, and malate dehydrogenase-2 reactions. (B) OXPHOS (complexes I-V). (C) Predicted glycogen storage. (D) Predicted TAG storage. ((E) Predicted respiratory quotient (RQ).

In order to identify reactions and pathways which modulate metabolic phenotypes associated with insulin resistance, I next performed *in silico* knockdowns (KDs) of each of the reactions within the model, both singly and in combination, and under varying extracellular nutrient conditions. ATP+Cr-P production was sensitive to KDs within key energy-producing pathways (e.g. TCA and OXPHOS, NADH

shuttles), and in both fasting and fed states. By contrast, reduced flux in lipid and branched chain amino acid oxidation pathways only reduced energy production in the fasting state—consistent with the more important role for these nutrients as energy sources in the fasting state—when glucose is limited. KDs which reduced cumulative TCA cycle flux were very similar to those reducing ATP production, a finding likely related to the role for TCA and OXPHOS as the “final common pathway” for energy production.

Conversely, relatively few KDs altered metabolic flexibility. Interestingly, metabolic inflexibility was not induced by isolated impairments in TCA or OXPHOS, but was induced by regulators of glucose oxidative metabolism (PDH), lipid uptake and metabolism (CD36 and ACSL), aspartate metabolism (AST), and the transport of extra-mitochondrial hydrogen to the respiratory chain (glutamate-aspartate shuttles). Of these, only knockdown of PDH also yielded significant reductions in ATP production and TCA cycle flux in the basal state.

In general, cellular metabolism was less sensitive to *in silico* experimental knockdowns when glucose or fatty acid availability was increased. However, no single knockdown (even PDH) yielded all 3 insulin resistance-related metabolic phenotypes under all conditions sampled. This is intuitive given that metabolic flux patterns differ in each nutrient condition, and redundancy could attenuate effects of a single knockdown. I thus hypothesized that defects in flux at multiple control reactions would be required to fully recapitulate the three insulin resistance phenotypes. Consistent with this notion, KD in PDH, when combined with either

electron-transferring-flavoprotein dehydrogenase (ETF_D) or FAT, did reduce ATP+Cr-P production, TCA flux, and metabolic flexibility (**Figure 12**). The combined knockdowns also modulated flux through key pathways to yield additional features of insulin resistance, including reduced fatty acid oxidation, increased incomplete fatty acid oxidation, and decreased glycogen storage.

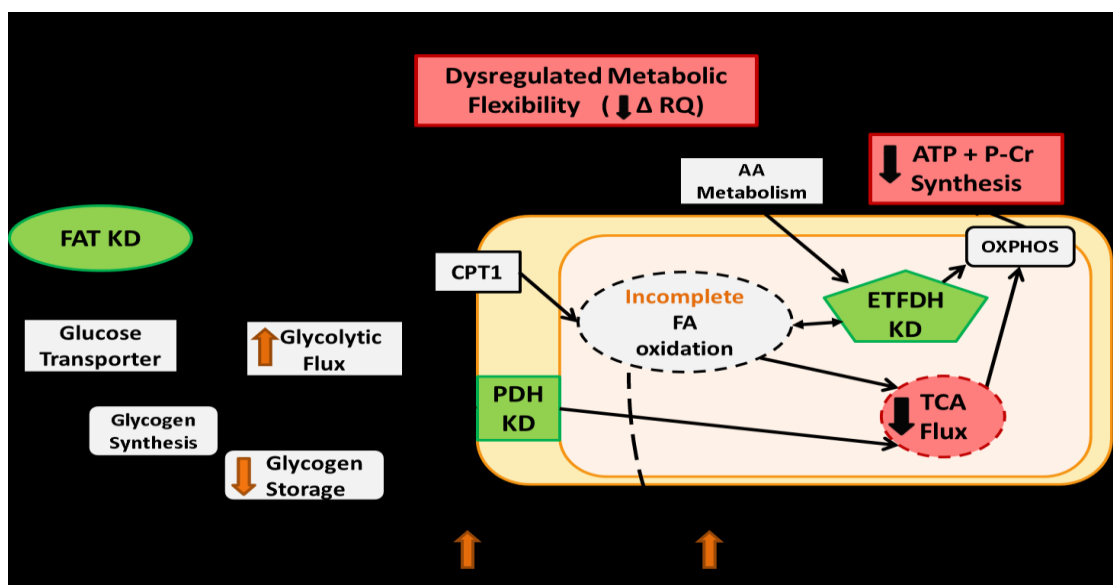


Figure 12. Schematic of targeted knockdowns that model phenotypes of insulin resistance. Knockdowns (KD; shown in green) of fatty acid transporter (FAT), pyruvate dehydrogenase (PDH), and electron transfer flavoprotein (ETF_D) recapitulated the metabolic phenotype of insulin resistance (shown in red), which was defined as decreased ATP+P-Cr synthesis and TCA flux and reduced metabolic flexibility, i.e., decreased change in respiratory quotient (RQ) in the fasted-to-fed transition. Additional metabolic alterations were observed (indicated by orange arrows), including increased glycolytic flux and release of non-oxidized pyruvate and parallel decrease in glycogen storage. Fatty acid oxidation was decreased, while increased incomplete fatty acid oxidation resulted in increased release of short-chain fatty acids.

The next step was to determine if one could reproduce these *in silico* results *in vitro* or *ex vivo*. First, we investigated the expression level of the genes which

encode the candidate enzymes in acutely IR-induced mouse model. Following the protocol established in the Melton Lab (Yi et al., 2013), Coelho isolated calf muscle tissue from control and IR induced mice, and performed RT-PCR for the genes in question. It was found that an acute IR induction can significantly alter expression levels in some of the genes queried: ETFb, PDHb, and CD36. This shows that under an acute induction of IR the expression of these genes are altered, and could lead to the dysregulated metabolism which cause the IR metabolic phenotypes. We next validated our *in silico* predictions *in vivo* using cultured myocytes. We modulated flux through PDH and ETFDH, singly and in combination, using a combination of genetic ablation (of PDK2/4) and siRNA targeting ETFDH. Notably, we demonstrate that lower PDH activity and ETFDH KD reduced ATP production, reduced TCA flux (measured by citrate synthase activity) and reduced metabolic flexibility (approximated by change in ECAR/OCR in response to glucose addition). Thus, these *in vivo* data demonstrate that alterations in flux through PDH and ETFDH can recapitulate elements of insulin resistant metabolism, validating the *in silico* predictions.

While these results look promising more work is necessary to elucidate the causes of IR phenotypes. The PDK-KO mouse model was one option to reproduce the differing fluxes between the *in silico* PDH normal and KD conditions. Another reproduction of the *in silico* experiments could have been to use a double siRNA KD scheme. Alternatively, another approach could have been introducing PDK directly which inhibits PDH, providing a method to knock down PDH activity. This

way, one could compare a direct *in silico* to *in vitro/vivo* KD, rather than inferring from a PDH overexpression model.

While the above options were considered, the method described here was chosen for two main reasons. First, as previously mentioned, it can be challenging to control for consistent double siRNA KDs. Second, the goal was to reproduce the *in silico* methods as closely as possible. The PDH was never completely knocked down and part of the hypothesis is that partial disruptions of PDH over long periods of time lead to the IR phenotypes.

In addition to the preliminary biological validation of the *in silico* data, these results are consistent with the central regulatory role for pyruvate dehydrogenase (PDH), a multi-enzyme complex that converts glycolysis-derived pyruvate to acetyl-CoA. Activity of PDH is regulated by its coenzymes (NAD⁺ and coenzyme-A), post-translational modifications (e.g., lysine acetylation (Wang et al., 2010), O-glycosylation (Kohda et al., 2010)), and by PDH kinases and phosphatases. Randle first proposed a key regulatory role for PDH in metabolism; increased fatty acid supply could increase ATP and NADH availability, inhibiting PDH activity and reducing both oxidative metabolism and uptake by muscle (Randle et al., 1963). Subsequent studies confirmed that PDH activity is reduced in humans with T2D or at risk for T2D (Mostert et al., 1999) and can also be reduced experimentally by lipid-induced insulin resistance (Pehmoller et al., 2012). Less severe reductions in PDH activity, potentially mediated by acetylation, have recently been linked with metabolic inflexibility in cardiac muscle in rodents (Vadvalkar et al., 2013).

Conversely, activation of PDH by PDK knockout (Jeoung and Harris, 2008), pharmacologic inhibition of PDH kinase (Mayers et al., 2005), or exercise (Kiilerich et al., 2008) improves insulin resistance and glycemia. Thus, these results build upon these prior findings by demonstrating that reductions in PDH flux may be a key contributor to deleterious metabolic phenotypes in insulin resistance.

Electron transfer flavoprotein localizes to the mitochondrial matrix and accepts electrons from dehydrogenases in fatty acid, choline, and amino acid metabolism. These electrons are then shuttled into the electron transport chain via electron-transferring-flavoprotein dehydrogenase (ETF₂NADH), which is located in the inner mitochondrial membrane, for reduction of ubiquinone. The function of these two enzymes is critical for energy metabolism; mutations in either cause multiple acyl-CoA dehydrogenase deficiency (MADD; type II glutaric aciduria) (Olsen et al., 2007), a rare inherited disorder leading to impaired oxidation of amino acids and lipids and increased plasma acyl-carnitines (Rinaldo et al., 2002). Recent genome-wide association studies also linked the ETF₂NADH locus to plasma acyl-carnitine levels in healthy individuals, suggesting a regulatory role in lipid and amino acid oxidative metabolism (Illig et al., 2010). Furthermore, expression of ETF₂NADH is regulated both by nutrients (up regulation after fatty acid exposure (Lockridge et al., 2008)) and in response to changes in insulin sensitivity. For example, ETF₂NADH is down regulated *in vivo* in insulin resistant mice (Sena et al., 2009) and humans (Viguerie et al., 2012) but up regulated by treatment with the PPAR γ agonist and insulin sensitizing drug rosiglitazone (Wilson-Fritch et al.,

2004). Thus, ETFDH plays a central role in lipid and amino acid oxidation; the model now identifies this enzyme complex as a key regulatory node which can interact with PDH to potentiate insulin resistance metabolic phenotypes.

Our model also predicts that reductions in fatty acid transport flux also potentiate effects of PDH. If fatty acid transport is compromised in such a “double-hit” scenario, intracellular lipid substrate availability would likely be reduced, limiting adaptive responses to maintain normal energetics. This concept is supported by experimental data indicating that reduced muscle fatty acid uptake (via CD36 or LPL) reduces mitochondrial function (Morino et al., 2012). Moreover, fatty acid transporters (e.g. FATP1) can interact with and modulate PDH activity in myotubes (Khajah et al., 2011).

Conclusion

While the conclusions drawn here are optimistic, there are limitations with the FBA framework. First, *in silico* models cannot fully recapitulate the complexities of inter-organ metabolism, hormonal responses, and intracellular signaling, and transcriptional responses which can further modulate flux within specific metabolic reactions. For example, in both studies (nutrition and IR metabolism), the question was to determine what acute response occurs under various conditions. It was assumed that the muscle had been primed for protein synthesis (i.e., after resistance exercise), and queried for the best acute supplementation strategy. IN addition, we know that IR phenotypes present earlier in life than T2D, and hypothesize that it is possible that small changes at more than one critical reaction, maintained over many years, could indeed contribute to important differences in muscle energetics, nutrient partitioning, and potentially increase risk for insulin resistance.

Another challenge in the application of FBA in studying metabolism of multicellular organisms is choosing an appropriate objective function for the organism or tissue (Shlomi et al., 2008). However, muscle tissue as compared to other tissues has more defined states which can be modeled: contraction, recovery/growth, fasted, and post-absorptive, to name a few. Because the objective was to increase muscle protein synthesis in response to supplementation in the first aim, the model's objective function would simply be the flux through the contractile protein

synthesis reactions. However, in order to elucidate the metabolism in IR, it was necessary to assume what the cell's "objective" was. *In vivo*, it is likely that a given cell has varying objective functions, affected by the prevailing hormonal, nutrient, or stimulated condition. Yet, I assumed that muscle tissue had evolved to store energy in the forms of ATP, Cr-P, glycogen, and TAG for subsequent use in contraction. Under this hypothesis, modeling from a fasted to fed state produced results consistent to what is seen *in vivo* (**Figure 5**). Depending on the state of the muscle tissue or the goal of the perturbations, one can envision other objective functions. For example, one can model muscle contraction by optimization ATP production. This can be done under differing oxygen availability, reflecting differing types of exercise: aerobic vs. non-aerobic.

In addition to the limitations of the FBA framework, there are shortcomings to the specific model developed here. The Nogiec Muscle Model (version 1.0 and 1.1) is less complex than previously published muscle models (Shlomi et al., 2008; Jerby et al., 2010; Agren et al., 2012). However, the Nogiec Muscle model was curated at the level of muscle cell metabolism and includes specific protein synthesis for contractile protein complex, while the other models do not. Yet, increasing the complexity by incorporating the specific protein synthesis into other published muscle models, can potentially allow one to investigate other nutrients and metabolites often used for supplementation. Either creating a muscle model *de novo* with increased complexity or providing better curation to the models

reconstructed from a general human muscle model may improve the potential of obtaining results more consistent with biology.

In addition to the future work suggested in the previous chapters, the FBA framework could have the potential in aiding the development of personalized (preventative) medicine. For example, in the case of the first application to muscle protein synthesis, this can be explored in many ways. Certain types of training lead to muscle tissue hypertrophy, which is mostly achieved by increasing the contractile proteins and scaffolding proteins in the muscle tissue. The contractile proteins differ slightly based on the muscle type: 1, 2a, 2x, and 2b. However, the amino acid composition of these proteins is similar enough that according to the model, amino acid supplementation effects protein synthesis similarly. This means that, similar supplementation regimes could be appropriate no matter the type of training goal. However, determining if there are differences between recovery and growth, one can slightly alter the objective function. For Type 1 muscle tissue (slow twitch), one could look at an objective function that would model increasing the concentration of mitochondria, while for Type 2 muscle tissue (fast twitch), the contractile protein synthesis may be more appropriate. To elucidate the differences even more, an objective function which incorporates a combination of mitochondrial proliferation and contractile muscle protein synthesis can be used to differentiate Type 2a, Type 2x, and Type 2b muscle tissues. Furthermore, the model predicts supplementation from fasting normo-aminoacidemia and post-absorptive states. These profiles were obtained by averaging the profiles of

multiple individuals. Perhaps, by knowing the specific amino acids levels of an athlete or patient, one can use this model to predict an individualized supplement regimen appropriate for which muscle tissue recovery is desired. In addition, I use plasma concentration levels of amino acids as a proxy for amino acid flux. Differing concentrations can lead to differing results. Ultimately, one would look at which uptake fluxes needed to be increased to achieve the desired results. Conceivably this can be adapted for personalized supplementation strategies. If the concentrations and/or amino acid uptake fluxes of individuals were known, one can determine the most effective supplementation strategy to achieve the individual's objective.

Moreover, because of the non-biased sampling of all the reactions in the model, FBA allows for *in silico* experimentation not permissible *in vivo* and permits the identification of novel candidate pathways contributing to insulin resistance phenotypes, which may otherwise be overlooked. Additional experimental validation and extension of these findings will be required in future studies.

In summary, the aims of this dissertation were (1) to show how novel applications of constraint-based modeling can aid in the investigation of human nutrition and (2) to elucidate disruptions in metabolic networks which cause metabolic phenotypes associated with IR/T2D. After constructing a unique metabolic model of muscle metabolism incorporating metabolism from the macronutrients, I addressed the first aim by asking whether or not this model can predict the efficacy

of amino acid supplementation on contractile protein synthesis. The results were qualitatively consistent with published data and showed an additional and/or alternative explanation as to why leucine and the other BCAAs increase muscle protein synthesis: BCAAs may be used as an acute energy source to support protein synthesis. While specific experiments would need to be done to test this hypothesis, these findings demonstrate potential in this framework. To elucidate metabolic phenotypes associated with IR/T2D, I also used the metabolic model, demonstrating great flexibility with this specific model. I incorporated reciprocal modulation of lipid oxidation and glucose uptake in order to model the fasted-to-fed transition, and using this approach, I demonstrated that key metabolic phenotypes characteristic of human insulin resistance can be recapitulated by *in silico* experimental reductions in activity of flux through the pyruvate dehydrogenase complex, in combination with reductions in cellular lipid availability (fatty acid transport) and/or lipid or amino acid metabolism (electron-transferring-flavoprotein dehydrogenase) (**Figure 14**). The combined knockdowns also modulate flux through key pathways to yield additional features of insulin resistance, including reduced fatty acid oxidation, increased incomplete fatty acid oxidation, increased lactate production, and decreased glycogen storage. I also demonstrate that experimental reductions in OXPHOS flux alter cellular energetics, as predicted, but do not alter metabolic flexibility; thus, this computational model predicts that isolated defects in OXPHOS flux are not likely to be solely responsible for insulin resistance-linked metabolic phenotypes. In

addition, to validate the *in silico* results, two mouse models were used. First, we looked at the effect of acute IR induction on the expression of the genes from the candidate enzymes. It was found that in this model, the expression of at least one of the genes in each of the candidate enzymes was lowered, which could lead to the metabolic dysregulation. To further validate that altered activity through these enzymes could lead to IR metabolic phenotypes, we employed a different mouse model. We used a PDK 2/4-KO mouse model to investigate differing PDH flux independently and in combination with ETFDH siRNA. The results show that cultured myotubes from cells with low PDH levels (WT) and ETFDH siRNA lead to decreased ATP production, citrate synthase activity, and metabolic flexibility (as inferred by the change in OCR/ECAR ratio), mirroring the *in silico* predictions.

Together, these findings are also consistent with the concept that insulin resistance is not likely to arise from a single gene defect, but rather from dysregulation of metabolic adaptations to energy/nutrient stress at several key nodes. More broadly, this analysis illustrates how computational approaches can be used to model metabolism and also provides a valuable resource which can be queried and expanded for further studies to identify novel candidate enzymes and pathways for type 2 diabetes pathogenesis and treatment.

Appendix A – Pathway Assignments

Pathway	Ala,_Asp,_and_ Glu	Arg_and_Orn_ metabolism	Arg_and_Pro_ Metabolism	Ascorbate_and _Alderate_Meta bolism	BCAA
KEGG ID	hsa00250	hsa00472	hsa00330	hsa00053	hsa00280
Model Abbreviation	ASTM GluDeh GlnSynth ALT ALDH4a1 ASNase ASNSynth	ALT Dr_orn	ASTM ALDH3A2 GluDeh GlnSynth ALT PRODH ALDH4a1 GATM GAMT ASNase P5CS PYCS PYRCR1 CKM MT_pro	DAGL Fum AKR1A1 ALDH3A2 RPE	G3PDehC ASTM CitSynth SucDeh-II ButyriCoADeh EnoCoADeh- But 3HA-CoADeh- But AcylCoAAT-But ALDH3A2 DLDH BCAT2-val BCKDHB-val BCKADE2-val ACADSB ECHS1 HIBCH HIBADH ALDH6A1 PCCB MCEE MUT BCKDHB-ile BCKADE2-ile ECHS1 HSD17B10_ ACAT1 BCAT2-leu BCKDHB-leu BCKADE2-leu IVD MCC1-MCC2 MGCA HMGCL OXCT HMGCS2 ALT Acetyl-coaLeak

					2a2hButLeak MT_val MT_ile MT_leu
--	--	--	--	--	---

Pathway	beta-alanine	Butanoate	Cys_and_Met_Metabolism	D-gln_and_D-glu_Metabolism	Fatty_Acid_Metabolism
KEGG ID	hsa00410	hsa00650	hsa00270	hsa00471	hsa00071
Model Abbreviation	ASTM Fum ALDH3A2 ECHS1 HIBCH	G3PDehC ASTM PyrSynth CitSynth Acon SucDeh-II Fum ButyrlCoAdeh EnoCoAdeh-But 3HA-CoAdeh-But AcylCoAAT-But ACSM-But ECHS1 ACAT1 HMGCL OXCT HMGCS2 ILVBL	ASTM Fum AKR1A1 SDS CBS CTH AdoHcyase MTR AdoMet	GluDeh Spont_Glu GLN_Elim MT_glu	SucDeh-II PalTK CPT1B-CHKL CPT2 AcylCoAdeh EnoCoAdeh 3HA-CoAdeh AcylCoAAT AcylCoAdeh-18-c EnoCoAdeh-18c 3HA-CoAdeh-18c AcylCoAAT-18c AcylCoAdeh-14-c EnoCoAdeh-14c 3HA-CoAdeh-14c AcylCoAAT-14c AcylCoAdeh-12-c EnoCoAdeh-12c 3HA-CoAdeh-12c AcylCoAAT-12c AcylCoAdeh-10-c EnoCoAdeh-10c 3HA-CoAdeh-10c AcylCoAAT-10c AcylCoAdeh-8-c EnoCoAdeh-8c 3HA-CoAdeh-8c AcylCoAAT-8c

					AcylCoADeh-6-c EnoCoADeh-6c 3HA-CoADeh-6c AcylCoAAT-6c ButyrlCoADeh EnoCoADeh-But 3HA-CoADeh-But AcylCoAAT-But ACSM-But ASCM-5c ASCM-6c ACSM-10c CPT1B-CHKL CPT2 AcylCoADeh-9-c EnoCoADeh-9c 3HA-CoADeh-9c AcylCoAAT-9c AcylCoADeh-7-c EnoCoADeh-7c 3HA-CoADeh-7c AcylCoAAT-7c AcylCoADeh-5-c EnoCoADeh-5c 3HA-CoADeh-5c AcylCoAAT-5c AKR1A1 ALDH3A2 ECHS1 ACAT1 GCDH Acetyl-coaLeak
--	--	--	--	--	---

Pathway	Folate_Metabolism	Fructose_and_mannose_metabolism	Galactose_Metabolism	Glutathione_metabolism	Glyc,_Ser,_Thre
KEGG ID	hsa00790	hsa00051	hsa00052	hsa00480	hsa00260
Model Abbreviation	AKR1A1 DHFR QDPR	Hex PFK FBP Ald	Hex PFK AKR1A1 PGM1	IsoDehnadph G6PD PGD GCL	G3PDdehC Fum AKR1A1 GLYCTK

		TPI G3PDehC AKR1A1	UGP2	GSS GSR GlutathLeak glutathxport	DLDH SDS CBS CTH GATM GAMT SHMT PHGDH PSA PSPH
--	--	--------------------------	------	---	---

Pathway	Glycerolipid	Glycerophosph olipid	Glycolysis	Glycylate_and _Dicarboxylate_ metabolism	Histidine_Metab olism
KEGG ID	hsa00561	hsa00564	hsa00010	hsa00630	hsa00340
Model Abbreviation	LPL MAGL Hex Acon Fum GK GPAT4 ABHD5 DAGZ-DAGK6 DGAT1 AKR1A1 ALDH3A2 GLYCTK St_TAG	DAGL G3PDehC GPAT4 ABHD5 DAGZ-DAGK6 BCAT-ile St_TAG	Hex PGI PFK FBP Ald TPI D3PDeh PGK PGM Eno PyrK PEPCarbK PyrSynth AKR1A1 ALDH3A2 DLDH PGM1	G3PDehC CitSynth Acon MalDehM ACSM-14c ACSM-18c AKR1A1 GLYCTK ASNase	TPI AKR1A1 ALDH3A2 GAMT HAL FLJ31300 MGC35366 FTCD1 ASNase

Pathway	Ketone_Metabo lism	Lysine	Nitrogen_metab olism	Once_Carbon_ Pool_by_folate	OxPhos
KEGG ID	hsa00072	hsa00310	hsa00910	hsa00670	hsa00190
Model Abbreviation	CitSynth AcylCoAAT-But ACAT1 HMGCL OXCT HMGCS2	AKGDeh EnoCoADeh- But 3HA-CoADeh- But AcylCoAAT-But ECHS1 ACAT1 AASS aAASADeh	GluDeh GlnSynth CTH SHMT HAL ASNase ASNSynth GLN_Elim ALA_Elim	G3PDehC MTR SHMT MTHFR DHFR FTCD1 FTCD2 FT ASNase PYRCR1	SucDeh-II NADHDeh-I UCytC-III CytCO-IV ATPSynth-V AMP_ADPSuppl y

		KATII GCDH ASNase lysdeg MT_lys			
--	--	---	--	--	--

Pathway	Pentose_and_glu cucouronate_inte rconversions	Pentose_Phosp hate	Phe,_Tyr,_Try_ Metabolism	Phe_metabolis m	Propanoate
KEGG ID	hsa00040	hsa00030	hsa00400	hsa00360	hsa00640
Model Abbreviation	TPI ALDH3A2 UGP2 RPE	PGI PFK FBP Ald AKR1A1 PGM1 G6PD PGLS PGD RPE RPIA TKT1 TKT2 TALDO RBSK	ASTM Fum AKR1A1 PAG	ASTM PalTK AKR1A1 ALDH3A2 ALT PAG	G3PDehC ASTM SunCoaSynth Fum ALDH3A2 ECHS1 HIBCH ALDH6A1 PCCB MCEE MUT ECHS1 ACAT1 ACAS2

Pathway	Pyruvate_meta bolism	TCA_Cycle	Tryptophan	Tyrosine	AminoAcid_Upt ake
KEGG ID	hsa00620	hsa00020	hsa00380	hsa00350	n-a
Model Abbreviation	PyrK PEPSynth PEPCarbK PEPCarbl LacDeh G3PDehC PyrSynth CitSynth MalDehM AcylCoAAT-But ALDH3A2 DLDH ACAT1	PEPCarbK PyrSynth CitSynth Acon IsoDeh IsoDehnadph AKGDeh SunCoaSynth SucDeh-II Fum MalDehM DLDH Acetyl-coaLeak MCT	AKGDeh EnoCoADeh- But 3HA-CoADeh- But AcylCoAAT-But ALDH3A2 ECHS1 ACAT1 ALT GCDH WARS	ASTM AKR1A1 GAMT	EAA_arg EAA_his EAA_ile EAA_leu EAA_lys EAA_met EAA_phe EAA_thr EAA_trp EAA_val NEAA_ala NEAA_asn NEAA_asp NEAA_cys

					NEAA_glu NEAA_gln NEAA_gly NEAA_pro NEAA_ser NEAA_tyr
--	--	--	--	--	--

Pathway	ATP_Metabolism	Carnitine_Transport	Cellular_Exchange	Creatine	MacroNutrient_Exchange
KEGG ID	n-a	n-a	n-a	n-a	n-a
Model Abbreviation	Obj_atp AMP_ADPSupply	SLC22A5- OCTN2 SLC25A20- CACT	12DAG GLUT4 MCT4 MCT_pyr FAT-CD36 FATprop FATbut FAT5c FAT6c FAT8c FAT9c FAT10c FAT12c FAT14c FAT18c Alc_glyc COA Xport_rib Dr_akg Dr_oaa	CKM Spont_CrP Nut_cr Dr_cr	Ex_ins Ex_gluc Ex_lac Ex_pyr Ex_pal Ex_prop Ex_but Ex_5c Ex_6c Ex_8c Ex_9c Ex_10c Ex_12c Ex_14c Ex_18c Ex_glyc Ex_tag Ex_dag Ex_mag Ex_akg Ex_oaa Ex_rib

Pathway	MicroNutrient_Exchange	Protein_Synthesis	Glycogen	NAD_NADH	FAD_FADH
KEGG ID	n-a	n-a	n-a	n-a	n-a
Model Abbreviation	Nut_o2 Nut_co2 Nut_h2o Nut_p Nut_hco3 Nut_coa Nut_carn Nut_dhf	YARS WARS TARS LARS IARS KARS AARS VARS	Hex PGI ATP2UTP UDP2ADP PGM1 UGP2 mGYG mGYS1	D3PDeh LacDeh MalDehC G3PDehC PyrSynth IsoDeh IsoDehnadph AKGDeh	G3PDehM SucDeh-II ETFUO AcylCoADeh AcylCoADeh-18-c AcylCoADeh-14-c

		MARS SARS DARS GARS PARS CARS EPRS QARS RARS FARS HARS NARS ACT MYOHC1-2x MYOHC2a MYOHC2b MYOLCk MYOLCp MYO1-2x MYO2a MYO2x MYO2b TMN1 TMN2 DIM-TMN1 DIM-TMN2 TPNC1 TPNC2 TPNI1 TPNI2 TPNT1 TPNT2 TPN1 TPN2 CONTR- COMP1 CONTR- COMP2a CONTR- COMP2x CONTR- COMP2b Str_CONTR- COMP1 Str_CONTR- COMP2a Str_CONT- COMP2x Str_CONTR- COMP2b	UDP2ADP mGYS1 ATP2UTP	MalDehM NADHDeh-I 3HA-CoAdeh 3HA-CoAdeh- 18c 3HA-CoAdeh- 14c 3HA-CoAdeh- 12c 3HA-CoAdeh- 10c 3HA-CoAdeh- 8c 3HA-CoAdeh- 6c 3HA-CoAdeh- 9c 3HA-CoAdeh- 7c 3HA-CoAdeh- 5c AKR1A1 ALDH3A2 DLDH HIBADH ALDH6A1 HSD17B10_ GluDeh AASS aAASADeh lysdeg ALDH4a1 MTHFR DHFR FT PHGDH PYCS PYRCR1 QDPR G6PD PGD GSR Recycle_nadp	AcylCoADeh- 12-c AcylCoADeh- 10-c AcylCoADeh-8- c AcylCoADeh-6- c ButyrlCoADeh AcylCoADeh-9- c AcylCoADeh-7- c AcylCoADeh-5- c ACADSB IVD PRODH
--	--	---	-----------------------------	---	--

Pathway	Mit_Shuttle	All_Pathways
KEGG ID	n-a	hsa01100
Model Abbreviation	Dr_akg Dr_oaa MalDehC ASTC G3PDehC Mal-AKGEX Glu-AspEx ASTM G3PDehM MalDehM	All reactions in the model

Bibliography

Agren R., Bordel S., Mardinoglu A., Pornputtapong N., Nookaew I., et al. (2012) Reconstruction of Genome-Scale Active Metabolic Networks for 69 Human Cell Types and 16 Cancer Types Using INIT. *PLoS Computational Biology* 8(5): e1002518. doi:10.1371/journal.pcbi.1002518.

Anderson, E.J., Lustig, M.E., Boyle, K.E., Woodlief, T.L., Kane, D.A., Lin, C.T., Price, J.W., III, Kang, L., Rabinovitch, P.S., Szeto, H.H., Houmard, J.A., Cortright, R.N., Wasserman, D.H., and Neuffer, P.D. (2009). Mitochondrial H₂O₂ emission and cellular redox state link excess fat intake to insulin resistance in both rodents and humans. *Journal of Clinical Investigation* 119(3): 573-581.

Aoki T.T., Brennan M.F., Müller W.A., Soeldner J.S., Alpert J.S., et al. (1976) Amino acid levels across normal forearm muscle and splanchnic bed after a protein meal. *The American Journal of Clinical Nutrition* 29: 340-350.

Befroy, D.E., Petersen, K.F., Dufour, S., Mason, G.F., de Graaf, R.A., Rothman, D.L., and Shulman, G.I. (2007). Impaired mitochondrial substrate oxidation in muscle of insulin-resistant offspring of type 2 diabetic patients. *Diabetes* 56: 1376-1381.

Blomstrand, E., Eliasson, J., Karlsson, H.K.R., Köhnke, R. (2006) Branched-Chain Amino Acids Activate Key Enzymes in Protein Synthesis after Physical Exercise. *The Journal of Nutrition* 136: 269S-237S.

Boyle, K.E., Canham, J.P., Consitt, L.A., Zheng, D., Koves, T.R., Gavin, T.P., Holbert, D., Neuffer, P.D., Ilkayeva, O., Muoio, D.M., and Houmard, J.A. (2011). A high-fat diet elicits differential responses in genes coordinating oxidative metabolism in skeletal muscle of lean and obese individuals. *Journal of Clinical Endocrinology and Metabolism* 96: 775-781.

Boyle, K.E., Zheng, D., Anderson, E.J., Neuffer, P.D., and Houmard, J.A. (2012). Mitochondrial lipid oxidation is impaired in cultured myotubes from obese humans. *International Journal of Obesity (Lond)* 36: 1025-1031.

Bowker-Kinley, M.M., Davis, W.I., WU, P., Harris, R.A., and Popov, K.M (1998). Evidence for Existence of Tissue-specific Regulation of the Mammalian Pyruvate Dehydrogenase Complex. *Biochemical Journal* 329: 191-196.

Cakir, T., Alsan, S., Saybasih, H., Akin, A., Ulgen, K.O. (2007) Reconstruction and flux analysis of coupling between metabolic pathways and astrocytes and neurons: application to cerebral hypoxia. *Theoretical Biology and Medical Modeling*: 4:48.

Centers for Disease Control and Prevention, HHS. National Diabetes Fact Sheet. www.cdc.gov/diabetes . 2011.

Cynober, L.A. (2002). Plasma Amino Acid Levels With a Note on Membrane Transport: Characteristics, Regulation and Metabolic Significance. *Nutrition* 18: 761-766.

Detimary, P., Jonas, J. C., and Henquin, J. C. (1995). Possible links between glucose-induced changes in the energy state of pancreatic B cells and insulin release. Unmasking by decreasing a stable pool of adenine nucleotides in mouse islets. *Journal of Clinical Investigation* 96:1738–1745

DeFronzo, R.A., Gunnarson, R., Biorkman, O., Olsson, M., and Warren, J. (1985). Effects of insulin on peripheral and splanchnic glucose metabolism in non-insulin dependent (Type II) diabetes mellitus. *Journal of Clinical Investigation* 76: 149-155.

Duarte, N.C., Becker, S.A., Jamshidi, N., Thiele, I., Mo, M.L., et al. (2007) Global reconstruction of the human metabolic network based on genomic and bibliomic data. *Proceedings of the National Academy of Sciences of the United States of America* 104 (6): 1777-1782.

Eriksson, J., Franssila-Kallunki, A., Ekstrand, A., Saloranta, C., Widen, E., Schalin, C., and Groop, L. (1989). Early metabolic defects in persons at increased risk for non-insulin-dependent diabetes mellitus. *New England Journal of Medicine* 321: 337-343.

Folger, O., Jerby, L., Frezza, C., Gottlieb, E., Ruppin, E., and Shlomi, T. (2011). Predicting selective drug targets in cancer through metabolic networks. *Molecular Systems Biology* 7: 501.

Gleeson, M. (2008) Dosing and Efficacy of Glutamine Supplementation in Human Exercise and Sport Training. *The Journal of Nutrition* 138: 2045S-2049S.

Gray, S.R., Soderlund, K., and Ferguson, R.A. (2008). ATP and phosphocreatine utilization in single human muscle fibres during the development of maximal power output at elevated muscle temperatures. *Journal of Sports Science* 26: 701-707.

Gordon, A.M., Homsher, E., Regnier, M. (2000) Regulation of Contraction in Striated Muscle (2000). *Physiological Reviews* 80(2): 853-924.

Illig, T., Gieger, C., Zhai, G., Romisch-Margl, W., Wang-Sattler, R., Prehn, C., Altmaier, E., Kastenmuller, G., Kato, B.S., Mewes, H.W., Meitinger, T., de Angelis, M.H., Kronenberg, F., Soranzo, N., Wichmann, H.E., Spector, T.D., Adamski, J., and Suhre, K. (2010). A genome-wide perspective of genetic variation in human metabolism. *Nature Genetics* 42: 137-141.

Jacob, S., Machann, J., Rett, K., Brechtel, K., Volk, A., Renn, W., Maerker, E., Matthaei, S., Schick, F., Claussen, C.D., and Haring, H.U. (1999). Association of increased intramyocellular lipid content with insulin resistance in lean nondiabetic offspring of type 2 diabetic subjects. *Diabetes* 48: 1113-1119.

Jeoung, N.H. and Harris, R.A. (2007). Knocking out PDK2 and PDK4 lowers fasting blood glucose levels, increases insulin sensitivity, and greatly improves glucose tolerance. *FASEB Journal* 21:1b171

Jeoung, N.H. and Harris, R.A. (2008). Pyruvate dehydrogenase kinase-4 deficiency lowers blood glucose and improves glucose tolerance in diet-induced obese mice. *American Journal of Physiology, Endocrinology, and Metabolism* 295: E46-E54.

Jerby, L., Shlomi, T., Ruppin, E. (2010) Computational reconstruction of tissue-specific metabolic models: application to human liver metabolism. *Molecular Systems Biology* 6:401.

Jin, W., Goldfine, A.B., Boes, T., Henry, R.R., Ciaraldi, T.P., Kim, E.Y., Emecan, M., Fitzpatrick, C., Sen, A., Shah, A., Mun, E., Vokes, V., Schroeder, J., Tatro, E., Jimenez-Chillaron, J., and Patti, M.E. (2011). Increased SRF transcriptional activity in human and mouse skeletal muscle is a signature of insulin resistance. *Journal of Clinical Investigation* 121: 918-929.

Jungas, R.L., Halperin, M.L., Brosnan, J.T. (1992) Quantitative Analysis of Amino Acid Oxidation and Related Gluconeogenesis in Humans. *Physiological Reviews* 72(2): 419-448.

Kacarovsky-Bielesz, G., Chmelik, M., Ling, C., Pokan, R., Szendroedi, J., Farukuoye, M., Kacarovsky, M., Schmid, A.I., Gruber, S., Wolzt, M., Moser, E., Pacini, G., Smekal, G., Groop, L., and Roden, M. (2009). Short-term exercise training does not stimulate skeletal muscle ATP synthesis in relatives of humans with type 2 diabetes. *Diabetes* 58(6): 1333-1341.

Kanehisa, M., Goto, S., Sato, Y., Furumichi, M., and Tanabe, M. (2012). KEGG for integration and interpretation of large-scale molecular data sets. *Nucleic Acids Research* 40: D109-D114.

Kelley, D.E. and Mandarino, L.J. (2000). Fuel selection in human skeletal muscle in insulin resistance: a reexamination. *Diabetes* 49: 677-683.

Kelley, D.E., Mokan, M., and Mandarino, L.J. (1992). Intracellular defects in glucose metabolism in obese patients with NIDDM. *Diabetes* 41: 698-706.

Kelley, D.E., Mokan, M., and Mandarino, L.J. (1993). Metabolic pathways of glucose in skeletal muscle of lean NIDDM patients. *Diabetes Care* 16, 1158-1166.
Kelley, D.E. and Simoneau, J.A. (1994). Impaired free fatty acid utilization by skeletal muscle in non-insulin-dependent diabetes mellitus. *Journal of Clinical Investigation* 94: 2349-2356.

Khajah, M., Millen, B., Cara, D.C., Waterhouse, C., and McCafferty, D.M. (2011). Granulocyte-macrophage colony-stimulating factor (GM-CSF): a chemoattractive agent for murine leukocytes in vivo. *Journal of Leukocyte Biology* 89: 945-953.

Kiilerich, K., Birk, J.B., Damsgaard, R., Wojtaszewski, J.F., and Pilegaard, H. (2008). Regulation of PDH in human arm and leg muscles at rest and during intense exercise. *American Journal of Physiology, Endocrinology, and Metabolism* 294: E36-E42.

Kohda, Y., Umeki, M., Kono, T., Terasaki, F., Matsumura, H., and Tanaka, T. (2010). Thiamine ameliorates diabetes-induced inhibition of pyruvate dehydrogenase (PDH) in rat heart mitochondria: investigating the discrepancy between PDH activity and PDH E1 α phosphorylation in cardiac fibroblasts exposed to high glucose. *Journal of Pharmacological Science* 113: 343-352.

Koves, T.R., Ussher, J.R., Noland, R.C., Slentz, D., Mosedale, M., Ilkayeva, O., Bain, J., Stevens, R., Dyck, J.R., Newgard, C.B., Lopaschuk, G.D., and Muoio, D.M. (2008). Mitochondrial overload and incomplete Fatty Acid oxidation contribute to skeletal muscle insulin resistance. *Cell Metabolism* 7: 45-56.

Kraegen, E.W., Sowden, J.A., Halstead, M.B., Clark, P.W., Rodnick, K.J., Chisholm, D.J., and James, D.E. (1993). Glucose transporters and in vivo glucose uptake in skeletal and cardiac muscle: fasting, insulin stimulation and immunolocalization studies of GLUT1 and GLUT4. *Biochemical Journal* 295 (Pt 1) : 287-293.

Lockridge, J.B., Sailors, M.L., Durgan, D.J., Egbejimi, O., Jeong, W.J., Bray, M.S., Stanley, W.C., and Young, M.E. (2008). Bioinformatic profiling of the transcriptional response of adult rat cardiomyocytes to distinct fatty acids. *Journal of Lipid Research* 49: 1395-1408.

MacLaren, D.P.M., Nevill, A.M., Take C.D., Campbell, I.T., Cheetham, E., et al. (2000) Human erythrocyte and plasma amino acid concentrations during exercise. *Medicine & Science in Sports & Exercise* 32(7): 1244-1249.

Malenfant, P., Joanisse, D.R., Theriault, R., Goodpaster, B.H., Kelley, D.E., and Simoneau, J.A. (2001). Fat content in individual muscle fibers of lean and obese subjects. *International Journal of Obesity and Related Metabolic Disorders* 25: 1316-1321.

Mandarino, L.J., Consoli, A., Jain, A., and Kelley, D.E. (1993). Differential regulation of intracellular glucose metabolism by glucose and insulin in human muscle. *American Journal of Physiology* 265: E898-E905.

Martin, B.C., Warram, J.H., Krolewski, A.S., Bergman, R.N., Soeldner, J.S., and Kahn, C.R. (1992). Role of glucose and insulin resistance in development of Type II diabetes mellitus: results of a 25-year follow-up study. *Lancet* 340: 925-929.

Mayers, R.M., Leighton, B., and Kilgour, E. (2005). PDH kinase inhibitors: a novel therapy for Type II diabetes? *Biochemical Society Transactions* 33: 367-370.

Mo, M.L., Palsson, B.Ø. (2009) Understanding human metabolic physiology: a genome-to-systems approach. *Trends in Biotechnology* 1:37-44.

Mootha, V.K., Lindgren, C.M., Eriksson, K.F., Subramanian, A., Sihag, S., Lehar, J., Puigserver, P., Carlsson, E., Ridderstrale, M., Laurila, E., Houstis, N., Daly, M.J., Patterson, N., Mesirov, J.P., Golub, T.R., Tamayo, P., Spiegelman, B., Lander, E.S., Hirschhorn, J.N., Altshuler, D., and Groop, L.C. (2003). PGC-1 α -responsive genes involved in oxidative phosphorylation are coordinately downregulated in human diabetes. *Nature Genetics* 34: 267-273.

Morino, K., Petersen, K.F., Sono, S., Choi, C.S., Samuel, V.T., Lin, A., Gallo, A., Zhao, H., Kashiwagi, A., Goldberg, I.J., Wang, H., Eckel, R.H., Maegawa, H., and Shulman, G.I. (2012). Regulation of mitochondrial biogenesis by lipoprotein lipase in muscle of insulin-resistant offspring of parents with type 2 diabetes. *Diabetes* 61: 877-887.

Mostert, M., Rabbone, I., Piccinini, M., Curto, M., Vai, S., Musso, A., and Rinaudo, M.T. (1999). Derangements of pyruvate dehydrogenase in circulating lymphocytes

of NIDDM patients and their healthy offspring. *Journal of Endocrinological Investigation* 22: 519-526.

Niklas, J., Schneider, K., Heinzle, E. (2010). Metabolic flux analysis in eukaryotes. *Current Opinion in Biotechnology* 21: 63-69.

Nogiec, C.D. and Kasif, S. (2013). To supplement or not to supplement: a metabolic network framework for human nutritional supplements. *PLoS ONE* 8: e68751.

Nutrition Business Journal. Supplements. *Nutritional Business Journal*. Retrieved August 23, 2010 from <http://nutritionbusinessjournal.com/supplements/>.

Oberhardt, M.A., Palsson, B.Ø., Papin, J.A. (2009). Application of genome-scale metabolic reconstructions. *Molecular Systems Biology* 5(320): 1-15.

Olsen, R.K., Olpin, S.E., Andresen, B.S., Miedzybrodzka, Z.H., Pourfarzam, M., Merinero, B., Frerman, F.E., Beresford, M.W., Dean, J.C., Cornelius, N., Andersen, O., Oldfors, A., Holme, E., Gregersen, N., Turnbull, D.M., and Morris, A.A. (2007). ETFDH mutations as a major cause of riboflavin-responsive multiple acyl-CoA dehydrogenation deficiency. *Brain* 130: 2045-2054.

Paddonn-Jones, D., Børsheim, E., Wolfe, R.R. (2004) Potential Ergogenic Effects of Arginine and Creatine Supplementation. *The Journal of Nutrition* 134: 2888S-2894S.

Patti, M.E., Butte, A.J., Crunkhorn, S., Cusi, K., Berria, R., Kashyap, S., Miyazaki, Y., Kohane, I., Costello, M., Saccone, R., Landaker, E.J., Goldfine, A.B., Mun, E., DeFronzo, R., Finlayson, J., Kahn, C.R., and Mandarino, L.J. (2003). Coordinated reduction of genes of oxidative metabolism in humans with insulin resistance and diabetes: Potential role of PGC1 and NRF1. *Proceedings of the National Academy of Science, USA* 100: 8466-8471.

Patti, M.E. and Corvera, S. (2010). The Role of Mitochondria in the Pathogenesis of Type 2 Diabetes. *Endocrine Review* 31(3): 364-395.

Petersen, K.F., Dufour, S., Befroy, D., Garcia, R., and Shulman, G.I. (2004). Impaired mitochondrial activity in the insulin-resistant offspring of patients with type 2 diabetes. *New England Journal of Medicine* 350: 664-671.

Pozefsky, T., Felig, P., Tobin, J.D., Soeldner, J.S., Cahill, G.F. Jr. (1969). Amino Acid Balance across Tissues of the Forearm in Post-absorptive Man: Effects of Insulin at Two Dose Levels. *The Journal of Clinical Investigation* 48: 2273-2282.

Petersen, K.F., Dufour, S., and Shulman, G.I. (2005). Decreased insulin-stimulated ATP synthesis and phosphate transport in muscle of insulin-resistant offspring of type 2 diabetic parents. *PLoS Medicine* 2: e233.

Ramakrishna, R., Edwards, J.S., McCulloch, A., and Palsson, B. Ø. (2001). Flux-balance analysis of mitochondrial energy metabolism: consequences of systemic stoichiometric constraints. *American Journal of Physiology. Regulatory, Integrative and Comparative Physiology* 280: R695-R704.

Randle, P.J., Garland, P.B., Hales, C.N., and Newsholme, F.A. (1963). The glucose fatty-acid cycle: Its role in insulin sensitivity and the metabolic disturbances of diabetes mellitus. *Lancet* 1: 785-789.

Rinaldo, P., Matern, D., and Bennett, M.J. (2002). Fatty acid oxidation disorders. *Annual Review of Physiology* 64: 477-502.

Romero, P., Wagg, J., Green, M.L., Kaiser, D., Krummenacker, M., and Karp, P.D. (2005). Computational prediction of human metabolic pathways from the complete human genome. *Genome Biology* 6: R2.

Sacchetti, M., Saltin, B., Olsen, D.B., and van, H.G. (2004). High triacylglycerol turnover rate in human skeletal muscle. *Journal of Physiology* 561: 883-891.

Schimomura, Y., Yamamoto, Y., Bajotto, G., Sato, J., Murkakami, T., et al. (2006). Nutraceutical Effects of Branched-Chain Amino Acids on Skeletal Muscle. *Journal of Nutrition* 136: 529S-532S.

Segre, D., Vitkup, D., and Church, G.M. (2002). Analysis of optimality in natural and perturbed metabolic networks. *Proceedings of the National Academy of Sciences of the United States of America* 99: 15112-15117.

Sena, S., Hu, P., Zhang, D., Wang, X., Wayment, B., Olsen, C., Avelar, E., Abel, E.D., and Litwin, S.E. (2009). Impaired insulin signaling accelerates cardiac mitochondrial dysfunction after myocardial infarction. *Journal of Molecular Cell Cardiology* 46: 910-918.

Shlomi, T., Cabili, M.N., Herrgård, M.N., Palsson, B.Ø., Ruppin, E. (2008). Network-based prediction of human tissue-specific metabolism. *Nature Biotechnology* 26(9): 1003-1010.

Simoneau, J.A. and Kelley, D.E. (1997). Altered glycolytic and oxidative capacities of skeletal muscle contribute to insulin resistance in NIDDM. *Journal of Applied Physiology* 83: 166-171.

Sleigh, A., Raymond-Barker, P., Thackray, K., Porter, D., Hatunic, M., Vottero, A., Burren, C., Mitchell, C., McIntyre, M., Brage, S., Carpenter, T.A., Murgatroyd, P.R., Brindle, K.M., Kemp, G.J., O'Rahilly, S., Semple, R.K., and Savage, D.B. (2011). Mitochondrial dysfunction in patients with primary congenital insulin resistance. *Journal of Clinical Investigation* 121: 2457-2461.

Sleigh, A., Stears, A., Thackray, K., Watson, L., Gambineri, A., Nag, S., Campi, V.I., Schoenmakers, N., Brage, S., Carpenter, T.A., Murgatroyd, P.R., O'Rahilly, S., Kemp, G.J., and Savage, D.B. (2012). Mitochondrial oxidative phosphorylation is impaired in patients with congenital lipodystrophy. *Journal of Clinical Endocrinology and Metabolism* 97: E438-E442.

Spirito, P., Seidman, C.E., McKenna, W.J., Maron, B.J. (1997). The Management of Hypertrophic Cardiomyopathy. *The New England Journal of Medicine* 336(11): 775-785.

Tabak, A.G., Jokela, M., Akbaraly, T.N., Brunner, E.J., Kivimaki, M., and Witte, D.R. (2009). Trajectories of glycaemia, insulin sensitivity, and insulin secretion before diagnosis of type 2 diabetes: an analysis from the Whitehall II study. *Lancet* 373: 2215-2221.

Tessari, P., Zanetti, M., Barazzoni, R., Vettore, M., Michielan, F. (1996). Mechanisms of Postprandial Protein Accretion in Human Skeletal Muscle: Insight from Leucine and Phenylalanine Forearm Kinetics. *The Journal of Clinical Investigation* 98(6): 1361-1372.

Thiele, I., Swainston, N., Fleming, R.M., Hoppe, A., Sahoo, S., Aurich, M.K., Haraldsdottir, H., Mo, M.L., et al, Palsson, B. Ø. (2013). A community-driven global reconstruction of human metabolism. *Nature Biotechnology* 31: 419-425.

Vaag, A., Henriksen, J.E., and Beck-Nielsen, H. (1992). Decreased insulin activation of glycogen synthase in skeletal muscles in young nonobese caucasian first-degree relatives of patients with non-insulin-dependent diabetes mellitus. *Journal of Clinical Investigation* 89: 782-788.

Vadvalkar, S.S., Baily, C.N., Matsuzaki, S., West, M., Tesiram, Y.A., and Humphries, K.M. (2013). Metabolic inflexibility and protein lysine acetylation in heart mitochondria of a chronic model of type 1 diabetes. *Biochemical Journal* 449: 253-261.

Varma, A. and Palsson, B. Ø. Metabolic Flux Balancing. *Nature Biotechnology* 12: 994-998. 10-12-1994.

Viguerie, N., Montastier, E., Maoret, J.J., Roussel, B., Combes, M., Valle, C., Villa-Vialaneix, N., Iacovoni, J.S., Martinez, J.A., Holst, C., Astrup, A., Vidal, H., Clement, K., Hager, J., Saris, W.H., and Langin, D. (2012). Determinants of human adipose tissue gene expression: impact of diet, sex, metabolic status, and cis genetic regulation. *PLoS Genetics* 8: e1002959.

Wang, Q., Zhang, Y., Yang, C., Xiong, H., Lin, Y., Yao, J., Li, H., Xie, L., Zhao, W., Yao, Y., Ning, Z.B., Zeng, R., Xiong, Y., Guan, K.L., Zhao, S., and Zhao, G.P. (2010). Acetylation of metabolic enzymes coordinates carbon source utilization and metabolic flux. *Science* 327: 1004-1007.

Wilson-Fritch, L., Nicoloso, S., Chouinard, M., Lazar, M.A., Chui, P.C., Leszyk, J., Straubhaar, J., Czech, M.P., and Corvera, S. (2004). Mitochondrial remodeling in adipose tissue associated with obesity and treatment with rosiglitazone. *Journal of Clinical Investigation* 114: 1281-1289.

Yi, P., Park, JS., Melton, DA. (2013). Betatrophin: a hormone that controls pancreatic β cell proliferation. *Cell* 153(4): 747-758.

Curriculum Vitae

